UNIVERSITAT POLITÈCNICA DE VALÈNCIA

Diseño y desarrollo de la electrónica de los emisores acústicos para los sistemas de posicionamiento y calibración de telescopios submarinos de neutrinos.

TESIS DOCTORAL:
Carlos David Llorens Álvarez
Gandía, mayo de 2017

DIRIGIDA POR:
Miguel Ardid Ramírez
Tomás Sogorb Devesa
Alicia Herrero Debón

II

A mis padres.
Por darme la vida y la oportunidad de llegar a donde he llegado.

A Núria y a Queralt.
Por ser las dos personas que dan sentido a mi vida y a las que más quiero.

Agradecimientos

En primer lugar, quería dar las gracias a mis compañeros del grupo “Acústica para la Detección de Astropartículas” ya que sin su trabajo y entrega el presente trabajo no habría sido posible. Gracias Joán, Manu, Silvia, Giusi, Maria e Ivan.

También quería darles las gracias a mis directores por su entrega y por la confianza puesta en mí. Gracias Miguel, Tomás y Alicia.

Quiero dar también las gracias a mis colegas de ANTARES, NEMO/SMO, KM3NeT y en especial al grupo del IFIC con el cual se ha colaborado coordinadamente durante la tesis.

Y por último darles las gracias a los proyectos que han financiado la investigación, así como a los entes que nos han permitido usar sus instalaciones para probar los desarrollos de la presente tesis:

Fondos Europeos:

European FEDER funds and 7th Framework Programmes.

Comisión Europea para el estudio del diseño de KM3NeT (FP6, numero de contrato DS 011937) y fase preparatoria (FP7, Grant No.212525).

Fondos Nacionales:

Ministerio de Ciencia e Innovación (Gobierno de España), referencias de los proyectos: FPA2009-13983-C02-02, FPA2012-37528-C02-02, ACI2009-1067, AIC10-D-00583.

Plan Estatal de Investigación, ref. FPA2015-65150-C3-2-P (MINECO/FEDER).

Fondos Regionales:

Generalitat Valenciana: Prometeo/2009/26, PrometeoII/2014/079, ACOMP/2015/175.

Resumen

Los telescopios de neutrinos son una nueva forma de observar el Universo. Desde hace más de una década se están diseñando este tipo de estructuras con el propósito de estudiar el Universo desde un nuevo punto de vista, el de las partículas que se generan en los aceleradores de partículas cósmicos. Estas infraestructuras no solo se limitan al estudio del Universo, sino que también pueden ser utilizadas en el campo de la Física de partículas e incluso en el estudio de la vida submarina.

La mayoría de estos telescopios se basan en la detección de la llamada luz de Cherenkov mediante fotomultiplicadores, la diferencia entre ellos radica en el medio en que se ubican (hielo o agua) y en la infraestructura utilizada. Concretamente, los telescopios europeos montan dichos fotomultiplicadores en una estructura vertical submarina anclada a gran profundidad, la cual está sometida a la influencia de las corrientes marinas. Por este motivo sufren desplazamientos que afectan a la localización de los fotomultiplicadores y se hace necesaria la implementación de un sistema de posicionamiento para que el telescopio sea funcional. Para ello se utiliza un sistema acústico consistente en unos emisores anclados al suelo marino y unos receptores situados en los diferentes niveles de la estructura vertical. Uno de los objetivos de la presente tesis es el desarrollo de estos emisores acústicos.

Con este fin se han desarrollado diferentes prototipos de laboratorio con los que se han ido escalando prestaciones hasta obtener un prototipo que ha sido instalado y testeado en los telescopios ANTARES y NEMO. Así se demostró que el prototipo funcionaba perfectamente dentro de los requisitos establecidos, pasándose a diseñar una versión final del emisor acústico mucho más potente y funcional para ser montada dentro de vasijas de aluminio junto con un traductor omnidireccional en las anclas del nuevo telescopio de neutrinos KM3NeT. Conjuntamente con la empresa MSM se elaboraron 18 equipos para KM3NeT-ARCA, dos de los cuales fueron instalados en la primera campaña marina a finales de 2015 comprobándose su correcto funcionamiento.

Por otro lado, la interacción de los neutrinos ultraenergéticos con la materia también produce un pulso termoacústico con forma bipolar, simetría axial y altamente directivo. Desde hace años se está estudiando la viabilidad de la técnica de detección acústica y la posibilidad de implementarla en dichos telescopios. Para poder poner a prueba y calibrar dicha técnica es necesario disponer de un sistema emisor acústico que sea capaz de generar una señal similar a la descrita. Este ha sido el segundo objetivo desarrollado en esta tesis.

Para ello se ha diseñado un calibrador compacto y versátil basado en un array de transductores acústicos usando generación paramétrica. Dada la complejidad del pulso a emular y lo novedoso de la técnica a utilizar, se ha requerido la realización de numerosas

pruebas de laboratorio con el fin de conseguir unos transductores adecuados y la electrónica capaz de hacerlos funcionar a la potencia y eficiencia requerida. Los positivos resultados obtenidos en esta línea hacen prever que, en breve, podremos obtener un calibrador acústico de neutrinos funcional.

Finalmente, cabe reseñar que he participado en las diferentes investigaciones y actividades que se describen en la tesis, siendo mi cometido principal el desarrollo tanto de la electrónica como de los diferentes softwares/firmwares implicados en los emisores acústicos desarrollados.

Resum

Els telescopis de neutrins són una nova forma d'observar l'Univers. Des de fa més d'una dècada s'estan dissenyant aquest tipus d'estructures amb el propòsit d'estudiar l'Univers des d'un nou punt de vista, el de les partícules que es generen en els acceleradors de partícules còsmics. Estes infraestructures no sols es limiten a l'estudi de l'Univers, sinó que també poden ser utilitzades en el camp de la Física de partícules i fins i tot en l'estudi de la vida submarina.

La majoria d'aquests telescopis es basen en la detecció de l'anomenada llum de Cherenkov per mitjà de fotomultiplicadors, la diferència entre ells radica en el mig en què s'ubiquen (gel o aigua) i en la infraestructura utilitzada. Concretament, els telescopis europeus munten dits fotomultiplicadors en una estructura vertical submarina ancorada a gran profunditat, la qual està sotmesa a la influència dels corrents marins. Per este motiu pateixen desplaçaments que afecten a la localització dels fotomultiplicadors i es fa necessària la implementació d'un sistema de posicionament per a què el telescopi siga funcional. Per a això s'utilitza un sistema acústic consistent en uns emissors ancorats al sòl marí i uns receptors situats en els diferents nivells de l'estructura vertical. Un dels objectius de la present tesi és el desenvolupament d'aquests emissors acústics.

Amb este fi s'han desenvolupat diferents prototips de laboratori amb els quals s'han anat escalant prestacions fins a obtindre un prototip que ha sigut instal·lat i testeat en els telescopis ANTARES i NEMO. Així es va demostrar que el prototip funcionava perfectament dins dels requisits establerts, passant-se a dissenyar una versió final de l'emissor acústic molt més potent i funcional per a ser muntada dins d'atuells d'alumini junt amb un traductor omnidireccional en les àncores del nou telescopi de neutrins KM3NeT. Conjuntament amb l'empresa MSM es van elaborar 18 equips per a KM3NeT-ARCA, dos dels quals van ser instal·lats en la primera campanya marina a finals de 2015 comprovant-se el seu correcte funcionament.

D'altra banda, la interacció dels neutrins ultraenergètics amb la matèria també produeix un pols termoacústic amb forma bipolar, simetria axial i altament directiu. Des de fa anys s'està estudiant la viabilitat de la tècnica de detecció acústica i la possibilitat d'implementar-la en els esmentats telescopis. Per a poder posar a prova i calibrar esta tècnica és necessari disposar d'un sistema emissor acústic que siga capaç de generar un senyal semblant al descrit. Aquest ha sigut el segon objectiu desenvolupat en aquesta tesi.

Per a això s'ha dissenyat un calibrador compacte i versàtil basat en un array de transductores acústics utilitzant generació paramètrica. Donada la complexitat del pols a emular i la novetat de la tècnica a utilitzar, s'ha requerit la realització de nombroses proves de laboratori a fi d'aconseguir uns transductors adequats i l'electrònica capaç de

fer-los funcionar a la potència i eficiència requerida. Els positius resultats obtinguts en esta línia fan preveure que, en breu, podrem obtindre un calibrador acústic de neutrins funcional.

Finalment, cal ressenyar que he participat en les diferents investigacions i activitats que es descriuen en la tesi, sent la meua comesa principal el desenvolupament tant de l'electrònica com dels diferents softwares/firmwares implicats en els emissors acústics desenvolupats.

Abstract

Neutrino telescopes are a new way of looking at the Universe. For more than a decade these structures are being designed to study the Universe from a new point of view, that is, from the particles generated in the cosmic accelerators of particles. These infrastructures are not only useful to study the Universe, but they can also be used in the field of Particle Physics and even in the study of underwater life.

Most of these telescopes are based on the detection of the so-called Cherenkov light using photomultipliers, the difference between them lies in the medium in which they are located (ice or water) and in the infrastructure used. Specifically, European telescopes mount these photomultipliers in an underwater vertical structure anchored at great depth, which is under the influence of sea currents. For this reason they suffer displacements that affect the location of the photomultipliers and it becomes necessary to implement a positioning system for the telescope to be functional. For this, an acoustic system consisting of emitters anchored to the sea floor and receivers located at the different levels of the vertical structure is used. One of the objectives of the present thesis is the development of these acoustic emitters.

For this purpose we have developed different laboratory prototypes with different features until obtaining an improved prototype that was installed and tested in ANTARES and NEMO telescopes. This showed that the prototype worked perfectly within the established requirements and then, we proceed to design a final version of the much more powerful and functional emitter, acoustic beacon, to be mounted inside aluminum vessels together with an omnidirectional acoustic transducer, which will be located in anchored positions of the new KM3NeT neutrino telescope. In collaboration with the MSM Company, 18 acoustic beacons were developed for KM3NeT-ARCA being two of them installed in the first marine campaign at the end of 2015, and being able then to verify their correct operation.

On the other hand, interaction of ultraenergetic neutrinos with matter also produces a thermoacoustic pulse with bipolar form, axial symmetry and highly directive. The feasibility of the acoustic detection technique and the possibility of implementing it in these telescopes have been under study for years. In order to test and calibrate this technique, it is necessary to have an acoustic emitter system able of generating a signal similar to the neutrino signature. This has been the second objective developed in this thesis.

To achieve this objective, a compact and versatile calibrator based on an array of acoustic transducers using parametric generation has been designed. Given the complexity of the pulse to emulate and the novelty of the technique to be used, it has been necessary to carry out different laboratory tests in order to obtain suitable transducers and electronics able of making them to work at the required power and efficiency. The positive results

obtained in this line suggest that we will be able to obtain a full functional neutrino acoustic calibrator soon.

Finally, I would like to mention that I have participated in the different research and activities described in the thesis, putting especial emphasis in the development of the electronics and the software/firmware of the developed acoustic emitters.

Índice

Diseño y desarrollo de la electrónica de los emisores acústicos para los sistemas de posicionamiento y calibración de telescopios submarinos de neutrinos.

Capítulo 1
Introducción general

1.1 Antecedentes y objetivos de la investigación.

La astronomía de neutrinos ofrece una nueva forma de mirar al Universo, complementaria a otras técnicas y con notables ventajas en algunos aspectos respecto a los mensajeros más tradicionales utilizados (véase Figura 1). Los fotones, en particular a altas energías, interaccionan con la radiación y la materia en su camino desde las fuentes astrofísicas que los producen. Los rayos cósmicos también son absorbidos y además, al ser partículas cargadas, son desviados por campos magnéticos galácticos y extra-galácticos, de manera que se pierde la información sobre qué fuentes los han producido. Los neutrinos, en cambio, viajan prácticamente inalterados desde su origen hasta nosotros ya que son neutros e interaccionan débilmente, por lo que son herramientas únicas para estudiar el Universo. Uno de los objetivos fundamentales de la astronomía de neutrinos es justamente identificar las fuentes que producen los rayos cósmicos de alta energía que llevamos décadas observando sin haber dilucidado aún su origen. Sean cuales sean las fuentes que los originan, esperamos que también produzcan neutrinos de alta energía. Además, la detección o no de neutrinos también permitirá entender si los rayos gamma que se observan en diversas fuentes astrofísicas son producidos por los llamados mecanismos leptónicos (sin neutrinos) o hadrónicos (con producción de neutrinos). Otro objetivo prioritario de los telescopios de neutrinos es la detección de materia oscura, que forma el 85% de la materia del Universo y de la que una de las pocas cosas que sabemos después de décadas de búsqueda es que no está hecha de partículas del Modelo Estándar. Los telescopios de neutrinos constituyen una alternativa complementaria a otros tipos de búsqueda de materia oscura, tanto directas

como indirectas, algo clave cuando se desconoce la naturaleza de las posibles partículas que pudieran componerla [ADR16, ARD17]. Por último, recientes estudios apuntan a que estos detectores pueden medir la jerarquía de masas de los neutrinos, una de las cuestiones que todavía quedan por resolver sobre estas partículas [ADR16b].

El principio de operación de los detectores consiste en la detección de la luz Cherenkov inducida por las partículas producidas en la interacción de neutrinos de alta energía en los alrededores del detector (véase Figura 2). Para poder detectar los flujos de neutrinos con suficiente sensibilidad es necesario disponer de detectores de grandes dimensiones, alrededor del kilómetro cúbico. ANTARES es un telescopio de neutrinos situado a unos 2500 metros de profundidad en el mar Mediterráneo, cerca de la costa francesa [AGE11]. Consta de 900 fotomultiplicadores (PMTs) de gran fotocátodo que detectan la luz Cherenkov inducida tras la interacción de neutrinos de alta energía en las proximidades del detector. Lleva tomando datos desde 2008 en su configuración completa. ANTARES fue el primer telescopio de neutrinos submarino y, aunque de menor dimensión que IceCube, ha servido para comprobar y demostrar su viabilidad y realizar los primeros análisis físicos, constituyendo la base para la nueva generación de telescopios de neutrinos submarinos KM3NeT. El detector KM3NeT tendrá dos configuraciones, llamadas en su fase intermedia ARCA y ORCA, lo que refleja la doble naturaleza de sus objetivos científicos: la física de astropartículas y la física de partículas elementales [ADR16]. La configuración de ARCA, de mayor volumen (un kilómetro cúbico) estará centrada en la búsqueda de fuentes astrofísicas de neutrinos. La configuración ORCA (1.8 Mton), más densa, tiene como objetivos fundamentales medir la jerarquía de masas de los neutrinos y dilucidar la naturaleza de la materia oscura. Durante la Fase 1 (2015-2018) se instalarán 7 líneas en el site francés y 24 en el italiano. Durante la Fase 2 se instalarán 115 líneas en Francia (ORCA) y 230 líneas en Italia (ARCA). Finalmente, en la Fase 3 se tendrá un total de 690 líneas entre ambos emplazamientos.

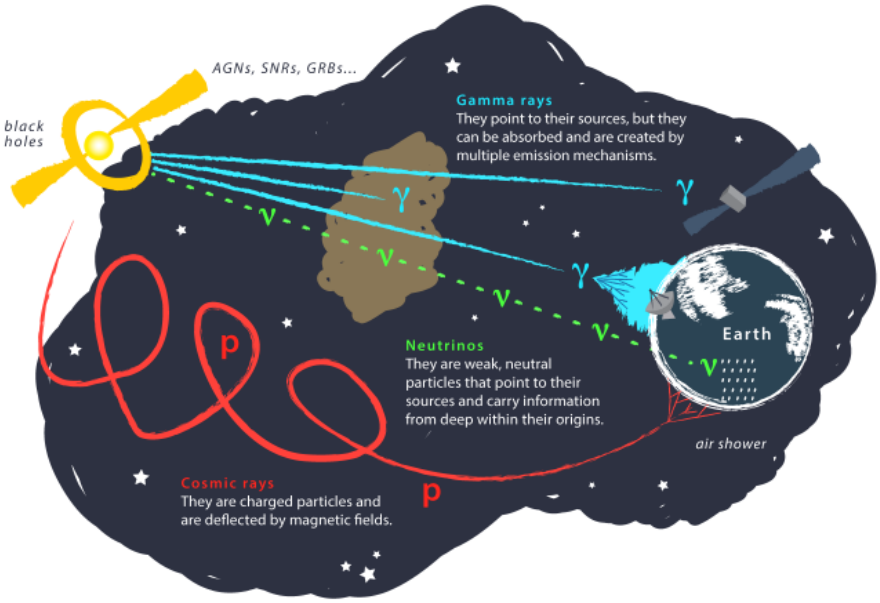

(credit: Juan Antonio Aguilar and Jamie Yang. IceCube/WIPAC)

Figura 1. Visión esquemática del estudio del Universo mediante diferentes mensajeros.

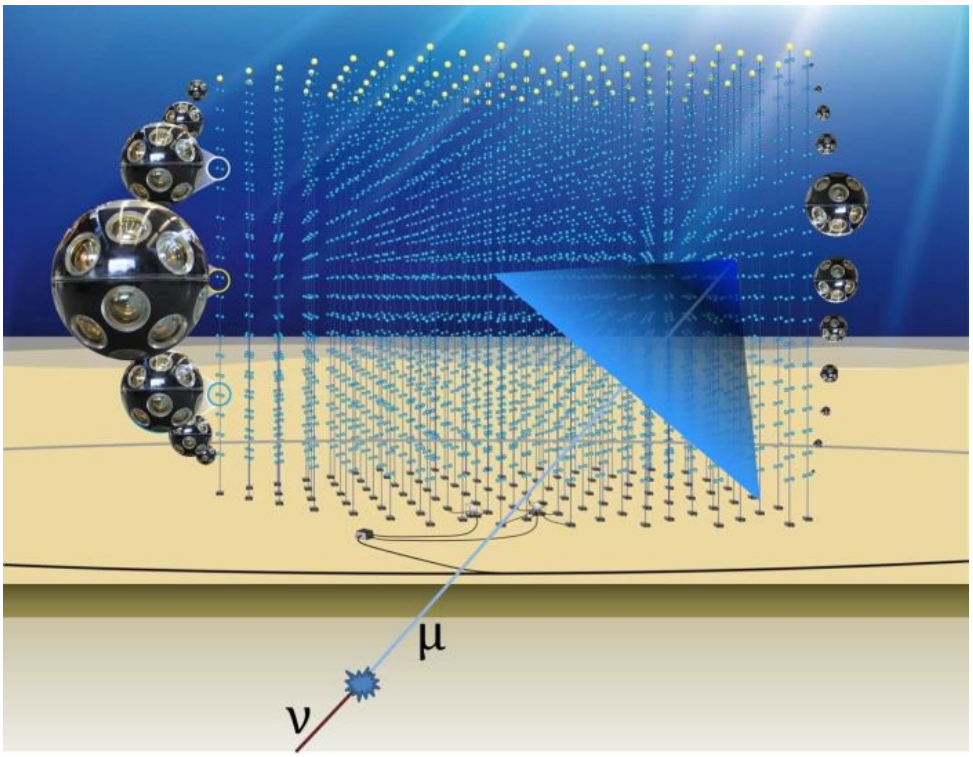

(credit: KM3NeT Collaboration)

Figura 2. Visión esquemática del telescopio de neutrinos KM3NeT y del principio de detección

Hay que destacar que la astronomía de neutrinos está en un momento crucial. ANTARES ha demostrado la viabilidad de esta técnica en detectores submarinos y, por otro lado, IceCube ha podido mostrar la existencia de un flujo de neutrinos cósmicos [AAR13]. Los datos tomados hasta ahora por ANTARES han permitido obtener una variada cosecha de resultados físicos [COY17], en algunos casos superando los resultados de IceCube, a pesar de tener este último un tamaño mucho mayor. La señal detectada por IceCube y la viabilidad de los telescopios de neutrinos submarinos demostrada por ANTARES son el mejor impulso para dar el siguiente paso, la construcción de KM3NeT, un detector aún mayor que IceCube y con las ventajas de operar en el agua y en el Hemisferio Norte. Además, se ha abierto también la posibilidad de medir la jerarquía de masas de los neutrinos con una parte de KM3NeT en configuración densa (ORCA).

La tesis que aquí se describe se enmarca en la participación desde el 2006 del grupo de investigación de la UPV “Acústica para la Detección de Astropartículas” en ambas colaboraciones internacionales, ANTARES y KM3NeT, financiadas con diferentes proyectos de ámbito europeo, estatal y regional. En algunas ocasiones el trabajo se ha

realizado conjuntamente con otros grupos nacionales y extranjeros de la Colaboración KM3NeT, y/o en colaboraciones con empresas valencianas, como se detallará posteriormente.

Uno de los aspectos clave para la correcta reconstrucción de eventos en un telescopio submarino de neutrinos es conocer la posición de los módulos ópticos con una precisión de unos 10 cm [VIO16]. Dado que el telescopio está formado por estructuras no rígidas consistentes en líneas de detectores ancladas al suelo y mantenidas en posición vertical por boyas, estas pueden sufrir desplazamientos de hasta decenas de metros debido a las corrientes marinas. Se hace, por tanto, necesario disponer de un sistema de calibración que permita monitorizar, cada minuto aproximadamente, la posición de los módulos ópticos con la precisión requerida. Para conseguirlo, se lleva a cabo una reconstrucción de la forma de la línea de detección y de la posición de los sensores ópticos a partir de la información del sistema de posicionamiento acústico, que proporciona la posición de diferentes puntos de la línea, y del sistema de brújulas/inclinómetros, que proporciona la orientación de los pisos [ADR12]. El sistema acústico, que constituye todo un reto en sí mismo por su complejidad, consiste en un sistema Long Baseline de emisores acústicos anclados en puntos fijos y que definen el sistema de referencia del telescopio, y de sensores acústicos (hidrófonos receptores) en las líneas. La posición de estos últimos se calcula por triangulación de distancias con los diferentes emisores a partir de la determinación del tiempo de vuelo de la onda acústica y la medida de la velocidad del sonido.

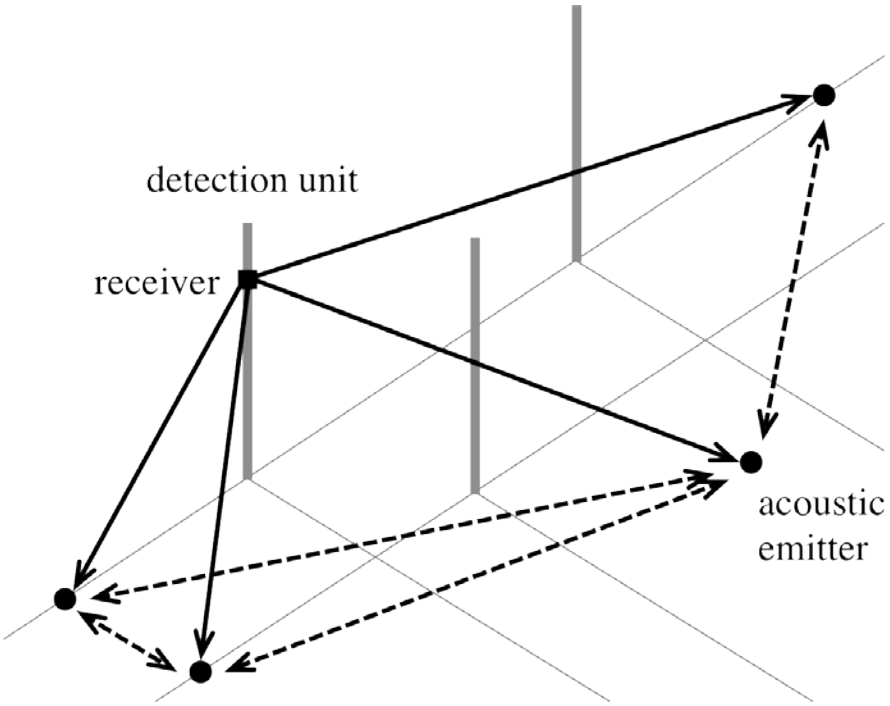

(Figura extraída de [ENZ13])

Figura 3. Visión esquemática del sistema de posicionamiento en telescopios submarinos de neutrinos.

El sistema de posicionamiento de ANTARES ha funcionado muy bien [ARD09, ADR12]. Sin embargo, se requiere de un nuevo sistema para las dimensiones de KM3NeT. En este aspecto el grupo de la UPV ha tenido una labor muy destacada en el diseño y desarrollo del mismo con nuevas propuestas como: el uso de nuevos emisores acústicos más económicos y mejor adaptados a la infraestructura del telescopio, el uso de *all-data-to-shore*, el uso de banda ancha de frecuencias y técnicas de procesado de señal, y el uso de sensores piezoeléctricos dentro de los módulos ópticos en combinación con hidrófonos. De especial relevancia ha sido el desarrollo de la tecnología para los emisores acústicos, incorporando las mejoras mencionadas, el cual ha sido llevado a cabo en las instalaciones del campus de Gandia de la UPV y ha demostrado su viabilidad con prototipos instalados in situ en la línea de instrumentación de ANTARES y en la torre de KM3NeT/NEMO-Phase II en el *site* de Sicilia. Cabe también mencionar aquí la firma del Contrato de Colaboración de investigación con la empresa Mediterráneo Señales Marítimas SL que, basándose en la tecnología diseñada por el grupo de la UPV, ha conseguido ganar el concurso para la producción de los 18 primeros emisores acústicos para KM3NeT. El trabajo desarrollado en esta tesis ha sido fundamental para lograr estos resultados.

Por otra parte, la detección acústica de neutrinos es una de las posibilidades más prometedoras para extender los telescopios de neutrinos al rango ultra-energético, ya que éstos al interaccionar en el agua producen un pulso termo-acústico que pensamos podría ser detectado mediante una red de hidrófonos [ASK57, ASK79]. Así, la detección acústica de neutrinos complementaría eficazmente la detección óptica. La ventaja de las señales acústicas, frente a las señales ópticas y electromagnéticas, es la débil atenuación que sufre a baja frecuencia en el agua lo que permitiría monitorizar un volumen extremadamente grande de agua (millares de kilómetros cúbicos) con un número razonable de sensores y de hecho es la única posibilidad para tener un telescopio submarino híbrido (óptico-acústico) en el mar que cubra el rango del GeV hasta 10^{12} GeV. El rango ultra-energético ha despertado mucho interés en los últimos años con la posibilidad de la detección de neutrinos GZK o provenientes de modelos top-down. Esta técnica se basa en la detección acústica del pulso de presión generado por el calentamiento del agua debido a la cascada hadrónica que se produce tras la interacción del neutrino. Las particularidades del pulso radiado (pulso bipolar altamente directivo con simetría axial) permitirían, por un lado, distinguirlo de otro tipo de señales mucho más abundantes, y por otro lado determinar la dirección de procedencia con unos pocos grados de resolución. Si bien es verdad que la viabilidad de la detección acústica de neutrinos aún no ha sido totalmente demostrada, los primeros estudios realizados con proyectos pilotos como SAUND [VAN05], ACORNE [THO08], NEMO-ONDE [RIC09] y sobre todo ANTARES-AMADEUS [AGU11], en el cual estamos implicados, apuntan a que sí sería posible. Además, el hecho de que KM3NeT incluya un elevado número de sensores acústicos para posicionamiento de los sensores ópticos con la filosofía de *all-data-to-shore* implica que automáticamente se constituirá en un detector que superará en varios órdenes de magnitud la sensitividad de sus predecesores. El calibrador acústico compacto basado en técnicas paramétricas no lineales [WES63], cuya electrónica desarrollaremos en esta tesis, será una herramienta fundamental para demostrar la viabilidad de esta técnica.

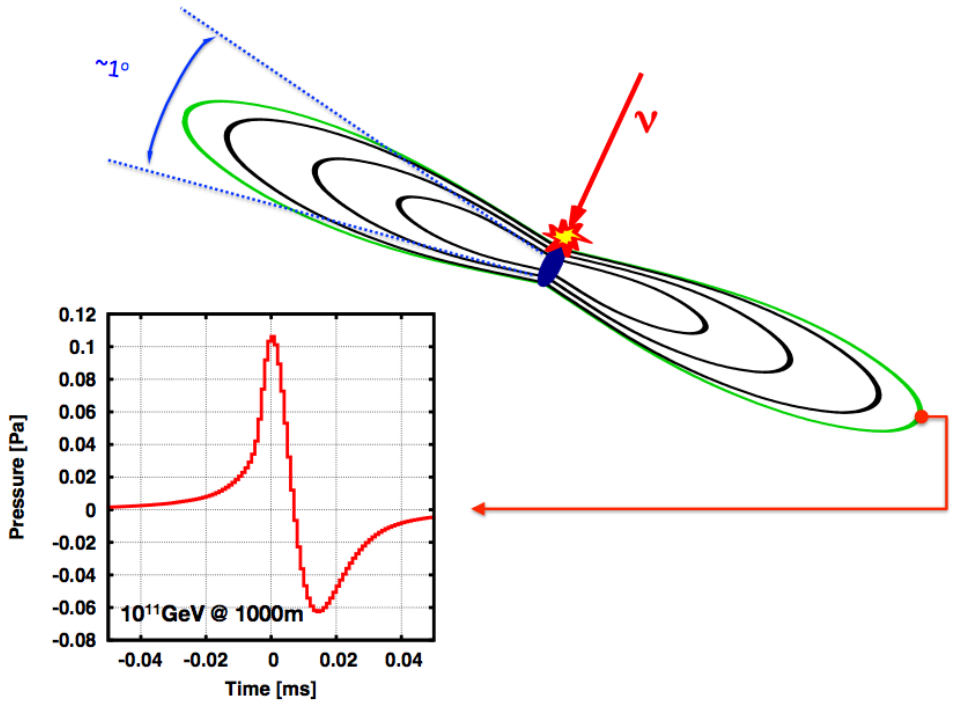

(Figura extraída de [RIC09b]).

Figura 4. Visión esquemática de la Interacción de un neutrino ultraenergético y de la generación y propagación del pulso termoacústico asociado.

Tras esta introducción a la situación actual y la identificación de algunas problemáticas y ámbitos de actuación a los que esta tesis pretende dar respuesta, los objetivos de investigación en el ámbito de la electrónica y del procesado de señal de los emisores acústicos de los telescopios de neutrinos que nos hemos planteado son los siguientes:

1. Selección del método de amplificación más apropiado para los sistemas emisores acústicos: dado los requisitos de rendimiento y potencia del sistema deberemos seleccionar el sistema de amplificación adecuado para estas aplicaciones con los transductores piezoeléctricos elegidos. Teniendo en cuenta que los requisitos de potencia son muy exigentes y las restricciones en estas infraestructuras son notables, este aspecto es un reto en sí mismo para ambas aplicaciones, especialmente si se considera que la esperanza de vida para un emisor del sistema de posicionamiento acústico debe ser mayor de 20 años.

2. Selección y cálculo de la red de adaptación apropiada: como los transductores piezoeléctricos suelen tener una impedancia con una parte real bastante elevada y una imaginaria aún más elevada y de tipo capacitivo, es necesaria una buena adaptación para

poder transferir suficiente energía al transductor y así poder cumplir con los requisitos de potencia y alcance necesarios para el sistema.

3. Sistema de generación de señal: para generar la señal precisaremos diseñar un sistema digital que pueda generar señales arbitrarias y excitar con ellas el amplificador de potencia. Para un amplificador basado en la polarización clase “D”, dichas señales de excitación son digitales por lo que no será necesario ningún tipo de conversión, pero en ese caso nuestro sistema debe ser capaz de generar las señales con modulación PWM para las altas frecuencias con las que trabajaremos.

4. Alimentación del sistema: uno de los requisitos imprescindibles es que la alimentación del sistema se ciña a las características del telescopio, las cuales son muy restrictivas. Por tanto, necesitaremos una forma de almacenar la energía (batería, condensador…) que sea capaz de entregarla rápidamente cuando se necesite.

5. Diseño de los sistemas de comunicación y control de los emisores acústicos: Se diseñará un sistema que permita la correcta comunicación con el resto de dispositivos de los telescopios de neutrinos y de manera que puedan controlarse todas sus funcionalidades.

6. Prueba del sistema en laboratorio y condiciones reales: será necesario probar los diferentes prototipos en primer lugar en las condiciones controladas del laboratorio para comprobar si se cumplen los requisitos y si el sistema es viable para el posicionamiento acústico del telescopio y para la calibración del sistema de detección acústico. Posteriormente se probará el sistema in situ, en un entorno más real, para comprobar si funcionan apropiadamente.

7. Análisis de las señales emitidas y recibidas y validación de los prototipos: para poder probar si podemos conseguir la precisión requerida analizaremos las señales emitidas y recibidas y emplearemos técnicas de procesado de señal para conseguir obtener el tiempo de vuelo de nuestras señales con suficiente precisión y ver si se han conseguido los diferentes objetivos de los sistemas de calibración.

1.2 Estructura de la Tesis.

En primer lugar, dado que se trata de una Tesis por compilación de artículos científicos y cada uno de ellos puede ser leído autónomamente, es importante recalcar que todos ellos constituyen un solo trabajo con un claro hilo argumental, tal y como hemos argumentado en el apartado anterior.

Así pues, la tesis se estructura en 4 capítulos:

1. Introducción general.
2. Publicaciones.
   - 2.1. Acoustic Transmitters for Underwater Neutrino Telescopes.
   - 2.2. The Sound Emission Board of the KM3NeT Acoustic Positioning System.
   - 2.3. Development of an acoustic transceiver for the KM3NeT positioning system.
   - 2.4. Acoustic signal detection through the cross-correlation method in experiments with different signal to noise ratio and reverberation conditions.
   - 2.5. Acoustic beacon for the positioning system of the underwater neutrino telescope KM3NeT.
   - 2.6. A compact array calibrator to study the feasibility of acoustic neutrino detection.
   - 2.7. Transducer development and characterization for underwater acoustic neutrino detection calibration.
3. Discusión de los resultados.
4. Conclusiones.

El cuerpo principal de la tesis lo constituye el **Capítulo 2**, el cual recoge siete artículos más significativos publicados en revistas científicas de prestigio.

El **primer artículo** se titula “Acoustic Transmitters for Underwater Neutrino Telescopes”. Este artículo se ha publicado en la revista de acceso abierto “Sensors” en marzo de 2012. De acuerdo con la edición de ese año del *Journal Citation Reports* esta revista figura con un índice de impacto de 1,953 y se encuentra en el primer cuartil del área “Instruments & Instrumentation” (concretamente en la posición 8 de 57). Esta revista es líder internacional en ciencia y tecnología de sensores y biosensores y todos sus artículos son revisados por pares.

En este primer artículo se muestra el estado de la investigación en 2012 tanto de la electrónica del primer prototipo como del estudio de los transductores propuestos para los sistemas de posicionamiento y calibrado. También se estudia el proceso de integración del primer prototipo de la *Sound Emission Board* y el transductor SX30 en la línea de instrumentación del telescopio de neutrinos ANTARES, trabajo que fue realizado en colaboración con el Instituto de Física Corpuscular (IFIC) ya que el emisor se instaló dentro de la misma vasija donde el IFIC tenía instalado su prototipo de

calibrador láser. Por este motivo nuestro emisor tuvo que ser adaptado al sistema de comunicaciones del telescopio (MODBUS sobre RS485). Además de esta adaptación, cabe destacar que nuestro emisor también se encargó de la tarea de control de las funciones de dicho calibrador láser.

Un motivo por el cual he elegido este artículo como primer artículo de la tesis es, no solo por el interés en sí mismo del emisor sino porque en él se puede ver el estudio detallado llevado a cabo y el proceso de selección de los transductores propuestos tanto para el sistema de posicionamiento como para el calibrador del sistema de detección acústica de neutrinos. Esto es de vital importancia puesto que la selección de estos transductores condiciona el diseño de la electrónica a utilizar.

El **segundo artículo** se titula "The Sound Emission Board of the KM3NeT Acoustic Positioning System". Este artículo fue presentado en el congreso TWEPP de 2011 en Viena siendo seleccionado para su publicación en la revista "Journal of Instrumentation" en enero de 2012. De acuerdo con la edición de ese año del *Journal Citation Reports* esta revista tiene un índice de impacto de 1,656 y se encuentra en el segundo cuartil del área "Instruments & Instrumentation" (concretamente en la posición 15 de 57).

En este segundo artículo se describe detalladamente el desarrollo del primer prototipo de la *Sound Emission Board* que se instaló para realizar las pruebas de campo para el sistema de posicionamiento acústico en los telescopios ANTARES y NEMO. También se explica cómo se ha desarrollado la parte de potencia para poder excitar el transductor propuesto en el primer artículo con el mejor rendimiento posible y se proponen posibles modificaciones para lograr cumplir todos los requerimientos necesarios para el telescopio KM3NeT.

El **tercer artículo** se titula "Development of an acoustic transceiver for the KM3NeT positioning system". Este artículo se presentó en el congreso VLVnT de 2011 en Erlangen y los proceedings fueron publicados en la revista "Nuclear Instruments and Methods in Physics Research Section A: Accelerators, Spectrometers, Detectors and Associated Equipment" de la editorial Elsevier en octubre de 2013. Esta revista, de acuerdo con la edición del 2013 del *Journal Citation Reports*, tiene un índice de impacto de 1,316 y se encuentra en el segundo cuartil del área "Nuclear Science & Technology", concretamente en la posición 9 de 33.

En este tercer artículo se detallan los diferentes tests que se realizaron con el primer prototipo de la *Sound Emmision Board* y los transductores SX30. En concreto se llevaron a cabo pruebas en tres entornos con características diferentes, uno muy reverberante en el tanque de agua del laboratorio de Física Aplicada de la Escuela de Gandía, otro más benigno en la piscina montada en el puerto de Gandía y por último otro en un entorno de alto nivel de ruido en el mismo puerto de Gandia. Del resultado de dichas pruebas se

extraen varias conclusiones: que el sistema emisor formado por la *Sound Emission Board* y el transductor SX30 con un nivel de presión sonora de 170 dB re 1µPa@1m cumple con los requisitos necesarios para formar parte del sistema de posicionamiento de un telescopio de neutrinos submarino, y que se puede mejorar en gran medida la precisión del sistema de posicionamiento empleando señales de banda ancha y correlación.

El **cuarto artículo** se titula "Acoustic signal detection through the cross-correlation method in experiments with different signal to noise ratio and reverberation conditions". Este artículo se presentó en el congreso MARSS de 2014 en Benidorm siendo seleccionado para su publicación en la revista "Lecture Notes in Computer Science" en febrero de 2015. Según la última edición publicada del Scimago Journal Ranking (2015) esta revista tiene un índice SJR de 0,252 y se encuentra en el segundo cuartil del área "Computer Science (miscellaneous)", concretamente en la posición 155 de 444.

En este artículo se aborda la detección de la señal acústica recibida en el entorno de los telescopios de neutrinos como continuación a los artículos anteriores. En ellos se ha visto que la mejor solución para mejorar la precisión en el sistema de posicionamiento es la emisión de señales de banda ancha (sweep, MLS …) y usar la correlación de la señal recibida con dichas señales para estimar el tiempo de vuelo de la señal con la mayor precisión posible. Por tanto, en este artículo se ponen a prueba diversas señales de emisión (seno, MLS y sweep) en múltiples entornos (alta reverberación, baja relación señal/ruido y muy baja relación señal/ruido) y se compara el cálculo del tiempo de vuelo de la señal mediante la detección de umbral con la detección por correlación. Además, también se ha simulado una emisión en el entorno del telescopio ANTARES. Para ello se ha simulado la propagación de la señal recibida en el laboratorio teniendo en cuenta la dispersión por onda esférica, la absorción del medio y la figura de ruido detectada in situ por los hidrófonos existentes en ANTARES.

El **quinto artículo** se titula"Acoustic beacon for the positioning system of the underwater neutrino telescope KM3NeT". Este artículo fue presentado en el congreso Tecniacústica que se celebró en Valencia en 2015 y publicado en los correspondientes *proceedings*, en las paginas 1322-1329.

En este artículo se describe el desarrollo final llevado a cabo para ser integrado en la primera fase del telescopio KM3NeT. Conjuntamente con la empresa Mediterráneo Señales Marítimas SLL se elaboraron 18 unidades para KM3NeT-ARCA . Para esta versión operativa del *Acoustic Beacon* se rediseñó la *Sound Emision Board* dividiéndola en tres placas independientes y mejorando la parte de potencia, alimentación y comunicaciones para ajustarse a los nuevos y más exigentes requisitos de KM3NeT. La principal mejora introducida es el aumento de la tensión de alimentación del amplificador clase D hasta los 60V mediante un *boost converter* que almacena la energía en un condensador electrolítico de mayor voltaje y capacidad. Para poder soportar este aumento de tensión los MOSFETs de la placa de potencia se han sustituido por unos

IRF540. También se ha mejorado el aislamiento tanto de las comunicaciones con el telescopio como de la placa de control con las placas de potencia y de alimentación para reducir al máximo cualquier posible interferencia electromagnética tanto con el telescopio como entre las diversas placas de la *Sound Emision Board*. Por último, en este artículo se describe también la vasija de aluminio anodizado y el soporte del transductor desarrollados por la empresa anteriormente mencionada.

El **sexto artículo** se titula "A compact array calibrator to study the feasibility of acoustic neutrino detection". Este artículo fue presentado en el congreso VLVnT de Roma en 2015 y publicado en la revista "EPJ Web of Conferences". De acuerdo con la última edición del "Scimago Journal Ranking" (2015) esta revista tiene un índice SJR de 0,142 y se encuentra en el cuarto cuartil del área "Physics and Astronomy (miscellaneous)", concretamente en la posición 221 de 247.

En este artículo se proponen unos nuevos transductores para el desarrollo del calibrador compacto de neutrinos. Aunque los transductores FFR-SX83 descritos en el primer artículo dieron buenos resultados generando el pulso bipolar requerido para el calibrador compacto de neutrinos, decidimos explorar nuevos transductores con la intención de mejorar la sensibilidad y la curva de impedancia que resultaba demasiado baja para el sistema amplificador clase D del primer prototipo. En el artículo se pueden ver los resultados tanto para la caracterización de dos transductores piezo-ceramicos de la empresa UCE ultrasonic Co. LTD que tienen la simetría apropiada para conseguir la directividad deseada, como para las pruebas realizadas para validar la emisión de un pulso bipolar usando la técnica paramétrica.

El **séptimo artículo** se titula "Transducer development and characterization for underwater acoustic neutrino detection calibration". Este artículo fue presentado en el "2nd Electronic Conference on Sensors and Applications" de 2015, siendo seleccionado para su publicación en la revista "Sensors". Según la última edición publicada del "Journal Citation Reports" (2015) esta revista tiene un índice de impacto de 2,033 y se encuentra en el primer cuartil del área "Instruments & Instrumentation", concretamente en la posición 12 de 56.

En este artículo se describe el diseño del transductor acústico con fines de calibración para la detección acústica de neutrinos. Cuando un neutrino ultra-energético interacciona con un núcleo del agua se produce un pulso de presión bipolar corto con directividad "pancake" que se propaga por el mar. Hoy en día, las redes de sensores acústicos se están desplegando en aguas profundas para detectar este fenómeno como un primer paso hacia la construcción de un telescopio de neutrinos acústico. Para estudiar la factibilidad del método, es crítico tener un calibrador que sea capaz de imitar la firma del neutrino. En trabajos anteriores se probó la posibilidad de utilizar la técnica paramétrica acústica para este fin. Con esta técnica, el array es operado a alta frecuencia y, por medio del efecto

paramétrico, se genera la emisión del impulso bipolar acústico de baja frecuencia imitando el impulso acústico producido por el neutrino ultra-energético. En este trabajo se describen todas las fases del desarrollo del transductor a utilizar en el array paramétrico. Se presentan el proceso de diseño del transductor, las pruebas de caracterización de la cerámica piezoeléctrica desnuda y la adición de capas de backing y de adaptación. Las eficiencias y los patrones de directividad obtenidos para los haces primarios y paramétricos confirman que el diseño del calibrador propuesto cumple todos los requisitos para el emisor y que se puede realizar un calibrador compacto versátil.

Capítulo 2
Publicaciones

2.1 Acoustic Transmitters for Underwater Neutrino Telescopes.

Miguel Ardid *, Juan A. Martínez-Mora, Manuel Bou-Cabo, Giuseppina Larosa, Silvia Adrián-Martínez and Carlos D. Llorens

Politècnica de València, Paranimf 1, E–46730 Gandia, València, Spain; E-Mails: jmmora@upv.es (J.A.M.-M.); maboca3@doctor.upv.es (M.B.-C.); giula@upv.es (G.L.); siladmar@upv.es (S.A.-M.); cdavid@upv.es (C.D.L.)

2.1.1 Abstract.

In this paper acoustic transmitters that were developed for use in underwater neutrino telescopes are presented. Firstly, an acoustic transceiver has been developed as part of the acoustic positioning system of neutrino telescopes. These infrastructures are not completely rigid and require a positioning system in order to monitor the position of the optical sensors which move due to sea currents. To guarantee a reliable and versatile system, the transceiver has the requirements of reduced cost, low power consumption, high pressure withstanding (up to 500 bars), high intensity for emission, low intrinsic noise, arbitrary signals for emission and the capacity of acquiring and processing received signals. Secondly, a compact acoustic transmitter array has been developed for the calibration of acoustic neutrino detection systems. The array is able to mimic the signature of ultra-high-energy neutrino interaction in emission directivity and signal shape. The technique of parametric acoustic sources has been used to achieve the proposed aim. The developed compact array has practical features such as easy manageability and operation. The prototype designs and the results of different tests are described. The techniques applied for these two acoustic systems are so powerful and versatile that may be of interest in other marine applications using acoustic transmitters.

Keywords: acoustic transceiver; sensor array; underwater neutrino telescopes; calibration; positioning systems; parametric sources

2.1.2 Introduction.

In this paper, different R&D studies and prototypes on acoustic transmitters are presented, that were conducted in the context of deep-sea neutrino telescopes. Acoustics are used in this type of facilities mainly in two areas: the acoustic positioning system used to monitor the positions of the optical sensors placed throughout the detector [1], and systems for acoustic neutrino detection technique [2], which is currently under study. Our research group has some responsibilities in these areas in two European partnerships for the design, construction and operation of undersea neutrino telescopes: ANTARES [3] (which is now operational and collecting data), and KM3NeT [4] (which is in the preparatory phase, that is definition and validation of the final design of the facility, and dealing with the legal and financial aspects for the construction). Conceptually both the ANTARES and KM3NeT projects are quite similar. The physics goals of deep-sea neutrino telescopes center on the fields of astronomy, dark matter, cosmic rays and high energy particle physics. Besides, these facilities also hold different equipment for long-

term continuous monitoring of environmental parameters interesting in several fields of Earth-Sea science such as biology, oceanography, geology, *etc*.

A deep-sea neutrino telescope is composed of several semi-rigid structures named Detection Units (DUs) that are anchored to the sea bed at great depths (events induced by neutrinos from astrophysical sources must be distinguished from other kinds of events which originate in the Earth's atmosphere). The mechanical structures of the DU contain several Optical Modules (OMs) with photomultiplier sensors detecting the Cherenkov light emitted by muons that are generated in neutrino interactions with matter near or in the detector. Since the DU structure is hundreds of meters high and is held vertically by a buoy located at the top of the structure, underwater sea currents produce inclination of the structures and thus the OMs can be displaced several meters from their nominal positions. For this reason, a positioning system is needed in order to monitor the positions of OMs. In particular, ANTARES is deployed at about 2,500 m depth, about 40 km off the coast of Toulon (France), and has 12 DU (Lines) with a separation between neighbouring lines of about 70 m. Each DU has 25 floors (storeys) with three OMs per storey. The vertical distance between adjacent storeys is 14.5 m. This layout—a 3-dimensional array of OMs over a volume of about 0.05 km^3—allows for a precise reconstruction of the muon tracks and thus of the primary neutrinos. KM3NeT will have a volume of several cubic kilometres becoming the next generation of deep-sea neutrino telescopes.

The performance of the telescope (particularly, an accurate reconstruction of the muon track) is highly sensitive to the knowledge of the OM relative positions. Hence it is necessary to monitor the relative positions of all OMs with accuracy better than 20 cm, equivalent to the ~1 ns precision of timing measurements [5]. The muon trajectory reconstruction and determination of its energy also require the knowledge of the OMs orientation with a precision of a few degrees. In addition, a precise absolute positioning of the whole detector has to be guaranteed in order to point to individual neutrino sources in the sky. For all these purposes, a positioning calibration system is needed. This system includes an Acoustic Positioning System (APS) composed of synchronized acoustic transceivers, anchored on fixed known positions at the sea bottom, and receiver hydrophones attached to the DUs structure, close to the position of the OMs. By measuring the time of flight between transceivers and hydrophones, and knowing the sound speed, it is possible to determine the distances between them. The position of the hydrophones is determined by a triangulation method using different transceivers. Using a mechanical model that explains the mechanical behaviour of the DUs and using the position information of the hydrophones (individual points on the DUs), it is possible to reconstruct the position of the OMs with the required accuracy [1]. The first part of this paper (Section 2) summarises the work, studies results and conclusions achieved in last years in the development process of an acoustic transceiver for the APS in the framework of the KM3NeT neutrino telescope. The implementation of the proposed transceiver into the detector is currently evaluated.

The other application of acoustic transmitters presented in this paper is related to the acoustic detection of neutrinos. The possibility of detecting ionizing particles by acoustic techniques was first pointed out by Askarian in 1957. The thermo-acoustic model predicts that an acoustic signal can be produced from the interaction of an Ultra-High-Energy (UHE) neutrino in water. This interaction produces a particle cascade that deposits a high amount of energy in a relatively small volume of the medium, which instantaneously forms a heated volume that gives rise to a measurable pressure signal [2]. Different simulations have been made on the acoustic signal generation and propagation. Details can be found in [6] and references therein. For this work, some reference figures for calibration purposes suffice. On average, 25% of the neutrino energy is deposed by a hadronic shower in a small, almost cylindrical, volume of a few cm in radius and several meters in length. The generated pressure signal has a bipolar shape in time and 'pancake' directivity, this means a flat disk emission pattern perpendicularly to the axis defined by the hadronic shower. As a reference example, we will consider that at 1 km distance, in direction perpendicular to a 10^{20} eV hadronic shower, the acoustic pulse has about 0.1 Pa peak-to-peak amplitude and about 40 μs width. With respect to the directivity pattern, the opening angle of the pancake is about 1°.

Both experiments, ANTARES and KM3NeT, consider acoustic detection as a possible and promising technique to cover the detection of UHE neutrinos with energies above 10^{18} eV. Also the combination of these two neutrino detection techniques to achieve a hybrid underwater neutrino telescope is possible, especially considering that the optical neutrino techniques need acoustic sensors for positioning purposes. Moreover, ANTARES has an acoustic detection system called AMADEUS that can be considered as a basic prototype to evaluate the feasibility of the neutrino acoustic detection technique. This system is a functional prototype array [7] composed of six acoustic storeys, three of them located on a special DU with instrumentation equipment (Instrumentation Line) and the other three on the 12th DU. Each storey contains six acoustic sensors. The system is operational and taking data. Despite all of the sensors having been calibrated in the laboratory, it would be desirable to have a compact calibrator that may allow for "*in situ*" monitoring of the detection system, to train the system and tune it, in order to improve its performance to test and validate the technique, as well as determining the reliability of the system [8]. The compact transmitter proposed may mimic the signature of a UHE neutrino interaction considering the high directivity of the bipolar acoustic pulse and, in addition, to have small geometrical dimensions that facilitates deployment and operation. In this paper, the studies and prototype developments towards such a transmitter based on the parametric acoustic sources techniques are presented in Section 3.

We believe that these transmitters (with slight modification) may also be used in other applications, such as marine positioning systems, alone or combined with other marine systems, or integrated in different Earth-Sea Observatories, where the localization of the sensors is an issue. Some of these techniques can be also applied for SONAR developments or acoustic communication, especially when very directive beams are

required and/or signal processing techniques are needed. In that case, the experience gained from this research can be of great benefit for other applications beyond underwater neutrino telescopes.

2.1.3 Transceiver Development for the KM3NeT APS.

The APS for the future KM3NeT neutrino telescope consists of a series of acoustic transceivers distributed on the sea bottom and receivers located on the DUs near the optical modules. Each of these acoustic transceivers is composed of a transducer and an electronic board to manage it. These two components and the performed tests on them are presented in the following sections.

2.1.3.1 The Acoustic Sensor.

The acoustic sensor has been selected to meet the specifications of the KM3NeT positioning which are: withstanding high pressure, a good receiving sensitivity and transmitting power capability, near omnidirectionality, low electronic noise level, a high reliability, and also affordable pricing for the units needed. Among the different options, we have selected a Free Flooded Ring (FFR) transducer SX30 model (FFR-SX30) manufactured by Sensor Technology Ltd. (Collingwood, Canada, http://www.sensortech.ca). FFR transducers have ring geometrical form maintaining the same hydrostatic pressure inside and outside, whilst reducing the change of the properties of the piezoelectric ceramic under high hydrostatic pressure. For these reasons they are a good solution to the deep submergence problem [9]. FFR-SX30s are efficient transducers that provide reasonable power levels over wide range of frequencies, and deep ocean capability. They work in the 20–40 kHz frequency range with an outer diameter of 4.4 cm, an inner diameter of 2 cm and a height of 2.5 cm. They can be operated in deep-sea scenarios with a transmitting and receiving voltage response at 30 kHz of 133 dB re 1 μPa/V at 1m and −193 dB re 1 V/μPa, respectively. The maximum input power is 300 W with 2% duty cycle. These transducers are simple radiators and have an omnidirectional directivity pattern in the plane perpendicular to the axis of the ring (XY-plane), whilst the aperture angle in the other planes depends on the length of the cylinder (XZ-plane), which is of 60° for the SX30 model. The cable on the free-flooded rings is a 20 AWG type, which is thermoplastic elastomer (TPE) insulated. The cable is affixed directly to the ceramic crystal. The whole assembly is then directly coated with epoxy resin. Both the epoxy resin and the cable are stable in salt water, oils, mild acids and bases. The cables are therefore not water blocked (fluid penetration into the cable may cause irreversible damage to the transducer). For this reason, and following KM3NeT technology standards, the FFR-SX30 hydrophones have been over-moulded with polyurethane material to block water and to facilitate its fixing and integration on mechanical structures. Figure 1 shows pictures of the FFR-SX30 transducer with and without over-moulding.

With the objective to study the possibility of using these transducers as emitters in the APS of the KM3NeT neutrino telescope several studies have been performed. In the

following, the results of tests carried out in our laboratory are presented, which characterize the transducers in terms of the transmitting and receiving voltage responses as a function of the frequency and as a function of the angle (directivity pattern). For the tests omnidirectional calibrated transducers, model ITC-1042 (transmitting voltage response 148 dB re 1 µPa/V @ 1m; http://www.itc-transducers.com) and RESON-TC4014 (receiving voltage response −186 dB ± 3dB re 1 V/µPa; http://www.reson.com), were used as a reference emitter and receiver, respectively. The measurements have been performed in a 87.5 × 113 × 56.5 cm^3 fresh-water tank using 10-cycle tone burst signals and a distance separation between transducers of about 10 cm. The emitter was fed with moderate voltage (less than 10 V) in order to avoid transient effects, and stable results were obtained with statistical uncertainties below 1 dB.

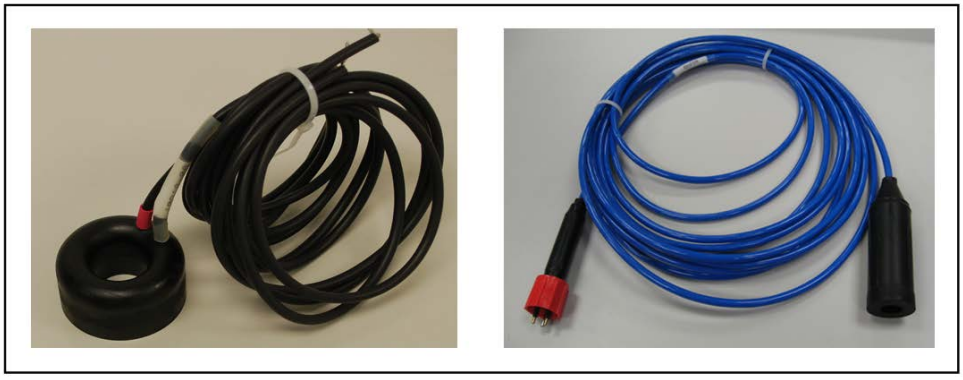

Figure 1 View of the Free Flooded Ring hydrophone: (left) without and (right) with over-moulding.

Figure 2 shows the transmitting voltage response and the receiving voltage response of the FFR-SX30 hydrophone as a function of the frequency (measured in the XY-plane, *i.e.*, perpendicular to the axis of the transducer). The results are consistent with the values given by the manufacturer and show that there are no strong irregularities in the 20–40 kHz frequency range.

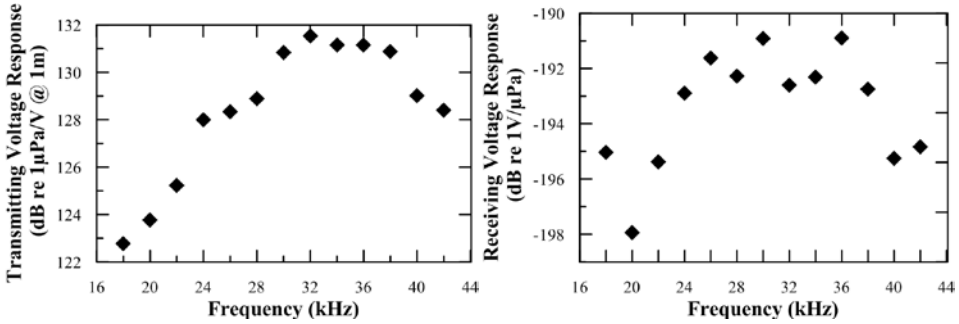

Figure 2. Transmitting and receiving voltage response of the FFR-SX30 hydrophones as a function of the frequency. The uncertainties on the measurements are 1.0 dB.

Figure 3 shows the transmitting voltage response and the receiving voltage response of the FFR-SX30 hydrophones as a function of the angle using a 30 kHz tone burst signal (measured in the XZ-plane where 0° corresponds to the direction opposite to cables). As expected, a minimum of sensitivity appears at an angle of ~30°. The variations of sensitivity are about 5 dB (almost 50%), which is a noticeable value, but can be handled without major problems for the KM3NeT APS application.

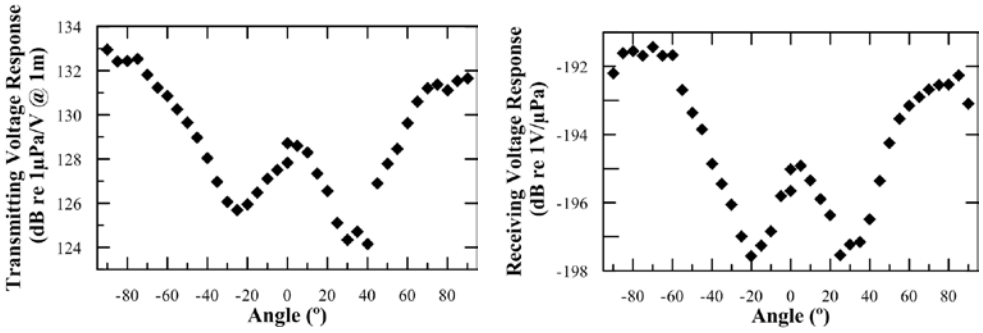

Figure 3. Transmitting and receiving voltage response of the FFR-SX30 hydrophones as a function of the angle in the XZ-plane. The uncertainties on the measurements are 1.0 dB.

One of the most important aspects that should be validated is the operability of the selected transducers under high pressure. For this reason a measurement campaign using the large hyperbaric tank at the IFREMER research facilities in Plouzanne (near Brest, France) was performed [10]. The behaviour of the FFR-SX30 transducers under different values of pressure weremeasured, in the frequency range of interest [24 kHz–40 kHz] and the relative acoustic power variations were observed. Figure 4 shows the results obtained from these measurements for the acoustic transmission between two FFR-SX30 transducers. From the measurements we can conclude that these transducers are quite stable with depth. The small variations that were observed are not problematic for the KM3NeT APS application.

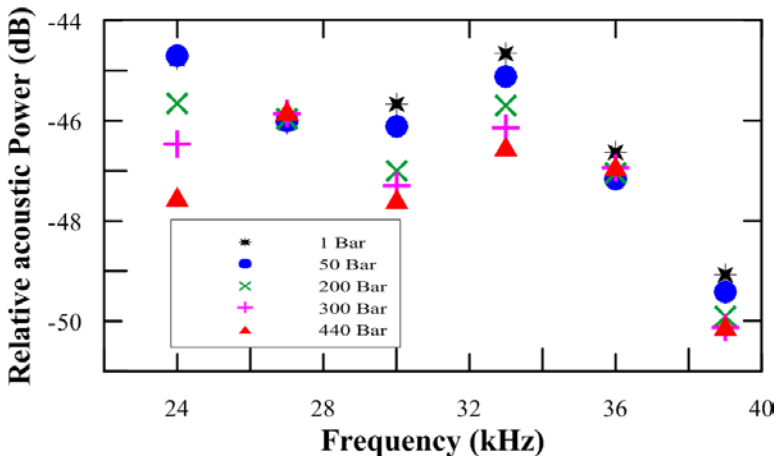

Figure 4. Pressure dependence of the FFR-SX30 hydrophones as a function of the frequency. The uncertainties of the measurement are 1.0 dB.

2.1.3.2 The Sound Emission Board.

Dedicated electronics, such as the Sound Emission Board (SEB) [11], have been developed for the communication with and the configuration of the transceiver, and furthermore, to control the emission and reception. Regarding the emission, it is able to generate signals for positioning with enough acoustic power that they can be detected by acoustic receivers at 1–1.5 km away from the emitter. Moreover, it stores electric energy for the emission, and can switch between emission and reception modes. The solution adopted is specially adapted to the FFR-SX30 transducers and is able to feed the transducer with a high amplitude of short signals (a few ms) with arbitrary waveforms. It has the capacity of acquiring the received signal as well. The board prototype diagram is shown in Figure 5. It consists of three parts: the communication and control which contains a micro-controller dsPIC (blue part), the emission part, constituted by the digital amplification plus the transducer impedance matching (red part), and the reception part (green part). In the reception part a relay controlled by the dsPIC switches the mode and feeds the signal from the transducer to the receiving board of the positioning system.

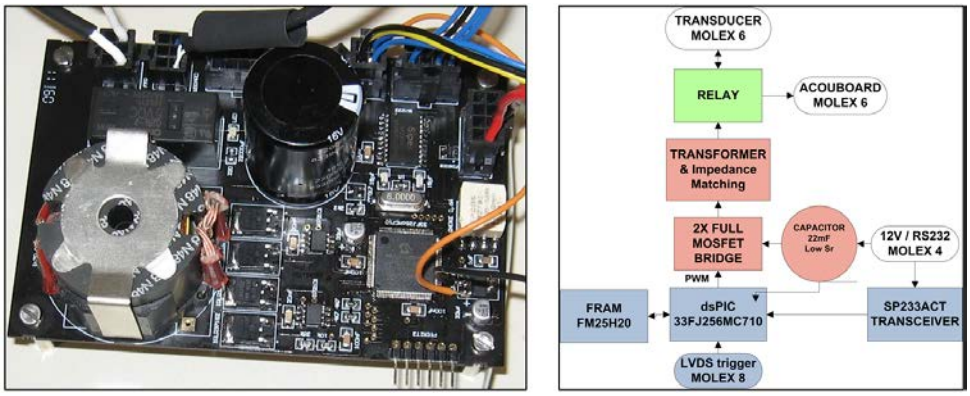

Figure 5. View and diagram of the Sound Emission Board.

The SEB has been designed for low-power consumption and it is adapted to the neutrino infrastructure using power supplies of 12 V and 5 V with a consumption of 1 mA and 100 mA, respectively, furnished by the power lines of the neutrino telescope infrastructure. With this, a capacitor with a very low equivalent series resistance and 22 mF of capacity is charged storing the energy for the emission. The charge of this capacitor is monitored using the input of the ADC of the micro-controller. Moreover, the output of the micro-controller is connected through a 2× Full MOSFET driver and a MOSFET full bridge; this is successively connected to the transformer with a frequency and duty cycle set through the micro-controller. The transformer is able to increase the voltage of the input signal to an up to 430 Vpp output signal.

The reception part of the board has the additional possibility to directly apply an anti-aliasing filter and return the signal to an ADC of the microcontroller. This functionality may be very interesting not only in the frame of the neutrino telescopes, but also for the implementation in different underwater applications, such as affordable sonar systems or echo-sounders.

The micro-controller runs the program for the emission of the signals and all the parts of the board control. The signal modulation is done using the Pulse-Width Modulation (PWM) technique [12] which permits the emission of arbitrary intense short signals. The PWM carry frequency of the emission signal is 400 kHz, frequencies up to 1.25 MHz have been successfully tested. The basic idea of this technique is to modulate the signal digitally at high frequency using different width of pulses, the lower frequency signal is recovered using a low-pass filter. A full H-Bridge is also used to increase the amplitude of the signal. The communication of the board with the control PC for its configuration is established through the standard RS232 protocol using a SP233 adapter on the board. To provide a very good timing synchronization the emission is triggered using a LVDS signal.

In summary, the board was designed for easy integration in neutrino telescope infrastructures, it can be configured from shore and can emit arbitrary intense short signals, or act as receiver with very good timing precision (the measured latency is 7 μs with a stability better than 1 μs), as shown in KM3NeT APS joint tests [13].

2.1.3.3 Tests of the Transceiver Prototype.

The transceiver has been tested in a fresh water tank in the laboratory, in a pool and in shallow sea water. After characterisation, it has been integrated in the instrumentation line of the ANTARES neutrino telescope for in situ tests in the deep-sea. In the following, the activities and results of these tests are described.

The measurement tests in the laboratory have been performed firstly in a fresh-water tank of 87.5 × 113 × 56.5 cm^3, and secondly in a water pool of 6.3 m length, 3.6 m width and 1.5 m depth. We have tested the system using the over-moulded FFR-SX30 hydrophone and the SEB. The complete over-moulding of the transducer has been done by McArtney-EurOceanique SAS. Moreover, a 10 meter-length cable 4021 type (http://www.macartney.com/) has been moulded onto a free issued hydrophones plus one connector type OM2M with its locking sleeves type DLSA-M/F. The mouldings are made of polyurethane, the connector body of neoprene and the locking sleeve of plastic.

Some changes to the SEB board have been made to integrate the system into the ANTARES neutrino telescope and also to test the system *in situ* at 2,475 m depth. For simplicity and due to limitations in the instrumentation line, it was decided to test the transceiver only as an emitter. The receiver functionality will be tested in other in situ KM3NeT tests. The changes made to the SEB are: to eliminate the reception part, to adapt the RS232 connection to RS485 connection and to implement the instructions to select the kind of signals to emit matching the procedures of the ANTARES DAQ system [3].

To test the system, the transceiver has been used with different emission configurations in combination with the omnidirectional transducers ITC-1042 and RESON-TC4014, which were used as emitter and receiver, respectively. Different signals have been used (tone bursts, sine sweeps, maximum length sequence (MLS) signals, *etc.*) to view the performance of the transducer in different situations.

Figure 6 shows the transmitting acoustic power of the transceiver as a function of the frequency (measured in the XY-plane). The transmitting acoustic power of the transceiver as a function of the angle (directivity pattern) using a 30 kHz short tone burst signal is also shown (measured in the XZ-plane, 0° corresponds to the direction opposite to cables). The measurements have been done in similar conditions to those of Figures 2 and 3.

Comparing the Receiving and Transmitting Voltage Response of the FFR-SX30 over-moulded with and without over-moulding, a loss of ~1–2 dB is observed for the over-moulded hydrophone. Figure 6 shows that the result for the transmitting acoustic power

in the 20–50 kHz frequency range is in the 164–173 dB re 1 μPa @ 1 m range, in agreement with the electronics design and the specifications needed. Despite this, acoustic transmitting power may be considered low in comparison with the ones used in Long Base Line positioning systems, which usually reach values of 180 dB re 1 μPa @ 1 m. The use of longer signals in combination with a broadband frequency range and signal processing techniques will allow us to increase the signal-to-noise ratio, and therefore allow for the possibility of having an acoustic positioning system of the 1 μs stability (~1.5 mm) order over distances of about 1 km, using less acoustic power, *i.e.*, minimizing the acoustic pollution. In order to study the transceiver over longer distances and also the possibilities of the signal processing techniques, tests were designed in shallow sea water at the Gandia Harbour (Spain). Here, the transceiver was used as an emitter and another FFR-SX30 hydrophone as a receiver with a distance of 140 m between them. The environment was quite hostile for acoustic measurements with a high level of noise existence and multiple reflection sites. However, our analysis showed that the use of broadband signals, MLS and sine sweep signals, is a very useful tool to increase the signal-to-noise ratio and allows for a better distinction of the direct signal from reflections. The latter could be misinterpreted as the direct ones giving a bad detection time [14].

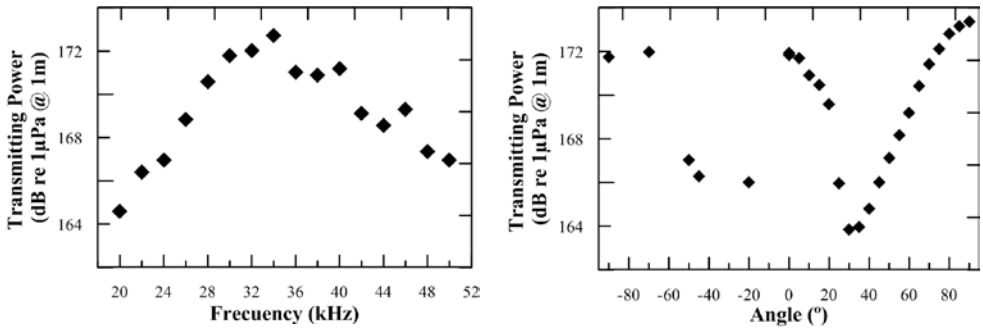

Figure 6. Transmitting acoustic power of the transceiver as functions of frequency and angle, respectively. The uncertainties on the measurements are 1.0 dB.

The system has been finally integrated into the active anchor of the Instrumentation Line of ANTARES. In particular, the SEB was inserted in a titanium container containing a laser and other electronic boards used for timing calibration purposes. A new functionality for the microcontroller was implemented to control the laser emission as well. The FFR-SX30 hydrophone was fixed to the base of the line at 50 cm from the standard transmitter of the ANTARES positioning system [1] with the free area of the hydrophone looking upwards.

Figure 7 shows some pictures of the final integration of the system in the anchor of the Instrumentation Line of ANTARES. Finally, the Instrumentation Line was successfully deployed at 2,475 m depth on 7th June 2011 at the nominal target position. The connection of the Line to the Junction Box, will be made when the ROV (Remotely

Operated Vehicle) will be available (probably in April 2012). Afterwards the transceiver will be tested in real conditions.

Figure 7. Picture of the anchor of the Instrumentation Line of ANTARES showing the final integration of the transceiver. Details of the FFR-SX30 hydrophone with its support and of the titanium container housing the SEB are also shown.

2.1.4 Compact Transmitter for Acoustic UHE Neutrino Detection Calibration.

In this section we present the R&D studies based on parametric acoustic sources techniques in order to develop a compact transmitter prototype for the calibration of acoustic neutrino detection arrays. The aim is to have a very versatile calibrator that not only is able to generate neutrino-like signals, but is able as well to calibrate the sensitivity of the acoustic sensors of the telescope, to check and train the feasibility of the UHE neutrino acoustic detection technique and to generate signals either for positioning or monitoring environmental parameters acoustically [8]. Moreover, a compact solution for the calibrator will result, most probably, in a system easier to install and deploy in undersea neutrino telescopes.

2.1.4.1 Parametric Acoustic Sources.

Acoustic parametric generation is a well-known non-linear effect that was first studied by Westervelt [15] in the 1960s. This technique has been studied quite extensively since then, being implemented in many applications in underwater acoustics, specifically to obtain very directive acoustic sources. The acoustic parametric effect occurs when two intense monochromatic beams with two close frequencies travel together through the medium (water, for example). Under these conditions in the regime of non-linear

interaction, secondary harmonics appears with the sum, difference, and double spectral components. One application of this effect is to obtain low-frequency very directive beams from very directive high-frequency beams, as secondary parametric beams have similar directivity pattern as the primary beams. Directive high-frequency beams are much easier to obtain, as the needed dimensions of the emitter scale with the wavelength. The technique application for a compact calibrator presents two difficulties: on one hand, it is a transient signal with broad frequency content, on the other hand, the directivity has cylindrical symmetry. To deal with transient signals it is possible to generate a signal with 'special modulation' at a larger frequency in such a way that the pulse interacts with itself while travelling along the medium, providing the desired signal. In our particular case the desired signal would be a signal with bipolar shape signal in time. Theoretical and experimental studies of parametric generation show that the shape of the secondary signal follows the second time derivative in time of envelope of the primary signal [16], following the equation:

$$p(x,t) = \left(1 + \frac{B}{2A}\right) \frac{P^2 S}{16\pi\rho c^4 \alpha x} \frac{\partial^2}{\partial t^2} \left[f\left(t - \frac{x}{c}\right) \right]^2 \qquad (1)$$

where P is the pressure amplitude of the primary beam pulse, S the surface area of the transducer, $f(t-x/c)$ is the envelope function of the signal, which is modulated at the primary beam frequency, x is the distance, t is the time, B/A the non-linear parameter of the medium, ρ is the mass density, c the sound speed and α is the absorption coefficient.

Parametric acoustic sources have some properties that are very interesting to be exploited in our acoustic compact calibrator:

- It is possible to obtain narrow directional patterns at small overall dimensions of primary transducer.
- The absence of side lobes in a directional pattern of the difference frequency.
- Broad band of operating frequencies of radiated signals.
- Since the signal has to travel long distances, primary high-frequency signal will be absorbed.

2.1.4.2 Evaluation of the Technique for the Application Proposed.

(a) Planar transducers

The first study to evaluate the parametric acoustic sources technique for the emission of acoustic neutrino like signal was to try to reproduce the bipolar shape of the signal. This study was done using planar transducers and was described in [17]. The results in terms of the bipolar signal generation from the primary beam signal, the studies of the signal shape, the directivity patterns obtained, the evidence of the secondary non-linear beam generated in the medium and the checking of the non-linear behaviour with the amplitude of the primary beam have been all coherent with the expectation from theory and

demonstrated that the technique could be useful for the development of the compact acoustic calibrator able to mimic the signature of the UHE neutrino interaction. Figure 8 shows the comparison between the emitted signal, the received signal and the secondary signal (obtained using a band-pass FIR filter: with corner frequencies 5 kHz and 100 kHz). The nonlinear behaviour of the secondary beam (filtered signal) in comparison to the primary beam (received signal) is also shown.

(b) Cylindrical symmetry

Once we have been able to reproduce the shape of the desired signal using the parametric technique, the next step was a more detailed study of the 'modulated signal' influence on the secondary beam generated, and on the other hand, to reproduce the 'pancake' pattern of emission desired using a single cylindrical transducer, a Free Flooded Ring SX83 (FFR-SX83) manufactured by Sensor Technology Ltd. (Collingwood, Canada). It has a diameter of 11.5 cm and 5 cm height. This transducer usually works around 10 kHz (the main resonance peak is at 10 kHz), but for our application we use a second peak resonance at about 400 kHz, which is the frequency used for the primary beam. This work is described in [18] and the results obtained agree with the previous ones using planar transducers, but now dealing with the complexity of the cylindrical symmetry generation obtaining a 'pancake' directivity of a few degrees.

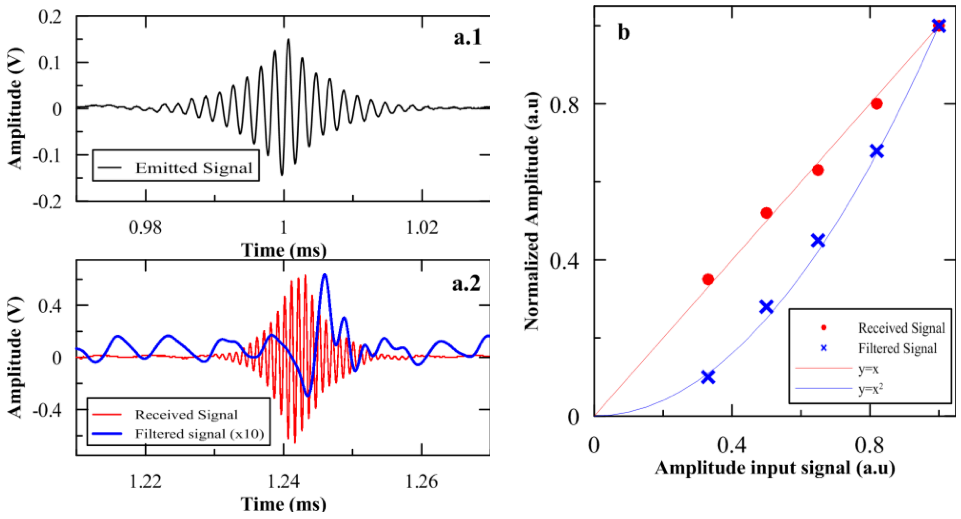

Figure 8. (a) Emitted and received signals. (b) Amplitude of the primary and secondary signals as a function of the amplitude of the input signal in the transducer. Statistical uncertainties are very small.

To verify the previous studies over longer distances, new measurements have been made in an emitter-receiver configuration in a pool of 6.3 m length, 3.6 m width and 1.5 m depth using as emitter a single FFR-SX83 transducer. It was positioned at 70 cm depth and the receiver hydrophone used to measure the acoustic waveforms was a spherical omnidirectional transducer (model ITC-1042) connected to a 20 dB gain preamplifier (Reson CCA 1000). With this configuration the receiver presents an almost flat frequency response below 100 kHz with a sensitivity of about −180 dB re 1 V/μPa, whereas it is 38 dB less sensitive at 400 kHz. The larger sensitivity at lower frequencies is very helpful for a better observation of the secondary beam. For these tests, the emitter and receiver are aligned and positioned manually with cm accuracy, which is enough for our purposes. A DAQ system is used for emission and reception. To drive the emission, an arbitrary 14 bits waveform generator (National Instruments, PCI-5412) has been used with a sampling frequency of 10 MHz. This feeds a linear RF amplifier (ENI 1040L, 400W, +55 dB, Rochester, NY, USA) used to amplify the emitted signal. The received signal was recorded with an 8 bit digitizer (National Instruments, PCI-5102) has been used with a sampling frequency of 20 MHz. Later, the recorded data are processed and different band-pass filters are applied to extract the primary and secondary beam signals and the relevant parameters.

Figure 9 summarizes the results of this study by comparing the amplitude of the primary and secondary beams. A different behaviour is observed in the evolution of both beams with the distance. The attenuation exponent for the primary beam is 0.81, which seems a reasonable value considering that we expect an exponent between 0.5 (pure cylindrical

propagation) and 1.0 (spherical propagation), being our case an intermediate situation. The attenuation exponent for the secondary beam is 0.50, which also seems reasonable since we expect an attenuation factor significantly lower than that of the primary beam, but higher than half of that exponent. This result is a clear evidence of the secondary bipolar pulse generation by the parametric acoustic sources. The directivity patterns were measured at a distance of 2.3 m. Despite the frequency components are very different both look quite similar (the opening angle differs about 10%).

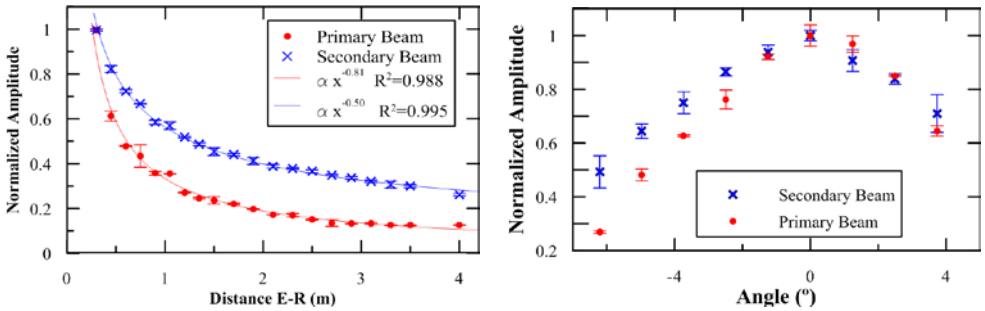

(a) (b)

Figure 9. Amplitude of the primary and secondary signals as a function of the distance, and directivity pattern for both beams. Normalization values (a) Primary beam: 166 kPa, Secondary beam: 200 Pa; (b) Primary beam: 27 kPa, Secondary beam: 80 Pa.

The positive results of the studies with a single transducer confirm that the parametric acoustic sources technique may be applied for the development of a transmitter able to mimic the acoustic signature of a UHE-neutrino interaction. Moreover, the technique presents advantages with respect to other classical solutions: such as the use of a higher frequency in a linear phased array implies that fewer elements are needed on a shorter length scale having a more compact design, and thus, probably easier to install and deploy in undersea neutrino telescopes. A possible drawback of the system is that the parametric generation is not very efficient energetically, but since bipolar acoustic pulses from UHE-neutrino interactions are weak, they can be emulated with reasonable power levels of the primary beams. At this point, it is necessary to design a fully functional array for integration in undersea neutrino telescopes or for application in calibration sea campaigns. There are two aspects that need to be dealt and solved for this: the mechanical design of the array and the necessary electronics to manage the array of acoustic sensors. In the following section, we describe some ideas and work on these aspects.

2.1.4.3 Design of the Compact Array.

Once the single cylindrical transducer had been characterized for the generation of the bipolar pulse using parametric generation in the previous studies, all the required inputs are available for the design of the array able to generate the neutrino-like signal with the 'pancake' directivity with an opening angle of about 1°. Figure 10(a) shows an example of the results for calculations performed by summing the contributions of the different sensors for far distances at different angles. In this example, a linear array of 3 FFR-SX83 transducers with a 20 cm separation from each other is enough to obtain an opening angle of about 1°. Moreover, to estimate the effect of the propagation caused in the bipolar parametric signal, received signals of the experimental measurements of the previous section (a single transducer in the pool), have been extrapolated to 1 km distance. For this an algorithm that works at frequency domain and propagates each spectral component considering the geometric spread of the pressure beams as 1/r and its absorption coefficient [19,20] has been used. The propagation has been done for the sea conditions of the ANTARES site, the value of the parameters are presented in Table 1. Figure 10(b) shows the results of propagating to 1 km the received signal of Figure 9 measured at 2.3 m distance and 0 º. In this case, no filter is applied, the propagation medium acts as a natural filter. High frequencies of the primary beam are absorbed and, at km range, only low frequencies remain. To be exact, there is still a small high-frequency component which is not observed at distances of 1.2 km (or higher). Notice that the high-frequency signal was three orders of magnitude higher than the secondary beam at a 1 m distance. It appears as well a kind of DC offset, it is due to the very low-frequency components of the signal (probably 50 Hz) which are also propagated.

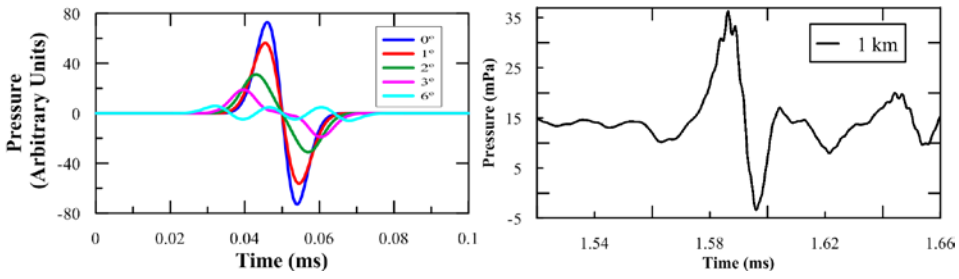

(a) (b)

Figure 10. (a) Pressure signal obtained at different angles for a three-element array. (b) Signal obtained by the propagation of the measured signal to a 1 km distance.

Table 1. Parameters used for the propagation and absorption coefficient examples [19,20].

Depth (m)	Sound speed (m/s)	Salinity (‰)	Temperature (ºC)	pH	Absorption coeff.,25 kHz (Np/m)	Absorption coeff., 400 kHz (Np/m)
2,200	1,541.7	38.5	13.2	8.15	0.00042	0.00983

To conclude this study, for a single element, it is expected to have a bipolar pulse with a 35 mPa amplitude peak-to-peak at 1 km. Considering the array configuration with three elements feeding in to phase with the maximum power it is expected to have, at least, a 0.1 Pa amplitude peak-to-peak, which is a good pressure reference for calibration of neutrino interactions of the 10^{20} eV energy range. Therefore, with the goal to reproduce the 'pancake' directivity, to cover long distances and to improve the level of signal of non-linear beam generated at the medium, an array of three elements configuration has been proposed as possible solution. It is composed by 3 FFR-SX83 transducers with a distance between elements of 2 cm, having the active part of the array at a total height of 20 cm. The three elements are maintained in a linear array configuration by using three bars with mechanical holders as shown in Figure 11. The bars can help to hold the array and also to help to orientate it.

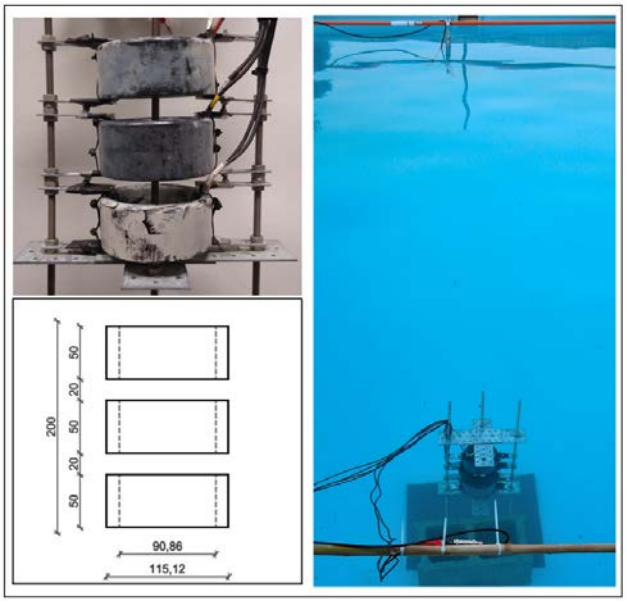

Figure 11. Picture of the array used for the tests and of the pool during the data taking. The emitter array and the receiver can be observed.

The measurements for the array characterization have been made using the same configuration than for the previous measurements. Figure 11 shows a drawing with the dimensions of the array, and pictures of the array and of the pool during the tests.

The results obtained from the array tests are summarized in Figure 12. An example of a received signal and the primary and secondary beams obtained after applying a band-pass FIR filter filters are shown in Figure 12(a), the secondary beam has been amplified by a factor of 3 for a better visibility. The corner frequencies of the primary beam are 350 kHz and 450 kHz, whereas the cut frequencies for the secondary beam are 5 kHz and 100 kHz. It is possible to see how the reproduction of the signal shape is achieved agreeing the results with our expectations from theory and previous observations. The directivity pattern measured at a longitudinal line defined by the axis of the array is shown in Figure 12(b). These measurements have been made at a 2.7 m distance between the array and the receiver. Notice that the absolute pressure values of Figure 12(b) are smaller than those of Figure 9(b). The reason for this is that the amplifier used is not very efficient to feed the three elements together due to a mismatch of electrical impedances, and therefore each transducer provides a lower pressure beam. Thus, for the final array system, it is very important to work on electronics and have a very good amplifier for each transducer. The design of the electronics for the array is further discussed in next section. In spite of these limitations, Figure 12(b) is quite interesting because it allows studying the angle distribution of both beams. Instead of having for the primary beam a thin peak, a wide peak with a no clear maximum is observed. This is due to the fact that the measurements were done at a distance which cannot be considered very large, and therefore the signals from the different transducers are not totally synchronous at 0°. However, the FWHM measured with the array for the secondary beam is about 7° (σ = 3°), that is, smaller than for the primary beam, and sensitively smaller than for a single element where the FWHM was about 14° (σ = 6°). This agrees with the expectations of the kind of calculations described for Figure 10(a), and considering that the signals for the three elements will be better synchronized at far distances (larger than 100 m), a more 'pancake'-like directive pattern with σ~1° is expected for far distances.

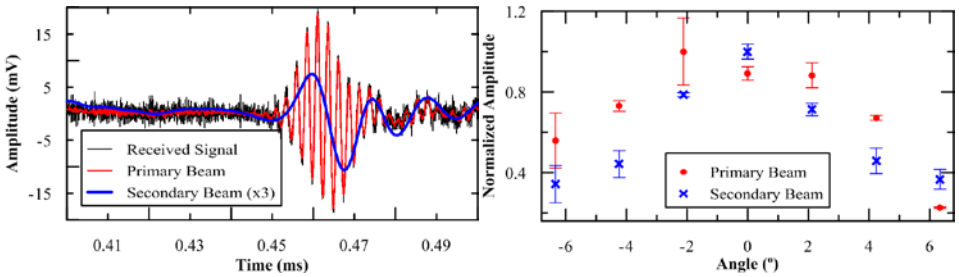

(a) (b)

Figure 12. (a) Example of a received signal and the primary and secondary beams obtained after applying the band-pass filters (the secondary beam has been amplified by a factor 3 for a better visibility). (b) Directivity patterns of primary and secondary beam measured with the array. Normalization values, Primary beam: 5.4 kPa, Secondary beam: 11.5 Pa.

2.1.4.4 Prototype of a Versatile Compact Array.

Our final goal is to have an autonomous and optimized compact system able to carry out several tasks related to acoustics in an underwater neutrino telescope, these tasks being: signal emulation for acoustic neutrino detection arrays, the calibration of acoustic receivers, and even performing positioning tasks, with all of them using the same transmitter. This could reduce the cost and facilitates the deployment in the deep sea. The new developments are orientated towards a mechanical array design improving the directivity and the operation, and the associated electronics to achieve a more powerful autonomous system.

For the prototype, the transducers have been fixed around an axis on flexible polyurethane. This offers water resistance and electrical insulation for high frequency and high voltage applications due to the nature of the cured polymer. Figure 13 shows the compact array prototype. Its compact design is remarkable with an active surface length of 17.5 cm. In order to use it in a future sea campaign with a vessel, a mechanical structure has been built that allows the device to be affixed to a boat, allowing control of the rotation angle. Due to the high directivity of the bipolar pulse, this is a very important point in order to be able to orientate the signal to the direction of the receivers.

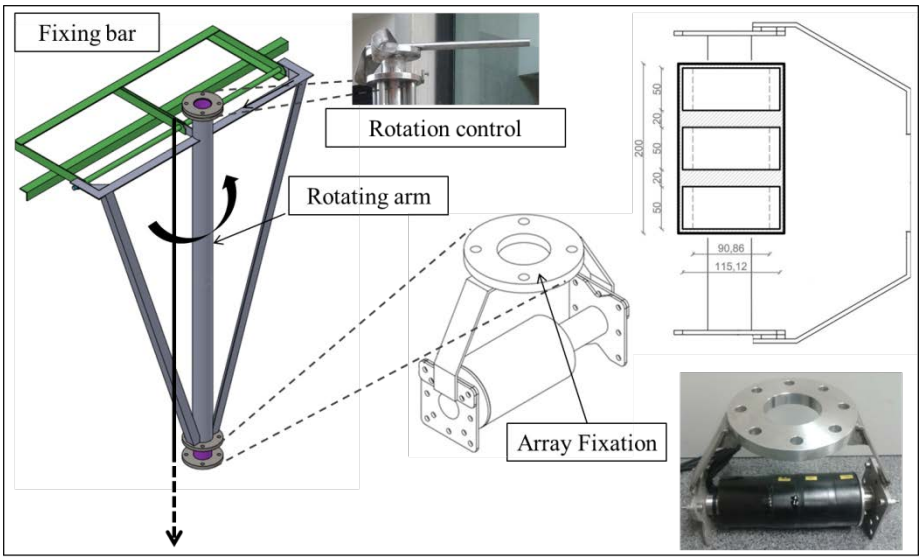

Figure 13. Compact array prototype and mechanical structure to hold and operate it from a boat.

Developments in electronics have been made to achieve an autonomous and optimized compact system able to work in a different frequency ranges and application modes. It has been necessary to develop an electronic device that controls the transmitter which generates and amplifies the signals, in order to have enough acoustic power in the nonlinear regime (parametric generation) and that standard signals can be detected at distant acoustic receivers (for calibration and/or positioning purposes). For this, an electronic board has been developed, based on the same principles as the SEB (described in Section 2.2), that was adapted to the particularities of the transmitter and applications considered. The board is able to communicate, configure the transmitter and control the emission mode (either for high or low frequency operation mode). Similarly to the electronics in the acoustic transceivers for positioning systems [11,21], the PWM technique has been used for the emission of arbitrary intense short signals to emit the necessary 'modulated signal' with the goal to obtain a secondary beam with the specifications desired.

Some of the advantages that this technique offers are:

- The system efficiency is improved because the system uses a class D amplification, this means that the transistors are working on switching mode, suffering less power dissipation in terms of heat, and therefore offering a superior performance.
- Simplicity of design. Analogic-digital converters are not needed. It is possible to feed directly the amplifier with digital signal modulated by the PWM technique.
- It is not necessary to install large heat sinks at amplifier transistors, reducing the weight and volume of the electronics system.
- In waiting mode, the power amplifier has a minimum power at idle state that allows storing the energy for the next emission in the capacitor very fast and efficiently.

The diagram of the board prototype is shown in Figure 14. It consists of three parts: the communication and control which contains the micro-controller (in blue) dsPIC33FJ256MC0710 implementing the PWM under motor control technology, the emission constituted by the digital amplification plus the transducer impedance matching (in red), differentiated for each frequency range, and the commuter between the two operation modes (in green). There are three identical parallel boards to manage the three transducers of the compact array. They can be used individually or, in parallel (standard operation mode).

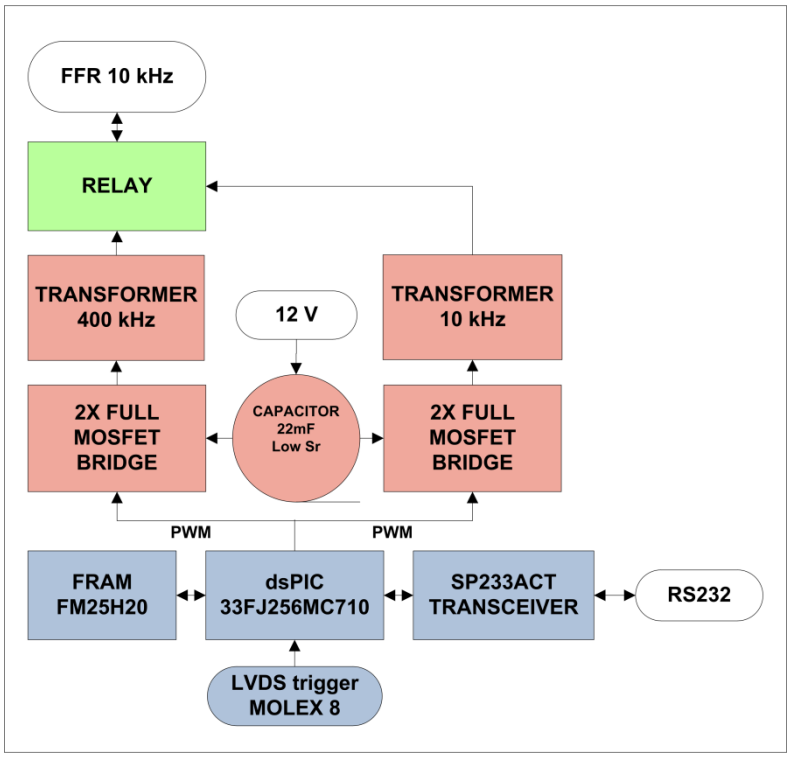

Figure 14. Electronics block diagram for the compact array transmitter.

Summarizing, the sound emission board has been designed for an easy integration into neutrino telescope infrastructures, using PWM to emit arbitrary intense short signals, to mimic the acoustic signature of neutrino using parametric acoustic generation, and tone bursts or arbitrary signals with low spectral content for positioning or calibration tasks.

2.1.5 Conclusions and Future Steps.

We have discussed the use and applications of acoustic sensors in underwater neutrino telescopes, and presented the acoustic transmitters developed either for the positioning system of KM3NeT (transceiver of the APS) or for calibration in acoustic neutrino detection systems (compact array prototype).

With respect to the transceiver for the APS, we have shown the results of the tests and measurements performed with FFR-SX30 hydrophones and a custom sound emission board, concluding that the transceiver proposed can be a good solution with the requirements and accuracy needed for such a positioning system.

With respect to the compact array, after showing the R&D studies made, we can conclude that the solution proposed based on parametric acoustic sources could be considered a good tool to generate the acoustic neutrino-like signals, achieving the reproduction of both specific characteristics of the signal predicted by theory: bipolar shape in time and 'pancake directivity'. Moreover, due to the versatility of the transceiver system, this prototype could be implemented to carry out several calibration tasks related to acoustic emission in underwater neutrino telescopes.

Furthermore, we consider that the techniques used for these transmitters are so powerful and versatile that it may be used in other kind of applications, such as marine positioning systems, alone or combined with other marine systems, or integrated in different Earth-Sea Observatories, where the localization of the sensors is an issue. Other applications, such as acoustic communication or SONAR, may benefit from the developments in obtaining very directive sources and in the implementation of signal processing techniques. Moreover, the developments and results may be of great interest for systems with cylindrical acoustic propagation or systems that can work in two operation modes (standard one and parametric acoustic sources one). In that sense, the experience gained from this research can be of interest to open new possible application uses in these areas.

The future work will consist of completing the characterization of the prototype systems, and integrating the transmitters into underwater neutrino telescopes using the framework of the ANTARES and KM3NeT neutrino telescopes. A very useful test for the *in situ* demonstration of the utility of the transmitters is to use them together with the ANTARES-AMADEUS acoustic system, and it is foreseen that these tests will be carried out during 2012.

2.1.6 Acknowledgments.

This work has been supported by the Ministerio de Ciencia e Innovación (Spanish Government), project references FPA2009-13983-C02-02, ACI2009-1067, AIC10-D-00583, Consolider-Ingenio Multidark (CSD2009-00064). Authors Manuel Bou-Cabo and Silvia Adrián-Martínez thank Multidark for the fellowships. The work has also been funded by Generalitat Valenciana, Prometeo/2009/26, and the European 7th Framework Programme, Grant No. 212525.

2.1.7 References and Notes.

1. Ardid, M. Positioning system of the ANTARES neutrino telescope. *Nucl. Instr. Meth. A* **2009**, *602*, 174-176.
2. Askariyan, G.A.; Dolgoshein, B.A.; Kalinovsky, A.N.; Mokhov, N.V. Acoustic detection of high energy particle showers in water. *Nucl. Instr. Meth.* **1979**, *164*, 267-278.
3. Ageron, M.; Aguilar, J.A.; Al Samarai, I.; Albert, A.; Ameli, F.; André, M.; Anghinolfi, M.; Anton, G.; Anvar, S.; Ardid, M.; et al. (ANTARES

Collaboration). ANTARES: The first undersea neutrino telescope. *Nucl. Instr. Meth. A* **2011**, *656*, 11-38.

4. The KM3NeT Collaboration. *KM3NeT Technical Design Report*; 2010. ISBN 978-90-6488-033-9. Available online: www.km3net.org (accessed on 20 March 2012).
5. Aguilar, J.A.; Al Samarai, I.; Albert, A.; André, M.; Anghinolfi, M.; Anton, G.; Anvar, S.; Ardid, M.; Assis Jesus, A.C.; Astraatmadja, T.; et al. (ANTARES Collaboration). Time calibration of the ANTARES neutrino telescope. *Astrop. Phys.* **2011**, *34*, 539-549.
6. Bevan, S.; Brown, A.; Danaher, S.; Perkin, J.; Rhodes, C.; Sloan, T.; Thompson, L.; Veledar, O.; Waters, D. (ACORNE Collaboration). Study of the acoustic signature of UHE neutrino interactions in water and ice. *Nucl. Instr. and Meth. A* **2009**, *607*, 398-411.
7. Aguilar, J.A.; Al Samarai, I.; Albert, A.; M.; Anghinolfi, M.; Anton, G.; Anvar, S.; Ardid, M.; Assis Jesus, A.C.; Astraatmadja, T.; Aubert, J.-J.; et al. (ANTARES Collaboration). AMADEUS-The acoustic neutrino detection test system of the ANTARES deep-sea neutrino telescope. *Nucl. Instr. Meth. A* **2011**, *626*, 128-143.
8. Ardid, M. Calibration in acoustic detection of neutrinos. *Nucl. Instr. Meth. A* **2009**, *604*, S203-S207.
9. Sherman, C.H.; Butler, J.L. *Transducers ad Array for Underwater Sound*; Springer: New York, USA, 2007.
10. Ardid, M; Bou-Cabo, M.; Camarena, F.; Espinosa, V.; Larosa, G.; Llorens, C.D.; Martínez-Mora, J.A. A prototype for the acoustic triangulation system of the KM3NeT deep sea neutrino telescope. *Nucl. Instr. Meth. A* **2010**, *617*, 459-461.
11. Llorens, C.D.; Ardid, M.; Sogorb, T.; Bou-Cabo, M.; Martínez-Mora, J.A.; Larosa, G.; Adrián-Martínez, S. The Sound Emission Board of the KM3NeT Acoustic Positioning System. *J. Instrum.* **2012**, *7*, C01001.
12. Barr, M. Introduction to Pulse Width Modulation. *Embed. Syst. Program.* **2001**, *14*, 103-104.
13. Simeone, F.; Ameli, F.; Ardid, M.; Bertin, V.; Bonori, M.; Bou-Cabo, M.; Calì, C.; D'Amico, A.; Giovanetti, G.; Imbesi, M.; et al. Design and first tests of an acoustic positioning and detection system for KM3NeT. *Nucl. Instr. Meth. A* **2012**, *662*, S246-S248.
14. Larosa, G; Ardid, M.; Llorens, C.D.; Bou-Cabo, M.; Martínez-Mora, J.A.; Adrián-Martínez, S. Development of an acoustic transceiver for the KM3NeT positioning system. *Nucl. Instr. Meth. A* **2012**, accepted.
15. Westervelt, P.J. Parametric acoustic array. *J. Acoust. Soc. Am.* **1963**, *35*, 535-537.
16. Moffett, M.B.; Mello, P. Parametric acoustic sources of transient signals. *J. Acoust. Soc. Am.* **1979**, *66*, 1182-1187.

17. Ardid, M; Bou-Cabo, M.; Camarena, F.; Espinosa, V.; Larosa, G.; Martínez-Mora, J.A.; Ferri, M. Use of parametric acoustic sources to generate neutrino-like signals. *Nucl. Instr. Meth. A* **2009**, *604*, S208-S211.
18. Ardid, M; Adrián, S.; Bou-Cabo, M.; Larosa, G.; Martínez-Mora, J.A.; Espinosa, V.; Camarena, F.; Ferri, M. R&D studies for the development of a compact transmitter able to mimic the acoustic signature of a UHE neutrino interaction. *Nucl. Instr. Meth. A* **2012**, *662*, S206-S209.
19. Francois, R.E.; Garrison G.R. Sound absorption based on ocean measurements. Part I: Pure water and magnesium sulfate contributions. *J. Acoust. Soc. Am.* **1982**, *72*, 896-907.
20. Francois, R.E.; Garrison G.R. Sound absorption based on ocean measurements. Part II: Boric acid contribution and equation for total absorption. *J. Acoust. Soc. Am.* **1982**, *72*, 1879-1890.
21. Ardid, M; Bou-Cabo, M.; Camarena, F.; Espinosa, V.; Larosa, G.; Llorens, C.D.; Martínez-Mora, J.A. R&D towards the acoustic positioning system of KM3NeT. *Nucl. Instr. Meth. A* **2011**, *626-627*, S214-S216.

Diseño y desarrollo de la electrónica de los emisores acústicos para los sistemas de posicionamiento y calibración de telescopios submarinos de neutrinos.

2.2 The Sound Emission Board of the KM3NeT Acoustic Positioning System.

C.D. Llorens, M. Ardid*, T. Sogorb, M. Bou–Cabo, J.A. Martínez-Mora, G. Larosa, S. Adrián

Universitat Politècnica de València representing the KM3NeT Consortium,

C/ Paranimf 1, E-46730 Gandia, Spain

2.2.1 abstract.

We describe the sound emission board proposed for installation in the acoustic positioning system of the future KM3NeT underwater neutrino telescope. The KM3NeT European consortium aims to build a multi-cubic kilometre underwater neutrino telescope in the deep Mediterranean Sea. In this kind of telescope, the mechanical structures holding the optical sensors, which detect the Cherenkov radiation produced by muons emanating from neutrino interactions, are not completely rigid and can move up to dozens of meters in undersea currents. Knowledge of the position of the optical sensors to an accuracy of about 10 cm is needed for adequate muon track reconstruction. A positioning system based on the acoustic triangulation of sound transit time differences between fixed seabed emitters and receiving hydrophones attached to the kilometre-scale vertical flexible structures carrying the optical sensors is being developed. In this paper, we describe the sound emission board developed in the framework of KM3NeT project, which is totally adapted to the chosen FFR SX30 ultrasonic transducer and fulfils the requirements imposed by the collaboration in terms of cost, high reliability, low power consumption, high acoustic emission power for short signals, low intrinsic noise and capacity to use arbitrary signals in emission mode.

KEYWORDS: Detector alignment and calibration methods; Large detector systems for particle and astroparticle physics;

2.2.2 Introduction.

The Sound Emission Board (SEB) presented in this article is part of the long baseline acoustic positioning system proposed for the future underwater neutrino telescope KM3NeT that will be located at the Mediterranean Sea.

The KM3NeT Consortium [1] aims to build an underwater neutrino telescope of at least one cubic kilometre volume. Due to the large instrumented volume needed, many of the hardware solutions adopted in the first undersea neutrino telescope ANTARES [2], hich is taking data since 2008 with an effective area of $0.1 km^2$, cannot directly be applied to KM3NeT; the costs and production period would be prohibitive. New designs of the detector sub-systems are required.

The detection principle used in underwater neutrino telescopes is based on the detection of the Cherenkov light produced by muons coming from ν_μ interactions with matter in

or near to the telescope. Both ANTARES and the future KM3NeT require knowledge of optical module positions with an accuracy of about 10 cm in order to properly reconstruct muon tracks detected by the photomultipliers. Since the mechanical structures holding the optical sensors are not completely rigid and can move due to sea currents, a positioning system is mandatory. In ANTARES, the positioning calibration system provides the positions of the optical modules with accuracy better than 10 cm [3]. While KM3NeT will be 20 times larger, the ANTARES positioning calibration system will not be directly scalable: a new design of the system has been necessary. The Acoustic Positioning System (APS) included in the KM3NeT general positioning calibration system is a Long Baseline System composed of a set of acoustic transceivers and the associated electronics (the subject of this paper) and an array of acoustic receivers (hydrophones) rigidly attached to the telescope mechanical structures. This APS should provide the position of the telescope mechanical structures, in a geo-referenced coordinate system with accuracy better than 1m (for a good pointing accuracy of the telescope) and also the positions of the 10000 + optical modules during continuous telescope operation in varying deep sea currents with a precision of about 10 cm. In addition, the acoustic devices installed in KM3NeT will be used in studies related to sea sciences (e.g. bioacoustics, geophysics, etc.) and possibly in the acoustic detection of ultra-high energy neutrinos.

An important aspect of the APS system is the transceiver. Following the idea of reducing cost and increasing reliability, a new design for this system has been proposed, and a prototype has been developed [4,5]. It basically consists of two parts: the acoustic transducer and the electronics: the Sound Emission Board (SEB). The selected transducer for this system is the FFR SX30 transducer manufactured by Sensortech. The most important reasons for choosing this transducer are:

- it can provide a reasonable acoustic power level for long distance transmission. Considering the transmission power level given by the manufacturer (133 dB Ref. 1 µPa/Volt @ 1 m) and the sensitivity of the receiver hydrophones developed by INFN – LNS [6], the required transducer excitation voltage has been calculated (figure 1). It has been found that 500 V is enough for reasonable levels in the receivers for distances up to 1.9 km. The calculation has been made for the 30 kHz resonant frequency: the impedance at this frequency is (130-1000j) Ω;
- it has an 'unlimited' depth (pressure) of operation according to the manufacturer specifications. Transducers were tested in a hyperbaric tank up to 440 bars checking the acoustic sensitivity for different frequencies under high pressure. Results obtained for this study were clearly satisfactory and no significant pressure-dependent changes in the expected behaviour of the transducer [4] were observed;
- the operation frequency range is 20kHz – 40 kHz; the optimum frequency range for positioning purposes.

2.2.3 The Sound Emission Board.

In this section we describe the specifications required for SEB operation in KM3NeT, its different parts, and the different solutions adopted to meet the imposed specifications, as follows;

- power consumption less than 1W at 5V (control part) & 12V (power part);
- low speed communication port required to configure the board and load arbitrary signals from shore. RS232 or RS485 communication ports have been implemented;
- time synchronization must work with an accuracy of about 1µs;
- the SEB must be able to work in emission and reception mode;
- trigger used in emission mode will be through a LVDS signal;
- the entire system life expectancy must exceed twenty years.

2.2.4 Basic block diagram.

In figure 2 the basic block diagram of the SEB is shown. The transducer is shown at the top of the diagram. The switching block allows transducer connection to the SEB driver or to an external acoustic board [6], which digitises the transducer signal when it is operated in receiver mode. When the transducer is operated as emitter, it is connected to the power amplifier through an impedance matching network. As the instantaneous power available through the telescope 12V DC distribution system is less than that needed to excite the transducer to cover long distances, it has been necessary to implement an energy storage block. In the lower part of the block diagram the signal generator that drives the power amplifier is shown. It has two inputs, one for the low bitrate communication port and one for the trigger signal.

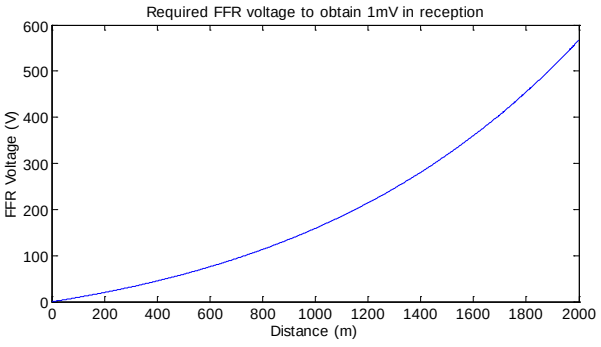

Fig.1. Required transducer excitation voltage needed to obtain the minimum signal a function of reception distance.

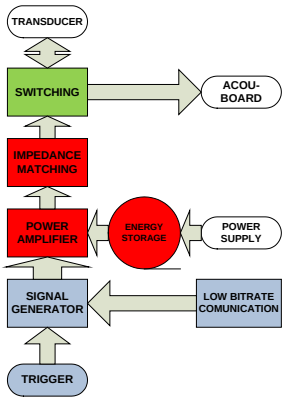

Fig.2. Conceptual block diagram of the SEB.

2.2.5 Impedance matching block.

As shown previously, the generation of an acoustic signal with enough power to be detectable at long distances requires more than 12VDC offered to feed the SEB. For this reason, a transformer - that also plays the main role of impedance matching - has been implemented in the SEB. While standard impedance matching networks interpose several inductors and capacitors between the power amplifier and transducer, the typical tolerances of inductors and capacitors (respectively 20% and 10%) would cause unacceptable variations in latency time between different SEB boards. For this reason, in the SEB we only use a single transformer for adapting the impedance, as shown in figure 3. Two variants of transformer have been implemented in the SEB prototype; the first with 1:20 turns ratio ($480V_{pp}$ output, without load), and the second with 1:30 turns ratio ($720V_{pp}$ output, without load).

2.2.6 Energy storage blocks.

In our system, we use capacitors to store the required transmission energy. The solution allows for fast charging, and correspondingly short time delays between successive emissions (the usual mode of operation is a high-power emission of a few ms duration every few seconds). The solution also offers a long life expectancy. The minimum capacitance needed for the emission has been calculated. Using the 1:30 transformer, the maximum output voltage achieved is 720 V_{pp}; with this voltage and the impedance of the transducer, the power applied is 65 W_{rms}. As the efficiency of the transformer is more than 80% and the power amplifier has more than 90% efficiency, the power required to feed the capacitor is around $90W_{rms}$ (7.5A @ 12V). Considering the maximum length of the signal of 1ms and a maximum capacitor discharge of 1V, the required capacitance exceeds 7.5mF.

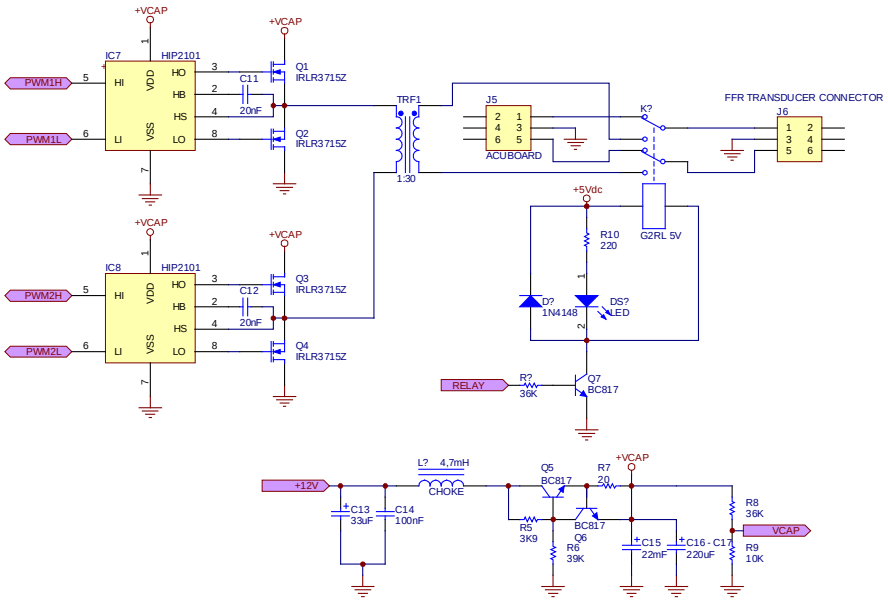

Fig.3. Power part schematic

2.2.7 The aluminium capacitor.

During tests of the first prototype a maximum transducer excitation of $400V_{pp}$ was seen using the 30:1 transformer (the value without the transducer was close to $720V_{pp}$). Some losses in the power amplifier and energy storage blocks were also observed. In order to correct this in the second prototype, the use of one hundred parallel tantalum capacitors has been considered. The individual tantalum capacitors usually have a much better ESL (Equivalent series inductance) than the aluminium capacitors, but they each have lower capacitance and slightly more ESR. However, using one hundred capacitors offers the possibility of multiplying the capacitance and reducing the ESL and ESR by one hundred. The MIL-HDBK-217F standard was used to determine the reliability of a single capacitor. Calculations were made for two different VISHAY models; the first of these (TR3E227K016C0100) is less expensive, but the second

(TR3E227K016C0100) has much greater reliability due to the bigger difference between the rated voltage and the used voltage (12 V). Table 1 presents the main parameters for each type.

Table1. Characteristics (Rated Voltage, ESR and Mean Time Between Failures) for tantalum capacitors and for the 100 parallel configuration.

MODEL	Rated V	ESR	ESR 100 parallel	MTBF years single	MTBF years 100 parallel
TR3E227K016C0100	16	0.1 Ω	1mΩ	2200	22
597D227X9020R2T	20	0.08 Ω	0.8 mΩ	50000	500

2.2.8 Power amplifier block.

The power amplifier solution adopted is a class D amplifier formed by a full bridge. The full bridge is composed of an Intersil HIP2101 MOSFET driver and four IRLS3715Z MOSFETs from International Rectifier. The main characteristics for the MOSFETs are the low R_{on} (transistor ON resistance) of 11 mΩ, the fast switching (13ns rise and 4.7ns fall) and low gate charge (Q_G = 7.2nC). Other important characteristics are the high drain current (I_d = 200 A, 0.1 ms signal) and the maximum drain to source voltage (20V). The SEB power part contains the transducer switching relay, the MOSFETs and their drivers, the energy storage capacitor with the corresponding current limiter and filter for the charging process.

For the new prototype we are considering several Infineon MOSFETs (all with R_{on} < 2mΩ). The most interesting types are not yet on the market. But from tests so far made our choice is the model BSC020N03LSG (R_{on}=1.7mΩ@V_{GS}=10V, Q_c=15nC, 7ns switching time and I_d=400A@0.1ms signal). Considering the lowest capacitor ESR and MOSFET Ron of the new prototype, we are improving the power part Z_{out} from 54mΩ to 5mΩ and - since the transducer impedance in the primary of the 30:1 transformer is close to (0,14-1j)Ω - the efficiency of the power part will be very much improved.

2.2.9 Signal generator block.

Having chosen the full bridge power amplifier, it must be fed with squared signals. This is not a problem if we want to send squared signals like an MLS (Maximum Length Sequence), which is a very useful signal that is extensively used in electro-acoustic measurements. The main characteristics of this signal are the plain spectrum and the non-correlation with any other signal. It can be used to obtain the impulse response of the entire system and for time of flight measurements. Moreover, if we wish to send standard sinusoidal or arbitrary signals we can take advantage of the fact that the transducer and the transformer are good band pass filters in our band of interest: we can emit a square signal in the band and all the highest frequencies that are out of the working band will be removed. We can also use square signals and obtain sinusoidal signals in the emission,

although the best technique - should we wish to send arbitrary signals by generating squared signals - is using PWM (Pulse Width Modulation) with a modulation frequency outside the main band. To implement PWM we must vary the width of the square signal in direct relation to the voltage of the desired signal (0-100% Pulse width). The classic way to do this is to compare the desired signal with a triangular or sawtooth signal in order to obtain a square signal at the output of the comparator. After the amplification, the desired signal is integrated (filtered by the transformer and the transducer) and the median value of the square signal is obtained. This median value is the desired signal.

For the signal generator we have decided to use the Microchip "Motor Control" function inside most of the DSPic microcontroller series. For the first prototype we selected the DSPic33FJ256MC710. This microcontroller has 40 MIPS of processing power, signal processing specific instructions, enough FLASH and RAM for our purposes and a 10bits@1MSps ADC converter. The "Motor Control" function is basically a digital counter that works with the main frequency of the microcontroller (40MHz). This device has all the necessary components to work with full MOSFET bridges (symmetric outputs, dead time generators, etc.), and for this reason matches perfectly for our purposes. We use two of the function modes of the motor control. The first is the "free run" mode; in this mode we can obtain a pulse with modulation similar to the classic one that compares the modulation signal with a saw tooth. Using this mode when the counter arrives to the PxTPER (maximum) value it is reset and starts again from zero. The device has also other comparators in order to establish the width of the pulse. The second mode we use is the "up/down" mode. The only difference between this and the previous mode is that when the counter arrives to PxTPER it starts counting down instead of resetting. This mode is similar to the classic PWM modulation that compares the signal with a triangular wave. With this mode we obtain a more symmetric square signal with fewer harmonics.

2.2.10 The Firmware.

We have developed different firmware versions in order to adapt our board to the communication prerequisites of the different test installations at the ANTARES and NEMO neutrino telescope sites (in ANTARES: with MODBUS over RS485; in NEMO: console over RS232). However, the basic working process is described in figure 4. The basic firmware has three main parts. The first is the processing of commands that arrive at the low bitrate communication port: these commands usually are for configuring the board or defining the signal to be emitted. The second block is in the main part of the program and is aware of the trigger port in order to start the emission when a trigger signal arrives. The third block is an interrupt code that works when the "Motor Control" counter arrives to the PxTPER register. This code changes the registers of the "Motor Control" device in order to obtain the next cycle of the desired square signal (frequency, pulse width, etc.)

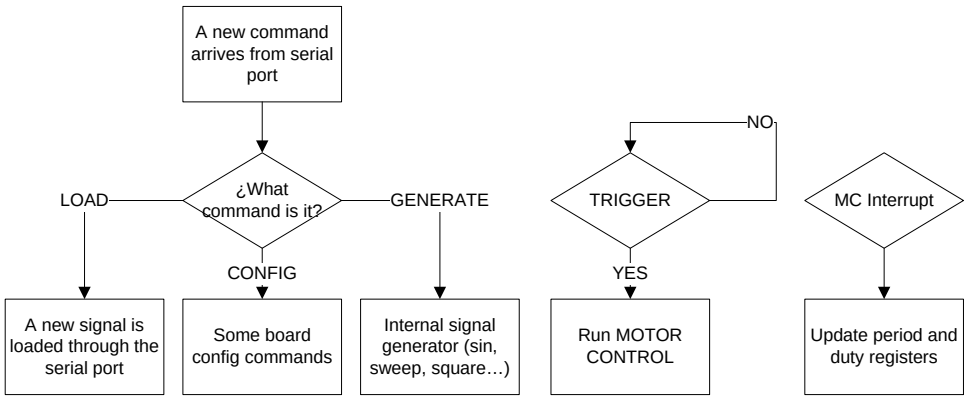

Fig. 4: Diagram of the firmware working process.

2.2.11 Tests.

Laboratory tests have verified that the different components behave as expected. The whole prototype has been fully tested in the lab in order to check that the power consumption, acoustic power emission, time stability, communication and configuration capability, and reliability conformto the specifications. During this process, several changes in the components were made to improve the board (as an example, a more powerful micro-controller is being used with respect to previous versions [4]). The final system described here has been shown in the lab tests to fulfill all the requirements and specifications: power consumption less than 1 W, good timing precision (measured latency around 5 μs with a stability better than 1 μs), well adapted to the standards used in deep-sea neutrino telescopes [7]. However, as mentioned, minor modifications have been derived and will be included in future versions in order to increase the efficiency of the power amplifier block.

In order to test the SEB prototypes under real conditions (in the hostile deep-sea environment) and to test their compatibility with neutrino telescope infrastructures in general and the positioning system in particular, our system is being integrated in two different sites: the Instrumentation Line of ANTARES (2500m depth: off Toulon, France) and the NEMO phase II[8] (3600m depth: off Capo Passero, Italy). The tests performed during the integration have shown the compatibility of the SEB with the rest of the elements of these neutrino telescopes, and we are presently waiting for the final deployment and deep sea connection of these KM3NeT prototypes to be able to test the SEB in situ.

2.2.12 Conclusions.

We have presented and described the solutions adopted for the Sound Emission Board for the KM3NeT acoustic positioning system. Our system is considered for the implementation in the final configuration of the KM3NeT detector. The first prototype developed has been tested in this framework. In order to test the system under real conditions (deep-sea), our system has been integrated in the Instrumentation Line of ANTARES (deployed and waiting for connection), and is also being integrated in NEMO phase II. Presently, a new prototype of the SEB improving the output impedance of the power part is being developed in order to be able to feed the transducer more efficiently.

2.2.13 Acknowledgments.

This work was supported by the European Commission through the KM3NeT Design Study (FP6, contract no. DS 011937) and Preparatory Phase (FP7, grant no. 212525) and also by the Ministerio de Ciencia e Innovación (Spanish Government), project references FPA2009-13983-C02-02, ACI2009-1067, Consolider-Ingenio Multidark (CSD2009-00064). It was also funded by Generalitat Valenciana, Prometeo/2009/26.

2.2.14 References.

[1] The KM3NeT Collaboration, *KM3NeT Technical Design Report*, (2010) ISBN 978-90-6488-033-9, available at http://www.km3net.org.

[2] The ANTARES collaboration, *ANTARES: the first undersea neutrino telescope*, Nucl. Instr. & Meth. A656 (2011) 11–38.

[3] M. Ardid, *Positioning system of the ANTARES neutrino telescope*, Nucl. Instr. & Meth. A602 (2009) 174-176.

[4] M. Ardid et al., *A prototype for the acoustic triangulation system of the KM3NeT deep sea neutrino telescope*, Nucl. Instr. & Meth. A617(2010) 459–461.

[5] M. Ardid et al., *R&D towards the acoustic positioning system of KM3NeT*, Nucl. Instr. & Meth. A 626-627 (2011) S214–S216.

[6] F. Ameli et al., *R&D for an innovative acoustic positioning system for the KM3NeT neutrino telescope*, Nucl. Instr. & Meth. A 626-627 (2011) S211–S213.

[7] G. Larosa et al., *Development of an acoustic transceiver for the KM3NeT positioning system*, in proceedings of *Very Large Volume Neutrino Telescope Workshop*, October, 12 - 14, 2011, Erlangen, Germany, VLVnT (2011) 91.

[8] M. Taiuti et al., *The NEMO project: A status report*, Nucl. Instr. & Meth. A 626-627 (2011) S25–S29.

2.2.15 Acronyms .

- MIL-HDBK-217F, Reliability Prediction of Electronic Equipment, is a military standard that provides failure rate data for many military electronic components.
- PxTPER is the PWM time base period register. It sets the maximum value of the counter.
- MODBUS is a communication protocol used in industrial environments.

2.3 Development of an acoustic transceiver for the KM3NeT positioning system.

G. Larosa, M. Ardid, C.D. Llorens, M. Bou-Cabo*, J.A. Martínez-Mora, S. Adrián-Martínez* (for the KM3NeT Consortium)

Institut d'Investigació per a la Gestiò Integrada de Zones Costaneres (IGIC)-Universitat Politècnica de València, C/Paranimf 1, 46730 Gandia, València, Spain

2.3.1 Abstract.

In this paper we describe an acoustic transceiver developed for the KM3NeT positioning system. The acoustic transceiver is composed of a commercial free flooded transducer, which works mainly in the 20-40 kHz frequency range and withstands high pressures (up to 500 bars). A sound emission board was developed that is adapted to the characteristics of the transducer and meets all requirements: low power consumption, high intensity of emission, low intrinsic noise, arbitrary signals for emission and the capacity of acquiring the receiving signals with very good timing precision.

The results of the different tests made with the transceiver in the laboratory and shallow sea water are described, as well as, the activities for its integration in the Instrumentation Line of the ANTARES neutrino telescope and in a NEMO tower for the in situ tests.

Keywords: underwater neutrino telescope; KM3NeT; calibration; acoustic positioning system; transceiver;

2.3.2 Introduction.

KM3NeT is a European Consortium with the goal to build and operate a multi-cubic-kilometre detector in the Mediterranean Sea. It will be composed from hundreds semi-rigid structures, containing optical modules (OMs), anchored on the seabed and maintained vertical with a buoy [1]. An Acoustic Positioning System (APS) is necessary to monitor the positions of all optical modules in the deep sea, as marine currents cause inclinations of the structures. Thus, the optical modules can be displaced up to several meters from their nominal positions. Precise knowledge of the relative positions of the optical modules (precision of about 10 cm) is needed for an accurate reconstruction of the muon tracks produced in neutrino interactions with the matter around the detector. A big effort has been made during the last years to develop an APS to the future KM3NeT neutrino telescope [4-6]. With respect to other commercial systems (as the ones used in ANTARES and NEMO) the new developments aim for a better integration to the KM3NeT infrastructure, cost reduction, more profound control of the system, better tuning of the acoustic power, and the possibility to use the acoustic data for other studies. The detector will have dimensions larger than 1 km^3, so the acoustic transceiver presented in this paper has been developed to attend to the distances involved (1–2 km), and to constraints imposed by a deep-sea neutrino telescopes (hostile environmental

conditions: high pressure, corrosion, etc.; technology standards: low-power consumption, specific communication protocols, etc.). Moreover, a transceiver prototype has been integrated in the Instrumentation Line of the ANTARES neutrino telescope [2] to be tested in situ. It is also being integrated in NEMO phase II tower [3]. These tests are very important for the final implementation in the KM3NeT detector.

2.3.3 Acoustic transceiver.

The acoustic transceiver is constituted of a transducer and an electronic board named S*ound Emission Board* (SEB), shown in Fig. 1. The transducer type is a Free Flooded Ring (FFR), model SX30 manufactured by Sensor Technology Ltd. It withstands high pressure (tested up to 440 bars) [7-8]. The FFR has dimensions of 2.5 cm height, 4.4 cm and 2 cm outer and inner diameter respectively. The operating frequency range is 20-40 kHz with good receiving sensitivity and transmitting power (-193 dB re 1V/μPa and 133 dB re 1μPa/V at 1m, respectively). The beam pattern is omnidirectional in the plane perpendicular to the axis of the ring, while in the planes containing the axis there is a minimum (reduction of 5 dB) of sensitivity responses at 60º. Moreover, the electronic noise is about -130 dB re $1V/(Hz)^{1/2}$ with a maximum input power of 300W with a 2% duty cycle.

The SEB [9] has been designed to match the characteristics of the FFR and for the requirements of the KM3NeT detector. The diagram of the SEB, which consists of three parts, is shown in Fig. 1. The first part, bottom part of the diagram, is a communication and control block which contains the microcontroller dsPIC. It manages the emission and the reception tasks and the settings, for instance setting the board with arbitrary waveforms. The emission block, in the middle, consists of the digital amplification plus the transducer impedance matching. It is able to store 1.6 J of energy for emission. Whit the energy stored on the capacitor it is possible to emit signals of 3ms length (at the maximum power) having a voltage drop l smaller than 1V. Successively the transformer converts the input digital signal to an output signal with higher voltage (in the range 35–400 V_{pp}) in order to have enough amplitude to feed the transducer for the emission of the acoustics signals to compensate for attenuation over the large distances involved in the KM3NeT detector. The last part, shown on top, is the reception part. The main component is a relay to use the transducer as receiver. Furthermore, the designed SEB allows the transducer to emit high amplitude short signals (a few ms length) with arbitrary waveform. Moreover, it has been designed for low-power consumption and adapted to the deep-sea neutrino telescope infrastructure using power supplies of 12 V and 5 V with a consumption of 1 mA and 100 mA respectively. To avoid initial high currents, there is a current limit of 15 mA when the capacitor starts to charge from the 12V line. Few seconds later the current stabilizes at 1mA. The communication of the board with a control PC is established through the standard RS232 protocol. In order to have very good timing synchronization the emission is triggered using a LVDS bus controlled by the dsPIC with stability better than 1 μs [8].

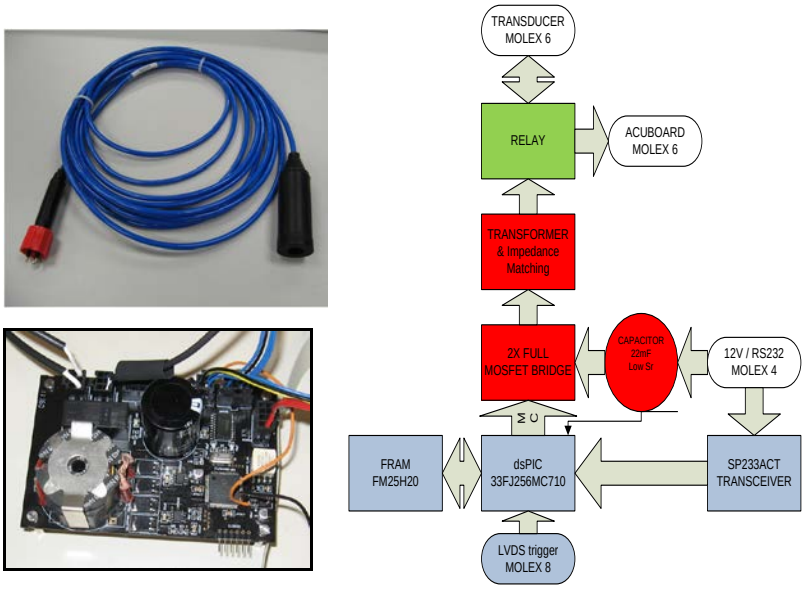

Figure 1: Views of the Free Flooded Ring transducer, of the Sound Emission Board, and its diagram.

2.3.4 Tests of the transceiver.

Different tests have been performed with the acoustic transceiver in order to check that the specifications are met. For instance, pressure tests were performed and reported in [8]. Other tests were performed in a tank of 87.5 x 113 x 56.5 cm^3 , and in a pool of 3.6 x 6.3 x 1.5 m^3 (fresh water in both cases) to study the transmitting voltage response and the directional response. The results have been reported in [5]. Here, we report the tests performed in the Gandia Harbour (Spain) to check the performance of the transceiver over longer distances and the response in a noisy environment. Particularly, we were interested in studying the use of different acoustic signals for positioning purposes. We were confident that the use of wideband signals, Maximum Length Sequence (MLS) signals and sine sweep signals, instead of pure sinusoidal signals may result in an improvement of the signal-to-noise ratio, and therefore resulting in an increase in the detection efficiency, as well as in the accuracy of the time of detection.

The transceiver (SX30 FFR plus SEB) was used as emitter. A second SX30 FFR with a RESON preamplifier, model CCA1000 (20 dB gain), was used as receiver hydrophone. Here, we show the results for a distance of about 140 m between the emitter and receiver. Figure 2 shows the receiving signals using a MLS signal (order: 11, sampling frequency: 200 kHz), a linear sine sweep signal (frequency range: 20-48 kHz, length: 4 ms), and a pure sinusoidal signal (frequency: 30 kHz, length: 4 ms). The signals were recorded

using an external trigger synchronization system between the emitter and the receiver. The system produces a delay of 8.25±0.03 ms in the receiver channel. The direct signal arrives at about 0.085 s. Since the noise is quite high (~Pa), and there are reflections, the signals are not easy to identify. However, as shown in Figure 3, looking at the correlation between the receiving and the emitted signal, the time when the signal appears is clearly observed. For the case of the MLS and sine sweep signals, a clear thin peak is observed, and therefore it is easy to determine the time of detection. The other peaks are due either to reflections or to the noise. The measurements were performed three times obtaining a time of detection of 85.08±0.03 ms (~4.5 cm uncertainty) for the MLS signal and of 85.075±0.015 ms (~2.3 cm uncertainty) for the sine sweep signal. Notice that the accuracy is similar to that of the synchronization system. Therefore, these measurements do not allow for the determination of the time detection uncertainty of the APS prototype, the measurements are compatible with those taken previously in the lab with uncertainties on the order of a microsecond.

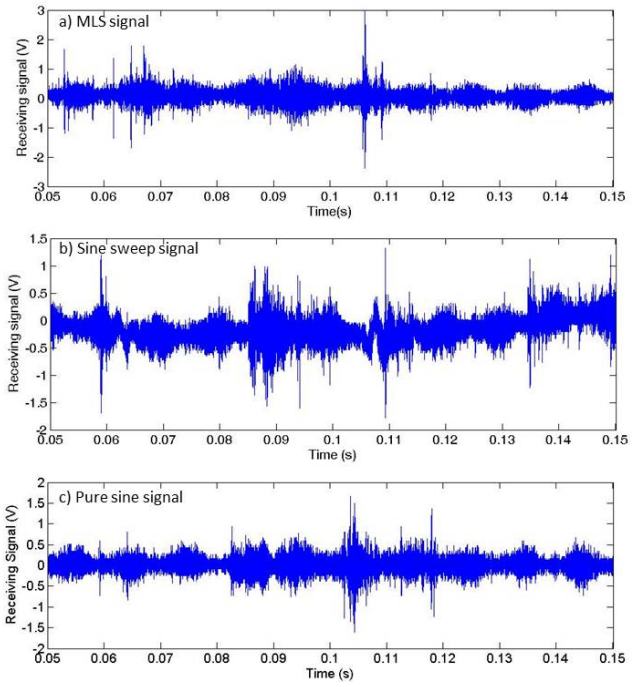

Figure 2: Receiving signal using three different kinds of signals.

The case of the pure sinusoidal signal is completely different. As shown in Figure 3, a very broad peak is obtained, the time of the maximum being quite sensitive to noise or reflections. Following the previous approach, an uncertainty of the millisecond order is

obtained, and therefore this method is not the best one for this kind of signals. Usually, a band-pass frequency filter is applied, and the detection time is determined by reaching a threshold level [11-12]. Doing this properly requires a very accurate calibration in order to determine the inertial delay of the hydrophone, and even so, it can give bad results in case of high noise or intense reflections nearby that can add to the waves constructively, as it happened during our measurement in the harbour. In contrast, the cross-correlation of broadband signals is less sensitive to these effects. The inertial delay, which affects mainly the start and end of the signal, is rendered less important by considering the whole duration of the signal. The effect of the reflections is reduced by distinguishing between different peaks of the cross-correlated signal, the first main peak being the one to consider.

Finally, in order to perform an in situ test, the system has been integrated in the active anchor of the Instrumentation Line of the ANTARES detector. The SEB was installed in a container which also houses a Laser system used for timing calibration purposes. A new functionality for the microcontroller of the SEB was implemented to control the laser emission as well The FFR hydrophone was fixed in the base of the line at 50 cm from the standard emitter transducer of the ANTARES positioning system with the area opposite to the moulding and the cable of the hydrophone looking upwards. It has been fixed through a support of polyethylene. The Instrumentation Line was successfully deployed at 2475 m depth on 7th June 2011 at the nominal target position. However, the connection of the Line to the Junction Box has been delayed and will be done when the ROV will be available (probably in April 2012). Once the line will be connected, the transceiver can be fully tested in real conditions. In addition, in April 2012 another transceiver prototype will be integrated in the NEMO phase II tower. As in the previous case, it will be fixed in the tower base and the SEB will be located inside a titanium container holding other electronic parts and a laser.

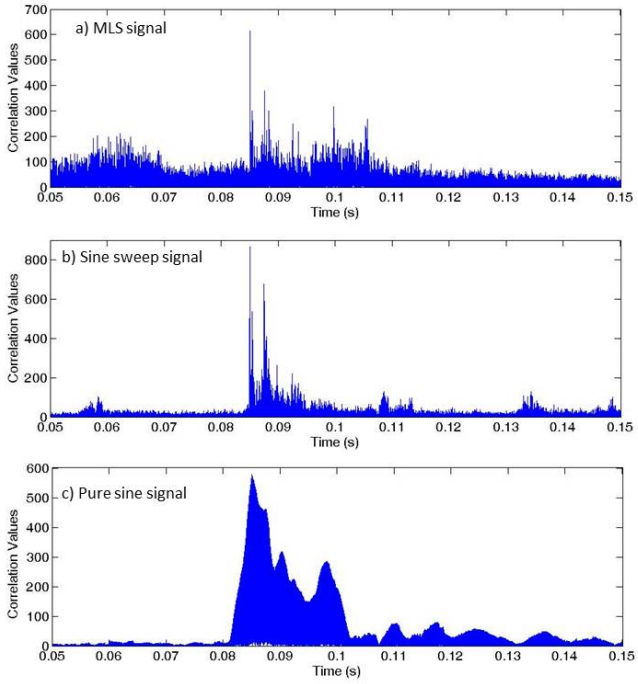

Figure 3: Correlation between emitted and received signals.

2.3.5 Summary and Conclusions.

An APS is needed in a deep-sea neutrino telescope and we have presented here studies and improvements done to develop a transceiver that will be implemented in KM3NeT. The tests and measurements done with the transceiver in the Gandia harbour do not allow for a measurement of the time detection uncertainty of the APS prototype with good precision, but allows us to say that the accuracy is better than 30 μs and the measurements are compatible with those taken previously in the lab with uncertainties on the order of a microsecond. Then, we can conclude that the transceiver seems to satisfy the requirements and accuracy needed for the APS. Moreover, the transceiver can handle a transmitting power above 170 dB re 1μPa@1m. Combined with adequate signal processing techniques positioning is possible with the system for the large distances involved in a neutrino telescope.

The system will be integrated in NEMO phase II tower in 2012 and it has been integrated in the ANTARES neutrino telescope (waiting for the connection of the Instrumentation Line) to test the transceiver in situ in the deep-sea.

2.3.6 Acknowledgments.

This work has been supported by the Ministerio de Ciencia e Innovación (Spanish Government), project references FPA2009-13983-C02-02, ACI2009-1067, AIC10-D-00583, and Consolider-Ingenio Multidark (CSD2009-00064). It has also been funded by Generalitat Valenciana, Prometeo/2009/26, and the European 7th Framework Programme, grant no. 212525.

2.3.7 References.

[1] KM3NeT Consortium, Technical Design Report, 2010, ISBN: 978-90-6488-033-9, available at <http://www.km3net.org>.
[2] M. Ageron et al. (ANTARES Collaboration), Nucl. Instr. and Meth. A 656 (2011) 11.
[3] M. Taiuti et al., Nucl. Instr. and Meth. A 626-627 (2011) S25.
[4] F. Ameli et al., Nucl. Instr. and Meth. A 626-627 (2011) S211.
[5] M. Ardid et al., Nucl. Instr. and Meth. A 626-627 (2011) S214.
[6] H. Motz, Nucl. Instr. and Meth. A 623 (2010) 402.
[7] C.H. Sherman and J.L. Butler, Transducers and Array for Underwater Sound, The Underwater Acoustic Series, Springer, 2007.
[8] M. Ardid et al., Nucl. Instr. and Meth. A 617 (2010) 459.
[9] C.D. Llorens et al., J. Instrum. (2012), *7*, C01001.
[10] F. Simeone et al., Nucl. Instr. and Meth. A 662 (2012), S246.
[11] M. Ardid (for the ANTARES Collaboration), Nucl. Instr. and Meth. A 602 (2009) 174.
[12] J.A. Aguilar et al. (ANTARES Collaboration), Nucl. Instr. and Meth. A 626–627 (2011) 128.

2.3.8 Acronyms.

ROV: Remotely Operated Vehicle.

2.4 Acoustic signal detection through the cross-correlation method in experiments with different signal to noise ratio and reverberation conditions.

S.Adrián-Martínez, M.Bou-Cabo, I.Felis, C.D. Llorens, J.A.Martínez-Mora, M.Saldaña, M.Ardid

Universitat Politècnica de València, Institut d'Investigació per a la Gestió Integrada de Zones Costaneres (IGIC)

Paranimf 1, 46730 Gandia, Spain

2.4.1 Abstract.

The study and application of signal detection techniques based on cross-correlation method for acoustic transient signals in noisy and reverberant environments are presented. These techniques are shown to provide high signal to noise ratio, good signal discernment from very close echoes and accurate detection of signal arrival time. The proposed methodology has been tested on different signal to noise ratio and reverberation conditions using real data collected in several experiences related to acoustic systems in astroparticle detectors. This work focuses on the acoustic detection applied to tasks of positioning in underwater structures and calibration such those as ANTARES and KM3NeT deep-sea neutrino telescopes, as well as, in particle detection through acoustic events for the COUPP/PICO detectors. Moreover, a method for obtaining the real amplitude of the signal in time (voltage) by using cross correlation has been developed and tested and is described in this work.

2.4.2 Introduction.

Acoustic signal detection has become an object of interest due to its utility and applicability in fields such as particle detection, underwater communication, medical issues, etc. The group of Acoustics Applied to Astroparticle Detection from the Universitat Politècnica de València collaborates with the particle detectors ANTARES [1], KM3NeT [2] and COUPP/PICO [3]. Acoustic technologies and processing analyses are developed and studied for positioning, calibration and particle detection tasks of the detectors.

Acoustic emitters and receivers are used for the positioning systems of underwater neutrino telescopes ANTARES [4] and KM3NeT [5] in order to monitor the position of the optical detection modules of these telescopes. The position of optical sensors need to be monitored with 10 cm accuracy to be able to determine the trajectory of the muon produced after a neutrino interaction in the vicinity of the telescope from the Cherenkov light that it produces [6]. An important aspect of the acoustic positioning system is the time accuracy in the acoustic signal detection since the positions are determined from triangulation of the distances between emitters and receivers, which are determined from the travel time of the acoustic wave and the knowledge of the sound speed. The distances

between emitters and receivers are of the order of 1 km. Therefore, the acoustic emitted signals suffer a considerable attenuation in the medium and arrive to the acoustic receivers with a low signal to noise ratio. The environmental noise may mask the signal making the detection and the accurate determination of its arrival time a difficult goal, especially for the larger future telescope KM3NeT with larger distances.

On the other hand, an acoustic test bench has been developed for understanding the acoustic processes occurred inside of the vessels of the COUPP Bubble Chamber detector when a particle interacts in the medium transferring a small amount of energy, but very localized, to the superheated media [7]. This interaction produces a bubble through the nucleation process. Under these circumstances the distance from the bubble to the vessel walls are very short (cm order) and a reverberant field generated by multiple reflections in the walls takes place. With these conditions, the distinction of the direct signal from reflection is quite difficult to achieve, being also quite complex to determine the time and amplitude of the acoustic signal produced.

The elaboration of protocols and post-processing techniques are necessary for the correct detection of the signals used in these tasks. Methods based on time and frequency analysis result insufficient in some cases. The first step consists of using the traditional technic of cross-correlation between the received signals and the emitted signals (expected) for localizing the source distance. In addition, the use of specific signals with wide band frequency or non-correlated such as sine sweep signals or Maximum Length Sequence (MLS) signal together with correlation methods increase the amplitude and the correlation peak narrows, this allows a better signal detection, improves the accuracy in the arrival time and the discernment of echoes.

In this work the detection of acoustic signals with a unique receiver under a reverberant field or a high noise environment is shown. The correlation method has been studied and applied for this purpose. Moreover, a method for obtaining the real amplitude of the signal (voltage) by using cross-correlation technique has been developed. Its validation has been done by comparing the results with the ones obtained by analytic methods in time and frequency domain, achieving a high reliability for the accurate detection of acoustic signals and the analysis of them. The results obtained in these tests in different environments using different kind of signals are shown.

In section 2 the cross-correlation technique is described, as well as the method proposed for signal detection. The application of the method under different situations: high reverberation, low signal-to-noise ratio (S/N) or very low S/N, is presented in section 3. Finally, the conclusions are summarized in section 4.

2.4.3 The cross-correlation method for signal detection.

Cross-correlation (or cross-covariance) consists on the displaced dot product between two signals. It is often used to quantify the degree of similarity or interdependence between two signals [8]. In our case, since all measurements were recorded using a digital acquisition system, all signals under study have been worked in discrete time, so that the correlation between two signals x and y with the same N samples length is expressed by the following expression:

$$Corr\{x, y\}[n] = \sum_{m=1}^{N} x[m] \cdot y[m+n] \tag{1}$$

If we do $y = x$ we obtain the autocorrelation of the signal x.

Figure 1 shows the appearance of the signals used in these studies: tones, sweeps, and MLSs. On top, there are these ideal signals in the time domain, that is, the generated signals by the electric signal generator equipment. In the middle row, the spectrum of each signal can be seen, where the different bandwidths can be appreciated. At the bottom, the autocorrelations of each signal show that the higher bandwidth signals have a narrower correlation peak, so, in principle, they are easier to detect. To understand the importance and convenience of using these signals in each detector, the reader can look at articles [9,10].

It is worth to note that, in the cases shown, the correlation peak amplitude ($V_{max,corr}$) is the same and equal to the number of samples of the signal in question (N). Therefore, it can be obtained the peak voltage of the signal (V_p) by the following expression:

$$V_p = \frac{2 V_{\max,corr}}{N} \tag{2}$$

Furthermore, this ratio does not vary with the amplitude of the signal and is less susceptible to the presence of noise.

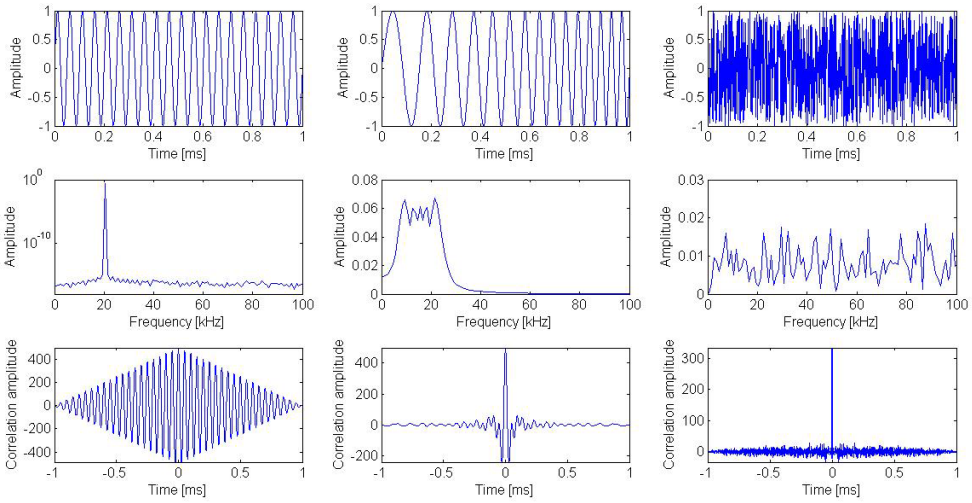

Fig. 1. Signals used for acoustic studies: tone, sweep and MLS.

However, the interest is the use of the method for the accurate detection of signals and the recorded signals will be influenced by reflections and noise that may vary the amplitude and profile of the direct signal detection.

Figure 2 shows the case of a tone, a sweep and MLS received signals with a distance of 112.5 m between emission and reception (E-R). On the top, the receiving signals in time domain after applying a high order band pass filter are shown (the original recorded signal in time is so noisy that the receiving signal is completely masked). On the bottom, it can be seen the cross-correlation of each signal (without prefiltering) where direct signal and reflections are easier and more effective to discern that working in the time or frequency domains, especially for high bandwidth signals (narrower auto-correlation peak).

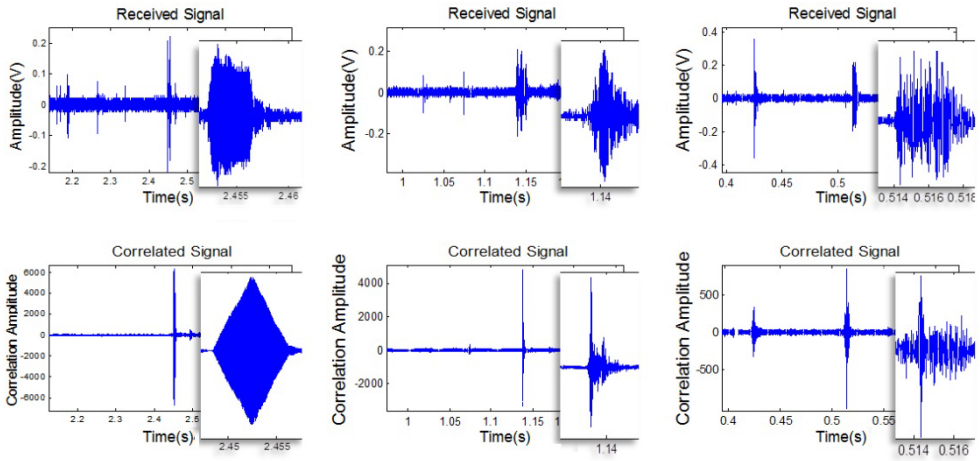

Fig. 2. Example of recorded signals at 112.5 m Emitter-Receiver distance in the harbor of Gandia.

Nevertheless, using this it is only possible to locate the signal but cannot know a priori the peak amplitude of the signal. This is because trying to tackle the problem from both time and frequency domains is completely crucial windowing temporarily the direct signal avoiding reflections to obtain a reliable value of its amplitude, which is not always possible.

Then, it would be important to obtain the corresponding relation between the maximum of the cross-correlation between received and emitted signal with the amplitude of the received signal avoiding reflections. This issue has been studied and has been found that if the amplitude of the signal sent ($V_{p,env}$), its number of samples (n_{env}) and the maximum correlation value ($V_{max,corr}$) corresponding to the detection of this signal are known, then it is possible to obtain the peak-amplitude voltage of the received signal applying the following expression:

$$V_{p,rec} = \frac{V_{\max,corr}}{V_{p,env}} \frac{2}{n_{env}} \tag{3}$$

In the following sections the results of applying this equation to the results of the correlations obtained and compared with values obtained applying time and frequency domain methods are presented. In addition, the improvements obtained by using this technique in terms of detection accuracy in different acoustical environments are also shown.

2.4.4 Application.

The different conditions in which the measurements of acoustic detection were performed are: inside a small vessel, in a tank of acoustic test, in a pool, in the harbor of

Gandia, and in ANTARES deep sea neutrino telescope. Although under different conditions of pressure, salinity and temperature, the acoustic propagation media in all the tests is water. Table 1 shows the relationship between the wavelength range associated with the studied signals (λ) and the geometrical dimensions of the places where acoustic processes occur (l).

Table 1. Characteristics of the acoustic conditions of the different measurements and tests.

Measure condition	*Characteristic distance l [m]*	*λ / l*
Vessel	*0.02*	*2.2*
Tank	*0.05-1*	*0.22*
Pool	*4*	*0.022*
Harbor	*120*	*0.0005*
Sea	*200*	*0.0003*

With this, it follows that conditions with higher ratio λ/l means working in a reverberant field, with a higher complexity, while configurations with a smaller λ/l ratio means that there is a less reverberant field, but usually a lower S/N ratio. As discussed below, both extreme situations make difficult the process of acoustic detection.

The results obtained in these conditions, the acoustic systems used in transmission and reception, and the results in terms of improvement of signal detection and S/N using cross-correlation method are shown in the following sections.

2.4.5 High reverberation conditions: vessel and tank.

When emitter and receiver are close and the dimensions of the enclosure where the acoustic processes occur are comparatively small, both signal and reverberation are high. This is the case of the configurations shown in Figure 3 that corresponds to a part of the acoustic test bench for COUPP detector [11]. On the left, the two experimental setups are shown. The first one corresponds to acoustic propagation studies inside a vessel, and the second one was used to study the acoustic attenuation. On the right the transducers used are shown. The signal was emitted with the pre-amplified ITC 1042 transducer and received with the needle-like RESON TC 4038 transducer.

Fig. 3. Experimental setups (left) and transducers used (right).

Figure 4 shows an example of a 30 kHz tone of 5 cycles of duration emitted and recorded under these conditions and their cross-correlation. It can be seen that the maximum of the correlation corresponds with the reception time of the received signal.

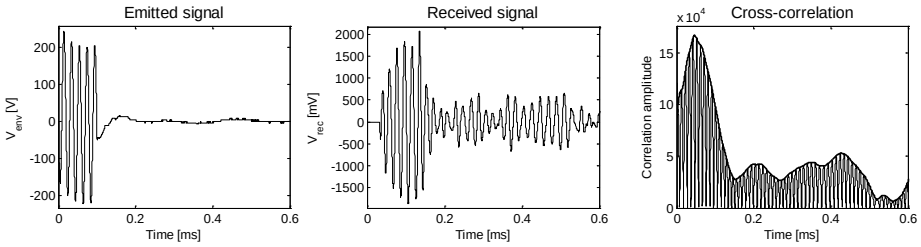

Fig. 4. Example of emitted signal, received signal, and cross-correlation.

Figure 5-left shows that for the tones studied between 10 kHz and 100 kHz the accuracy of this method is quite good, with an error smaller than 10 %. Considering the characteristic dimensions of the problem and 1500 m/s as sound propagation speed, this uncertainly is of the same order of magnitude of the experimental uncertainly (1 mm). As expected, the maximum deviation corresponds to lower frequencies, and it seems there is some frequency dependent fluctuations. This can be another argument in favor of using broadband signals for cross-correlation techniques.

The received amplitudes of the signals have been obtained using equation (3). The results are shown in Figure 5-right compared to the results obtained with standard techniques in time and frequency domains. It can be observed that the results are very similar.

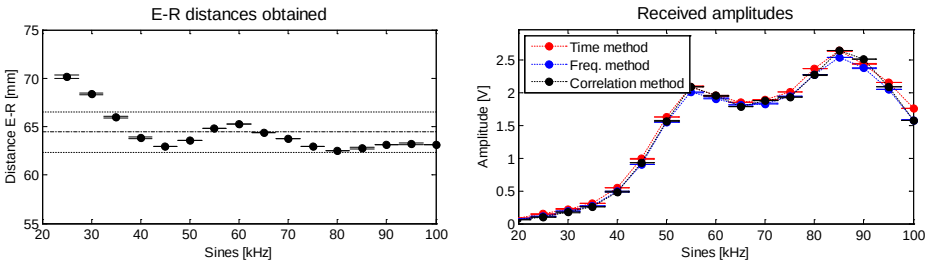

Fig. 5. Left: distances obtained between emitter and receiver by cross-correlation with tones between 20 kHz to 100 kHz. Right: Received amplitudes through the cross-correlation method using Eq.3 and using time and frequency domain methods.

2.4.6 Low signal to noise ratio conditions: pool.

The following configuration used is an intermediate step between high signal to noise ratio (section 3.1) and very low signal to noise (measurements in the harbor and in the ANTARES neutrino telescope, presented in the next section 3.3 and 3.4 respectively). This is the case of measurements taken on a pool as shown in figure 6 (left). In this experimental setup, the transmitter consists of an array of three transducers FFR SX83 (middle) and an electronic board to generate and amplify the different acoustic signals. This system can operate in three different modes: emitting with a single element, with the three elements connected in series and the three elements connected in parallel [10]. Our measures were made with the transducers connected in parallel so, in this embodiment, higher transmission power is obtained. The reception was performed using a FFR SX30 (right).

Fig. 6. Experimental setup (left), emitter (middle) and receiver (right) transducers.

Using tones between 10 kHz and 60 kHz in these conditions, we have calculated the emitter-receiver distances from flight times, as described above. The results are shown in figure 7 and compared with those obtained directly in time-domain method. In this case, we can see that the deviation of the measurements relative to a mean value is 5%, which corresponds to an uncertainty less than ± 20 cm. However, if we discard some out-layer measure (sine of 40 kHz) the deviation of the values is reduced to 2.3%, i.e., ± 9 cm. We think that a reason for the relatively large variation between different measurements at different frequencies might be the interference between the three emitters of the array, which depends on the frequency. Again here, the use of broadband signals with the cross-correlation method may help to mitigate this problem since it will average the response of the different frequencies.

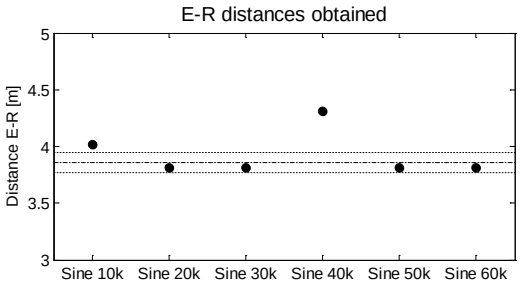

Fig. 7. Emitter-receiver distances obtained by cross-correlation method using tones between 10 kHz to 60 kHz (considering 1500 m/s as the sound propagation speed).

The plots of figure 8 show the results obtained by comparing the voltages (left) and the S/N ratios (right) both in cross-correlation method and time-domain method (in this case, since the signals can be windowed properly, avoiding the presence of reflections, values obtained in time and frequency domains are coincident).

As before, using the Eq. 3 very similar results to the usual techniques are obtained. On the other hand, the S/N ratio increases considerably (at least 20 dB) for the set of signals used using correlation method. This improvement is crucial for a correct detection of the signals.

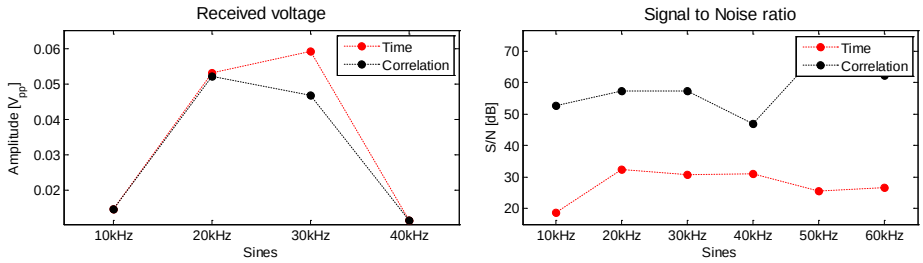

Fig. 8. Comparison of cross-correlation and time domain method to obtain the received voltage amplitude (left) and the S/N ratio (right).

2.4.7 Very low signal to noise ratio conditions: harbour.

The first kind of measures taken in very low signal to noise ratio condition has been done in the port of Gandia. The acoustic signals were emitted from one side of the harbor and received from the other side, as it can be seen in figure 9 (left), the distance between the emitter and the receiver was about 120 m. The emitter and receiver transducers used were the same as the ones used in pool measurements (section 3.2).

Fig. 9. Measured conditions (left), emitter (middle) and receiver (right) transducers.

In this case, tones of 10 kHz and 30 kHz, a sweep between 5 to 50 kHz and a MLS signals were used. As it can be shown in figure 10, with these signals we have obtained the distances between emitter and receiver around 113 m with a precision of ± 30 cm.

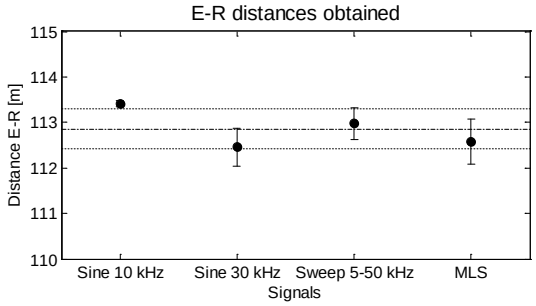

Fig. 10. Emitter-receiver distances obtained by cross-correlation method using tones of 10 kHz and 30 kHz, 5 to 50 kHz sine sweep and MLS signals.

In these measures, the amplitudes obtained in time and cross-correlation present more deviation by using a 10 kHz tone, however these amplitudes are very close if we look at higher frequencies, as it can be shown in figure 11. Additionally, the signal to noise ratio increases more than 10 dB in the signals analyzed using the cross-correlation method, which helps significantly its detection in this noisy environment.

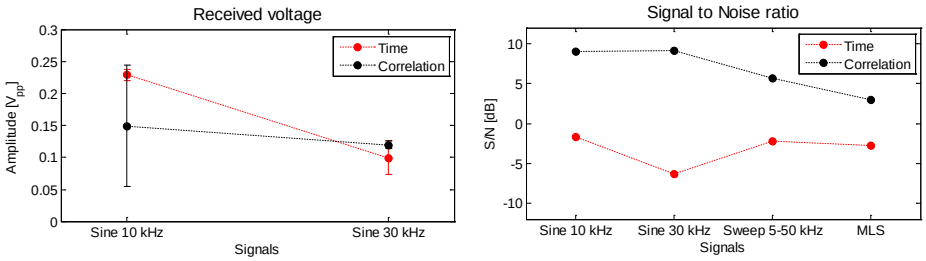

Fig.11. Comparison of cross-correlation and time domain method to obtain the received voltage amplitude (left) and the S/N ratio (right).

2.4.8 Very low signal to noise ratio: sea.

The more complex environment in which this study has been performed is the acoustic measurements made in situ in deep-sea at the ANTARES site. In this case, the distance between emitter and receiver was about 180 m and the S/N ratio was quite low. Figure 12 shows on the left an artistic and schematic view of the telescope. The emitter was a FFR SX30 transducer, shown in the middle, with an electronic board designed specifically for this type of transducer to optimize and amplify the signal sent [10,12], and the receiving hydrophone was a HTI-08 transducer, shown on the right [13].

Fig. 12. View of the ANTARES neutrino telescope (left) and pictures of the emitter FFR SX30 (middle) and of the receiver HTI-08 (right) transducers.

Since in this ANTARES test synchronization between transmitter and receiver was not available, it is not possible to calculate absolute flight times. However, the received amplitude expression as well as the increase of the S/N ratio obtained by cross-correlation method can be evaluated here, as shown in figure 13. In this case, sine signals of 20, 30 and 40 kHz, 20 to 48 kHz and 28 to 44 kHz sweep signals and MLS (order 11) signals were used.

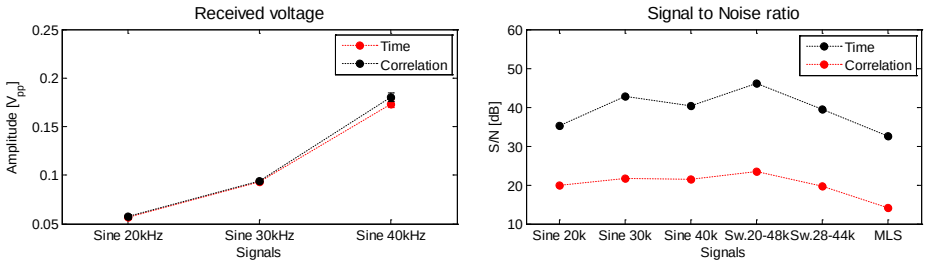

Fig. 13. Received amplitude (left) and S/N ratio (right) both in cross-correlation and time domain method.

It can be concluded from these measurements that using the cross-correlation method is possible to obtain the signal amplitude accurately and obtain an increase of 15 to 20 dB in the S/N ratio, with a consequent improvement in the acoustic detection.

Additionally, and with the aim of applying this technique for post-processing signals in the future KM3NeT neutrino telescope, simulations of propagation of signals measured in ANTARES over longer distances have been done. The received signals measured have been propagated to further distances (up to 2.16 km) in order to know the pressure levels reached and the amplitude signal received by the hydrophones and its correlation amplitude. The signals received are propagated applying the spherical divergence loss transmission and the sea water absorption coefficient per frequency. The propagation has been performed following the steps shown in the diagrams of Figure 14. The diagram on the left shows the digital processes in order to know the expected amplitude per distance. The diagram on the right shows the processes to obtain the time detection by correlation method with the propagated signals added to real noise in different time position. Figure 15 shows, the improvement in the S/N ratio as a function of the distance using the different signals and methods.

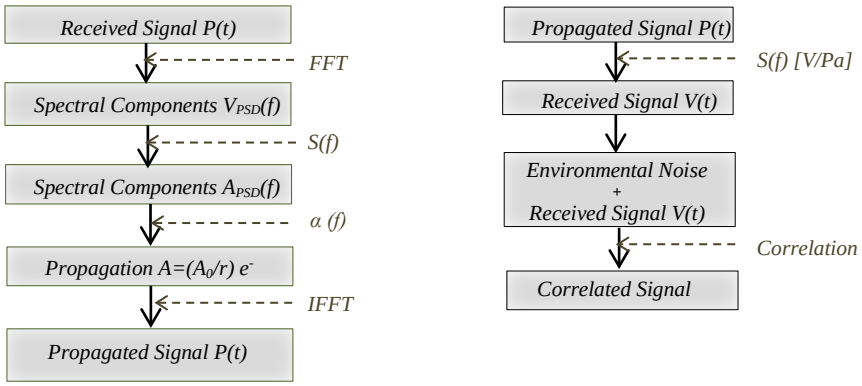

Fig. 14. Block diagrams of the received signal propagation

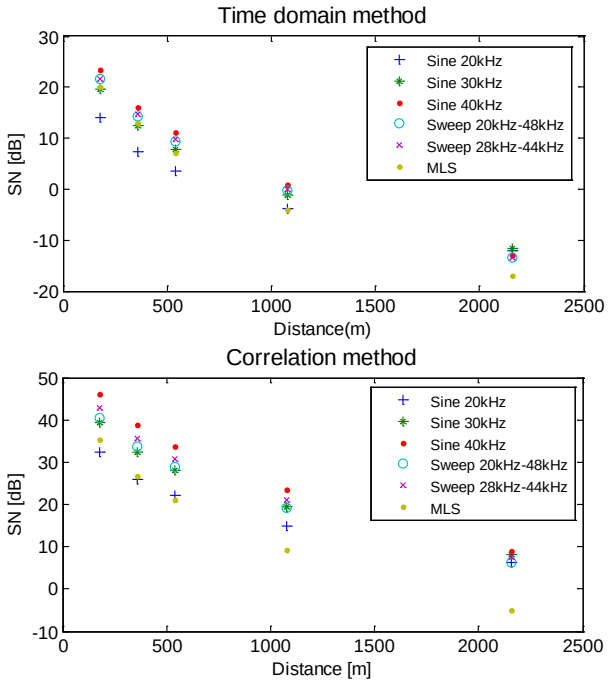

Fig. 15. S/N ratio obtained using time domain method (top) and cross-correlation method (bottom).

Finally, in order to determine the reach of the system in terms of time detection accuracy, propagated signals have been introduced in 100 random (but known positions) of noise recorded. We have studied the ability of detecting them as a function of the distance (from 180 m to 2.16 km) using the correlation method.

An example of the figures obtained in the processing performed are shown in Fig.16, the analysis with the sine sweep signal received at 180 m from the transmitter inserted to the 0.08 s of a section of 0.14 s noise is shown:

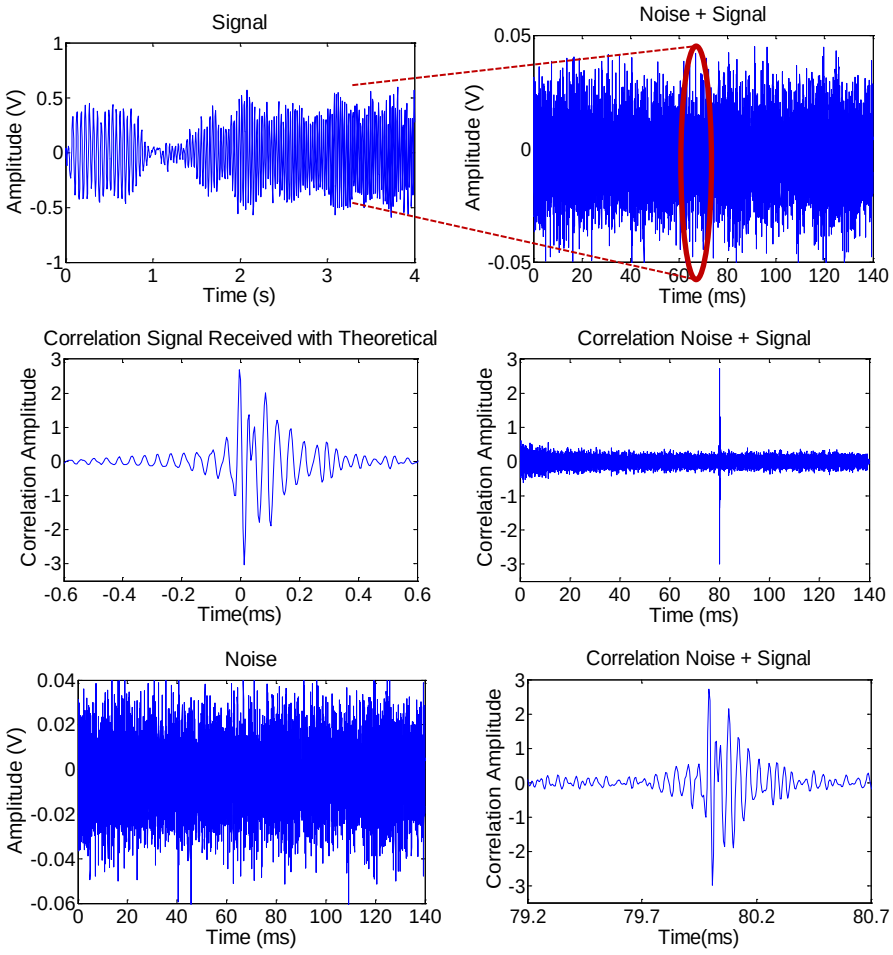

Fig. 16. Signal processing steps for the simulation of signal received at 180 m with noise.

The values of deviation time (mean and standard deviation) for the detected signal with respect the true time are shown in Fig. 17. The obtained results show that the sweep signal can be detected at a distance of 2.16 km with good accuracy. Notice, that even if the signal to noise ratio is not favorable, it is possible to detect the signals emitted up to 2.16 km with reasonable accuracy by using the detection signal technique describe above. By using this method, the acoustic emitter requires less acoustic power to reach the large distances needed and consequently it allows producing less acoustic pollution in the media.

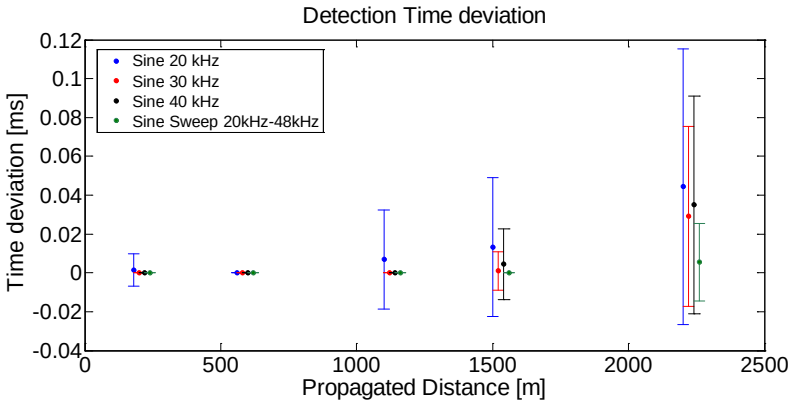

Fig. 17. Values of deviation time (mean and standard deviation), with respect the true time, for the detected propagated signal with noise. It is determined by the correlation detection method.

2.4.9 Conclusions.

We have seen that, using different signal emission-acquisition systems, working on a wide range of distances and in very different environmental conditions, good acoustic detection through the technique of cross-correlation between the emitted and received signals can be obtained. This technique is more favorable for broadband signals (sweeps and MLS) because they have a narrower correlation peak and consequently they are easier to discern than others peaks. Furthermore, this technique is powerful in measurement conditions with a reduced S/N ratio, as the case in marine environments over long distances where the recorded signal is weak, or in environments with high background noise. In addition, we have obtained a relation between the peak value of the cross-correlation and the voltage value of the received signal, which synthesizes and optimizes the signal analysis.

2.4.10 Acknowledgements.

This work has been supported by the Ministerio de Economía y Competitividad (Spanish Government), project ref. FPA2012-37528-C02-02 and Multidark (CSD2009-00064). It has also being funded by Generalitat Valenciana, Prometeo/2009/26, and

ACOMP/2014/153. Thanks to the ANTARES Collaboration for the help in the measurements made in the ANTARES deep-sea neutrino telescope.

2.4.11 References.

1. M. Ageron et al. (ANTARES Collaboration), *ANTARES: the first undersea neutrino telescope*, Nucl. Instr. And Meth. A, vol. 656 (2011) pp. 11-38.
2. The KM3NeT Collaboration, *KM3NeT Technical Design Report* (2010) ISBN 978-90-6488-033-9, available on www.km3net.org.
3. E. Behnke et al. (COUPP Collaboration), *First dark matter search results from a 4-kg CF3I bubble chamber operated in a deep underground site*, Phys.Rev.D 86, 052001 (2012).
4. M. Ardid, *Positioning system of the ANTARES neutrino telescope*, Nucl. Instr. and Meth. A, vol. 602 (2009) pp. 174-176.
5. G. Larosa and M. Ardid, *KM3NeT Acoustic position calibration of the KM3NeT neutrino telescope*, Nucl. Instr. and Meth. A, vol. 718 (2013) pp. 502-503.
6. M. Ardid, ANTARES: *An Underwater Network of Sensors for Neutrino Astronomy and Deep-Sea Research*, Ad Hoc & Sensor Wireless Networks, vol. 8 (2009), pp. 21-34.
7. M. Bou-Cabo, M. Ardid and I. Felis, *Acoustic studies for alpha background rejection in dark matter bubble chamber detectors*, Proc. of the IV International Workshop in Low Radioactivity Techniques. AIP Conference Proceedings, Vol. 1549, pp. 142-147 (2013).
8. J.G.Proakis & D.G.Manolakis, *Digital Signal Processing*, 3ed Prentice Hall (1996).
9. M.Saldaña. *Acoustic System development for the underwater neutrino telescope positioning KM3NeT*, Bienal de Física (2013).
10. M. Ardid et al., *Acoustic Transmitters for Underwater Neutrino Telescopes*, Sensors, vol. 12 (2012), pp. 4113-4132.
11. I.Felis, M.Bou-Cabo, M.Ardid, *Sistemas acústicos para la detección de Materia Oscura*, Bienal de Física (2013).
12. C.D. Llorens et al., The sound emission board of the KM3NeT acoustic positioning system, Journal of Instrumentation, vol. 7 (2012) C01001.
13. K. Graf, *Experimental Studies within ANTARES towards Acoustic Detection of Ultra High Energy Neutrinos in the Deep Sea*, Ph.D. thesis, U. Erlangen (2008) FAU-PI1-DISS-08-001.

2.5 Acoustic beacon for the positioning system of the underwater neutrino telescope KM3NeT.

M. Saldaña; M. Ardid; I. Felis; C.D Llorens; J. A. Martínez-Mora

Institut d'Investigació per a la Gestió Integrada de les Zones Costaneres (IGIC), Universitat Politècnica de València (UPV), 46730 Gandia, València, España.

2.5.1 Abstract.

The design and development of an acoustic beacon as part of the positioning system for the underwater neutrino telescope KM3NeT is presented. Acoustic positioning system is used to monitor the position of the optical sensors of the telescope (with 10 cm accuracy over distances of about 1 km), in which the acoustic beacons are the active elements. The acoustic beacon is able to generate high-power short signals in a frequency range of 20-60 kHz, hence signal processing techniques can also be used to improve the performance of the positioning system.

2.5.2 Introduction.

The Acoustic beacons have been developed to be part of the acoustic positioning system (APS) for the multi-cubic-kilometre underwater neutrino telescope KM3NeT located at the depths of the Mediterranean Sea. Currently, KM3NeT project is in its first construction phase, after the preparatory and design phases. At the end of this phase the detector will consists of 24 Detection Units (DUs) deployed off-shore in Capo Passero, Italy, (KM3NeT-IT) and 7 DUs, deployed off-shore in Toulon, France (KM3NeT-FR). Each DU hosts 18 digital optical modules (DOMs), each one equipped with 31 photo-multipliers tubes (PMTs) [1].

The KM3NeT telescope will detect neutrinos by measuring the Cherenkov light emitted by charged secondary particles produced in neutrino interactions with the sea water or the rock beneath. Since neutrinos interact so weakly, a huge volume of water must be observed to collect a sufficient number of such events. The direction of the incoming neutrino can be reconstructed with the telescope and its energy estimated. Accumulations of neutrino events pointing to particular celestial directions will establish the coordinates and characteristics of cosmic accelerators or other astrophysical neutrino sources.

During the telescope operation, in order to effectively reconstruct muon tracks, generated by the interaction of cosmic neutrinos with water nuclei, via the optical Cherenkov technique, the coordinates of the optical sensors must be known with an accuracy of about 10 cm. In the deep sea, DUs are anchored to the sea bed but they are free to move along their vertical expansion under the effect of currents, thus their positions must be determined and monitored. A long baseline (LBL) of acoustic transmitters placed on the seabed in known positions and an array of acoustic receivers rigidly connected to the

mechanical structures of the telescope will be used, therefore the optical sensor positions could be continuously calculated via triggered emission of acoustic signals. The distances from acoustic emitters and receivers of the line are of the order of 1 km, so acoustic signals emitted suffer a considerable attenuation.

2.5.3 Long Base-Line (Lbl) Positioning System.

The LBL positioning system of KM3Net is composed by an array of acoustic transmitters and receivers hosted on the DUs bases and on the Calibration Units bases (CBs). Each DU base will host a digital hydrophone, each CB will host an acoustic beacon and a digital hydrophone placed at known distance from the beacon. The LBL of the acoustic beacons installed on the CBs is complemented by an array of autonomous acoustic emitters (battery powered and driven by local clock) placed outside the footprint of the telescope, that improve the resolution of triangulation calculation for receivers placed on DU at the edge of the telescope field. Moreover, autonomous beacons must be used, during the installation of the first CBs, to create a temporary LBL field [2].

The positions of acoustic beacons, receivers and autonomous beacons must be geo-referenced during the deployment operation using GPS signal, available on board the ship that performs the deployment, with an accuracy of ±1 m. The main LBL system is time-synchronized and phased with the detector master clock. This allows the implementation of LBL auto-calibration and the possibility to accurately measure the Time of Flight (ToF) of acoustic signals emitted by each acoustic beacon to reach the acoustic receivers on DUs. The LBL acoustic beacons are reconfigurable by dedicated RS-232 bidirectional link between shore station and CU base electronics: acoustic emission signal parameters (amplitude, waveform, and timing) can be set for “in situ” optimization of the signal detection.

2.5.4 LBL Acoustic Beacon.

The acoustic beacon (MAB-100) developed by our group in cooperation with Mediterráneo Señales Marítimas SLL for the LBL positioning system is a broadband range acoustic emitter (20 kHz - 60 kHz) able to work at rating depths up to 400 bar in underwater environments. It provides the emission of short intense signals (Sound Pressure Levels of 180 dB re 1 µPa @ 1 m at 34 kHz) and has LBL functionality. The system is composed by a piezo-ceramic transducer and an electronic board integrated in an only piece system by a cylindrical hard-anodized aluminium vessel (Fig. 1) The transducer is a Free Flooded Ring (FFR SX30). The electronic board is specifically design to fulfil the positioning system requirements of the telescope, enabling the transducer communication and the signal emission control and amplification. It disposes of a serial interface communication via RS-232 for signal configuration from shore.

Figure 1. Acoubeacon MAB-100 device

2.5.5 AcouBeacon Piezo-Ceramic Transducer.

The FFR SX30 acoustic transducers are able to work in the frequency range of 20 kHz to 50 kHz with transmitting voltage responses of 130 dB re 1 µPa/Volt @ 1 m at 30 kHz. The maximum input power is 300 W with 2% duty cycle. They are able to operate at very large depth, satisfactory tested up to 440 bar maintaining good stability. These transducers have an omnidirectional directivity pattern on the radial plane and a toroidal (60°) directivity pattern on the axial plane [3, 4].

In order to ensure the transducer holding and protection, the nude transducer is moulded with a polyurethane material joined to a BH2M hard-anodized aluminium connector as shown in Fig. 2. It is screwed into one side of the vessel and connected to the electronic board placed inside.

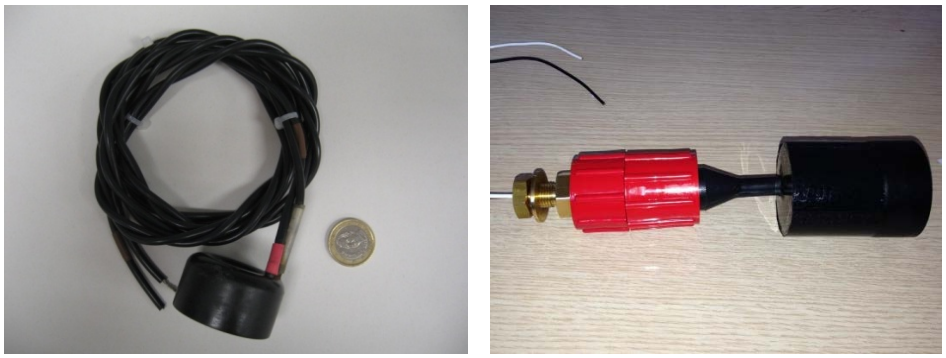

Figure 2. Nude (left) and molded (right) FFR SX30 Transducer

2.5.6 Acoustic specifications of the AcouBeacon.

The *AcouBeacon* emits a Sound Pressure Level (SPL) of 180 dB re 1 µPa @ 1 m at 34 kHz with a variation of ± 6 dB in the frequency range of 20 kHz to 60 kHz. The radial beam pattern is omnidirectional with ± 2 dB for each work frequency and the axial beam pattern is toroidal with ± 10 dB of variation at 60º and ± 5 dB at 180º. The acoustic

emission parameters are configured by commands through a RS-232 serial interface allowing signal reconfiguration from shore. There is a graphical interface for facilitating the user interaction. The signals parameters can be configured as following:

- Signal Emitted length: from 0 to 50 ms.
- Maximum emission amplitude: 180 dB @ 34 kHz re 1 µPa a 1 m.
- Type of acoustic signals:
  - Monochromatic signals configurable from 1 kHz to 80 kHz.
  - Sine Sweep signals configurable from 1 kHz to 80 kHz.
  - Maximum Length Sequence (MLS) signals with lengths from 5.12 ms to 40.96 ms (from 10th to 13th order and sampled at 200 kS/s).
- Modality of emission: external trigger response (LVDS with galvanic isolation). It disposes two operation emission modes; single and automatic (continue) emission.
- Variable temporal interval of emission between a signal and the successive one for the automatic emission mode from 0.5 s to 300 s.

The sound pressure level (dB re 1µPa@1m) of the acoustic beacon obtained with different capacitor charge (5V, 20V, 40V and 60V) is shown in Figure 3, in both radial and axial directions. Figure 4 shows the *AcouBeacon* directivity at axial direction.

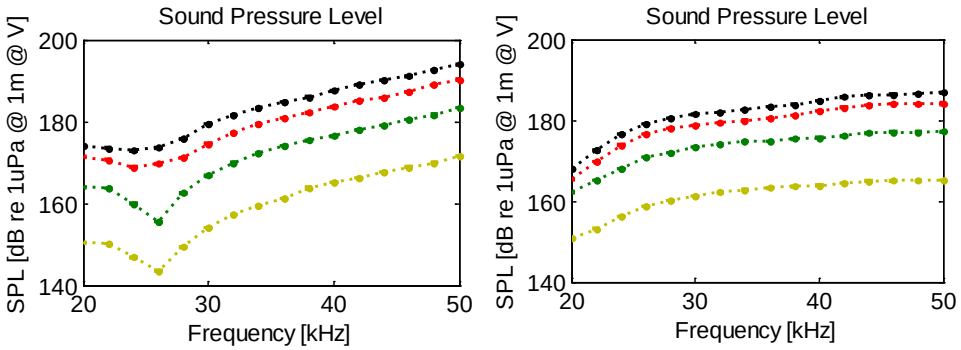

Figure 3. Sound Pressure Level (SPL) of the Acoubeacon at axial direction (left) and radial direction (right) for different capacitor charge.

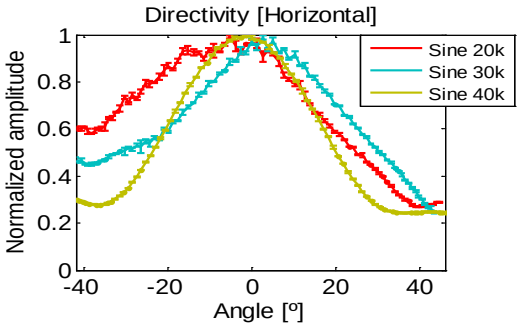

Figure 4. Directivity of the Acoubeacon

Positioning acoustic pulses will be emitted in the range of frequencies from 20 kHz to 50 kHz. In this range acoustic signals emitted in water with a SPL of 180 dB re 1 µPa at 1 m can effectively propagate until a distance of 2 km with about 110 dB re 1 µPa (depending on frequency) and it can be easily recognised by the acoustic receivers of the telescope.

2.5.7 Electronic specifications of the Acoubeacon.

The *Beacon Board* has been carefully designed to accomplish all the positioning requirements, as well as, to optimize and amplify the signal power emission [5]. The board is piloted by a dedicated electronics integrated at the base of the Calibration Units (CBs) that provides the bidirectional link to shore; this enables emission signal reconfiguration for 'in situ' signal detection optimization. Acoustic waveforms to be emitted are stored in a local memory that can be updated from shore via RS-232 link. The signal emission trigger is received from the CB electronics, synchronized with the detector master clock. The time synchronization and calibration with respect to the detector master clock is accurate and stable. The technical specifications of the Acoubeacon electronics are described in Table 1.

Table 1. Electronic specifications of the Acoubeacon for the LBL

Supply Voltage	12 V
current consumption	250 mA
Communications	Serial Port RS-232. Baud rate 9600, 8bits No parity 1 stop bit
Trigger Signal	Differential 1Vpp galvanic isolated Accuracy >±1µs
Emission Latency	<10 µs
Synchronization accuracy	<1 µs
Dimensions	Three boards (240x70mm all)
Lifespan	>=20 years

.

Figure 5. Acoubeacon Board

The electronic beacon board consists of three boards (Fig. 5): In the block diagram the yellow part is related with the DsPIC Board, the orange part related to the Supply Board and the red one to the Bridge Board.

The DsPIC Board has the main DsPIC processor that generates the PWM signal for the class D amplifier, a RS-232 isolated driver to receive the configuration commands protecting the supply of the telescope from emission noise, a galvanic isolated differential trigger reception to synchronize the emission of the beacon, a flash memory to store configuration and signals, and a temperature and humidity sensor to check the internal vessel status. The DsPIC board can also be connected to an external RS485/MODBUS pressure and temperature sensor that can check the external vessel conditions.

The Supply Board receives the 12 V external supply and uses it by means of a common mode filter and a current limiter that protects the telescope supply from

noise and inrush current. After this protection the board has two DC-DC converters; one to feed the DsPIC board with 5 V and the other to provide 60 V for the emission. The 60 V are used to charge/discharge the main capacitor in the Bridge Board using a constant current source and a constant current sink. The main capacitor is charged slowly up to the desired emission voltage which is read from the main DsPIC using an ADC input.

Finally, the Bridge board consists of a power Mosfet H Bridge which amplifies the PWM signal that comes from the DsPIC using the energy stored in the main capacitor. The H Bridge is coupled to the transducer through a transformer that reduces the impedance.

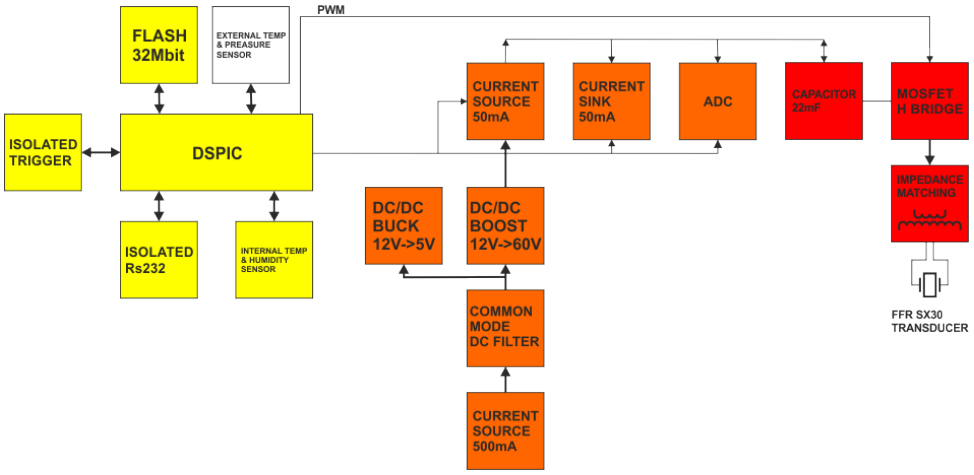

Figure 6. Block diagram of the electronic board

2.5.8 Mechanical specifications of the AcouBeacon.

The AcouBeacon mechanical assembly consists of a cylindrical pressure vessel with a transducer screwed on the front endcap and hold firmly with a clamp (Fig. 7). The total length of the system is 575 mm; 400 mm length of the vessel including connector and 175 mm length of the complete transducer. The pressure vessel is a sealed system that contains the internal electronics in a secure environment, it isolates the electronics from external pressure and water and keeps them in proper humidity conditions. It is able to safely support pressure levels up to 400 bars.

The pressure vessel is composed of a closed aluminium hull and two removable endcaps with collar hulls and a light inner chassis where the electronic board is located. The endcaps have double O-ring seals to ensure sealing and closing by collar hulls. There are entries on both end caps of the vessel; one in the rear endcap for the passage of the power supply to the electronic board, using a Seacon Microwet MC-BH-6M hard-anodized aluminium connector, and one on the front endcap for the acoustic transducer connection to the board through a BH2M hard-anodized aluminium connector. The vessel material is hard anodized aluminium L6082-T6 of 60 microns and the hardware used is AISI316 (A4).

The acoustic transducer FFR SX30 is located in the front of the vessel conveniently moulded to cable signal using a polyurethane mould. The moulded transducer joint is subject to the vessel by means of a plastic (Arnite) clamp that guarantee the correct stability and strength of the issuer, without affecting the acoustic properties of the transducer, especially the directivity.

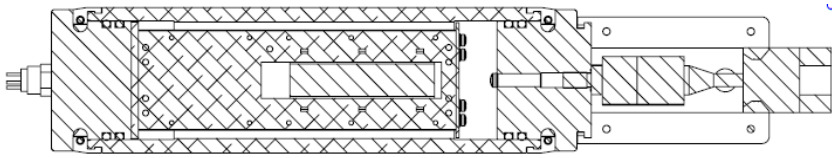

Figure 7. Drawing of the Acoubeacon, internal mechanical structure.

2.5.9 Signal processing technics for detection optimization.

Protocols and post-processing techniques have been developed for the correct detection of the signals used for the positioning system. The distance from the emitters and receivers can be of the order of 1-2 km, therefore acoustic emitted signals suffer a considerable attenuation and arrive to the acoustic receivers of the detection units with a low signal to the environmental noise ratio. The noise masks the signal making its detection and the accurate knowledge of its arrival time a difficult goal [6].

The time of arrival (ToA) is determined by the difference between the emission time and the initial time of the receiving signal. The receiving time is obtained by two different methods: the threshold method used for sine signals mainly and the cross-correlation method of the received signal used mainly for the broadband signals: sine sweep and maximum length sequence (MLS) signals [7].

The threshold method determines the initial time of the received signal by taking a rise time value of the received signal envelope after applying a band-pass filter centred in the frequency of the emitted signal. The cross-correlation method determines the arrival time of the received signal by taking the interval of time corresponding to the maximum peak of the cross-correlated signal with the expected emitted signal. This technique is more favourable for broadband signals (sweeps and MLS) because they have a narrower correlation peak and consequently the mean peak is easier to discern than the other peaks. Figure 8 shows a tone, a sweep and MLS received signals with a distance of 112.5 m between emission and reception (E-R) in some measurement tests made in Gandia's harbour. On the top, the receiving signals in time domain after applying a high order band pass filter are shown (the original recorded signal in time is noisy so the receiving signal is masked). On the bottom, it can be seen the cross-correlation of each signal (without prefiltering) where direct signal reflections are easier and more effective to discern that working in the time or frequency domain, especially for the broad bandwidth signals (narrower auto-correlation peak).

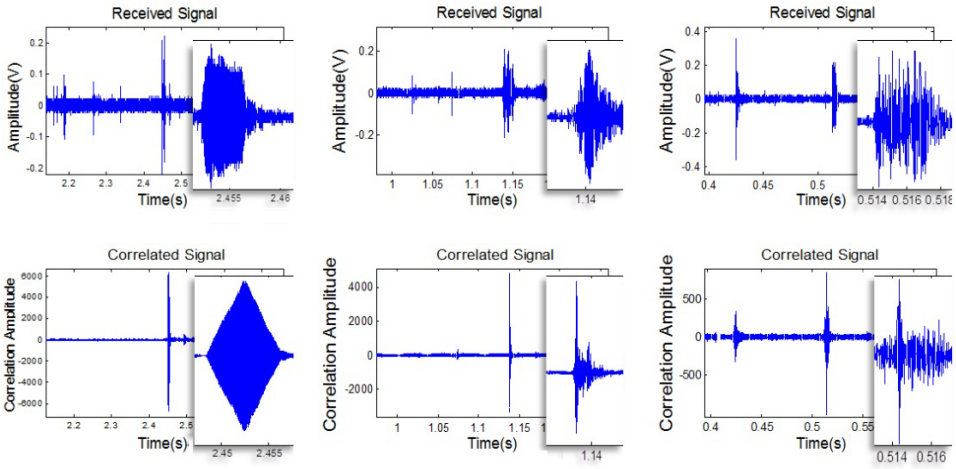

Figure 8. Example of recorded signals at 112.5 m E-R in the harbour of Gandia.

In situ test with the first's acoustic beacon prototypes have been performed in the neutrino telescope infrastructures installed in Capo Passero (NEMO) [8] and in ANTARES site [9, 10]. The emitted signals were sine signals of 20 kHz, 30 kHz and 40 kHz, sine sweep signals from 20 kHz to 48 kHz and from 28 kHz to 44 kHz, and MLS signal.

The data recorded in NEMO tower test (3500 m depth) was taken by hydrophones from all floors of the tower in which the emitter is located on the base. The distance from emitter to the first floor is about 100 m and between floors is around 40 m and the line has a total of 8 floors with two hydrophones per floor. As an example of the ToA obtained at the NEMO test, Fig. 9 shows the ToA obtained from the sine sweep signal from 20 kHz to 48 kHz applying the cross-correlation method. Table 2 shows the stability of the ToA values obtained from all hydrophones per signal.

Table 2. Stability of ToA values from all hydrophones per signal.

	THRESHOLD METHOD	CORRELATION METHOD
SIGNAL	SIGMA [ms]	SIGMA [ms]
Sine 20 kHz	0.065	0.103
Sine 30 kHz	0.031	0.046
Sine 40 kHz	0.029	0.029
Sweep 20kHz48kHz		0.027

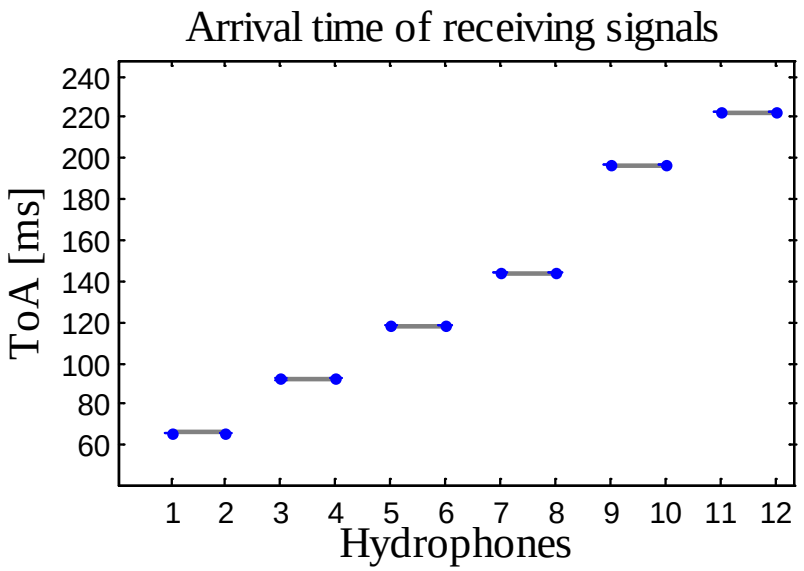

Figure 9. Time of arrival (ms) with the 20 kHz- 48 kHz sine sweep.

The results of the tests performed in situ show that the time of arrival obtained matches with the expected distances from the emitter to the hydrophones, as well as, a good stability is obtained.

The signal to noise ratios obtained by using the filter and threshold in time and cross-correlation methods to determine the amplitude; are shown in Fig. 10 for a distance between the emitter and receiver of 180 m.

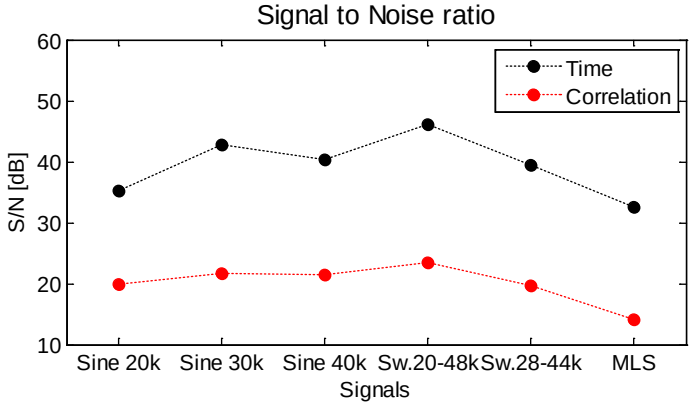

Figure 10. S/N ratio both in cross-correlation and time domain method.

Figure 10 shows that using the cross-correlation method is possible to obtain accurately the signal amplitude and getting an increase of between 15 and 20 dB in the S/N ratio, with a consequent improvement in the acoustic detection.

2.5.10 Conclusions.

The acoustic beacon developed satisfies all the requirements for the KM3NeT-LBL acoustic positioning system. The beacon works properly in terms of functionality, matching, operation modes, signal configuration and power emission. The tests and calibration performed show stable and favourable results.

From the study of the signal processing technics with the analysis realized from the different measures performed in situ, we can conclude that by using the cross-correlation method with broadband signals (sweeps and MLS) the signal detection is optimized; it enlarges the S/N ratio improving the arrival time detection and its accuracy.

2.5.11 Acknowledgements.

This work has been supported by the Ministerio de Economía y Competitividad (Spanish Government), project ref. FPA2012-37528-C02-02, by Generalitat Valenciana, projects ACOMP/2015/175 and PrometeoII/2014/079, by the project Multidark (CSD2009-00064), and the European FEDER and 7th Framework Programmes, Grant no. 212525. Thanks to KM3NeT, ANTARES, and NEMO/SMO Collaborations for the help.

2.5.12 Bibliography.

[1] The KM3NeT Collaboration, KM3NeT Technical Design Report (2010) ISBN 978-90-6488-033-9, available on www.km3net.org.
[2] S. Viola (KM3NeT Collaboration) in proceedings of 34th ICRC. PoS (ICRC2015)1169 (2015)
[3] M. Ardid et al., Sensors 12 (2012) pp. 4113-4132.
[4] G. Larosa et al, Nucl. Instr. and Meth. A 725 (2013) 215–218.
[5] C.D. Llorens et al, J. Instrum. 7 (2012) C01001.
[6] S. Adrián-Martínez et al., MARSS (2014). arXiv:1502.05038 [physics.ins-det]
[7] M. Saldaña et al., Elsevier, Physics Procedia, vol. 63 (2015) pp. 195-200
[8] S. Viola et al., Nucl. Instr. and Meth. A, vol. 725 (2013) pp. 207-210.
[9] M. Ageron et al., Nucl. Instr. and Meth. A (2011), vol. 656, pp. 11-38.
[10] M. Ardid, Nucl. Instr. and Meth. A, vol. 602 (2009) pp. 174-176

2.6 A compact array calibrator to study the feasibility of acoustic neutrino detection.

M. Ardid, F. Camarena, I. Felis, A. Herrero, C.D. Llorens, J. Martínez-Mora, M. Saldaña

Institut d'Investigació per a la Gestió Integrada de les Zones Costaneres (IGIC) - Universitat Politècnica de València, C/ Paranimf 1 , 46730 Gandia, Spain

2.6.1 Abstract.

Underwater acoustic detection of ultra-high-energy neutrinos was proposed already in 1950s: when a neutrino interacts with a nucleus in water, the resulting particle cascade produces a pressure pulse that has a bipolar temporal structure and propagates within a flat disk-like volume. A telescope that consists of thousands of acoustic sensors deployed in the deep sea can monitor hundreds of cubic kilometres of water looking for these signals and discriminating them from acoustic noise. To study the feasibility of the technique it is critical to have a calibrator able to mimic the neutrino 'signature' that can be operated from a vessel. Due to the axial-symmetry of the signal, their very directive short bipolar shape and the constraints of operating at sea, the development of such a calibrator is very challenging. Once the possibility of using the acoustic parametric technique for this aim was validated with the first compact array calibrator prototype, in this paper we describe the new design for such a calibrator composed of an array of piezo ceramic tube transducers emitting in axial direction.

2.6.2 Introduction.

The study of Ultra-High-Energy (UHE) neutrinos by means of the detection of the acoustic pulse generated by the energy deposition after interacting with a nucleus in water was proposed already in 1950s [1]. This phenomenon induces a local heating in a very short period of time leading to a sub-millisecond pressure pulse signal with bipolar shape and very directive flat disk-like pattern, with the bipolar pulse being emitted perpendicularly to the shower axis direction.

The feasibility of the acoustic detection neutrino technique is currently being studied in the Mediterranean Sea [2, 3] and could be implemented in the new deep-sea Cherenkov neutrino telescope under construction, the KM3NeT telescope [4], which will have a volume of several cubic kilometres. Thus, the acoustic detection is a promising technique to cover the detection of UHE neutrinos, being possible to combine these two neutrino detection techniques for a hybrid underwater neutrino telescopes, especially considering that the optical neutrino detection technique needs acoustic sensors for monitoring the position of the optical sensors [5, 6]. A key tool to study the viability of the acoustic detection is an acoustic calibrator able to imitate the bipolar pulse signal. This will be needed to calibrate the sensors, as well as, to improve and train the classification and discernment of the neutrinos bipolar pulse signals from noise or other background transient signals. The proposed design, described in this paper, is a compact calibrator composed of an array of piezo-ceramic tube transducers emitting in axial direction. The

emission of the low-frequency acoustic bipolar pulse is generated by parametric emission at high-frequency. For this, specific electronics adapted to the ceramics in order to feed them efficiently are required, as well as, to allow and control the different functionalities the calibrator has to provide.

2.6.3 Compact Array Calibrator Approach.

The use of parametric acoustic sources to generate neutrino-like signals with cylindrical transducers has been achieved and validated in previous studies [7]. The acoustic parametric effect occurs when two intense monochromatic beams with two close frequencies travel together through the medium. Under these conditions, in the region of nonlinear interaction, secondary harmonics of these frequencies are produced at lower frequency with a beam pattern directivity similar to the primary beam. Since this technique offers the advantage of generating a parametric signal much more directive, it allows designing a compact array with fewer units with respect to classical solutions, and thus reducing costs and facilitating the deployment and operation issues. The array calibrator under development will be constituted of a few tube piezo ceramics aligned with optimal distance separation for obtaining an opening angle of about 1º and phased emission of the multi-element array. The array of transducers will emit at high frequency (hundreds of kHz) in the perpendicular direction to the axis and produce a bipolar pulse (with lower frequency spectrum, tens of kHz) due to the interaction of parametric signals generated for each element.

The first phase of the calibrator design presented in this paper consists of the study and selection of transducers, their characterization, and the emission of neutrino-like signals with a single transducer using the parametric technique. In a second phase, a study on matching layer materials and transmission loses has to be studied and finalizing the studies of the parametric emission for single and group of transducers, moulding them, designing the electronics and testing them. The last phase will be completing the integration of the system and testing it for long distances. Afterwards, the calibrator will be ready for in situ tests and use either installed in the deep-sea neutrino telescope or from the surface of the sea in a sea campaign with a vessel.

The array calibrator will be able to work in different operation modes; at linear low frequency range by emitting long non-directive signals (easy to detect), at high frequency range by emitting long parametric directive signals, and at high frequency range by emitting the transient and directive parametric bipolar signal. This will allow to use the array transmitter for different functionalities, such as training and tuning the acoustic detector, cross-checking the detector hydrophones, and other marine applications. On the other hand, the different operation modes will allow us to plan a sea campaign in order to facilitate the signal detection in the three steps with increasing difficulty.

2.6.4 Transducer Characterization.

Two types of piezo-ceramic tube transducers from UCE ultrasonic Co. LTD have been selected as candidates for the emitters of the array calibrator. The choice was based on resonance frequencies, power emission, dimensions, and costs. Both are able to emit high frequency signals within high power emission and they have a reasonable power level at lower frequencies as well. The first candidate is the piezo-ceramic UCE-534541 with dimensions: outer diameter of 5.3 cm, inner diameter of 4.5 cm and height of 4.1 cm. The primary resonance frequency is at 490 kHz, but it has also a secondary resonance at low frequency, around 35 kHz. The second candidate is the piezo-ceramic UCE-343020 with dimensions: outer diameter of 3.4 cm, inner diameter of 3 cm and height of 2 cm. The primary resonance frequency is at 890 kHz, with a secondary resonance frequency around 75 kHz.

The piezo-ceramics have been characterized both at high and low resonance frequencies in a water tank of 87.5 × 113 × 56.5 cm^3 with fresh-water at the laboratory. The calibration of the ceramics has been performed by measuring the Transmitting Voltage Response (TVR) and directivity in emission. The signals used for calibration have been tone bursts with the different frequency ranges of interest of each transducer. The hydrophones used for the calibration are omnidirectional, model RESON-TC40348 for high frequency and model RESON-TC4034 for low frequency. Figure 1 shows the characterization of both ceramics, the left plot shows the sensitivity obtained at high frequency with resonance frequency (F_R) of 490 kHz for the UCE-534541 and 890 kHz for the UCE-343020. The TVR of the UCE-534541 is 159 dB (re µPa/V at 1m) at F_R (490 kHz) with a directivity of ±5º. On the other hand, the TVR of the UCE-343020 is 162 dB (re µPa/V at 1m) at F_R (890 kHz) with a directivity of ±7º. The TVR at lower frequencies, 10 kHz to 100 kHz, is in the range 132 – 143 dB (re µPa/V at 1m) for both ceramics [8], so it will be possible to use these ceramics as well for generating low frequency signals directly, which is very useful for calibration purposes.

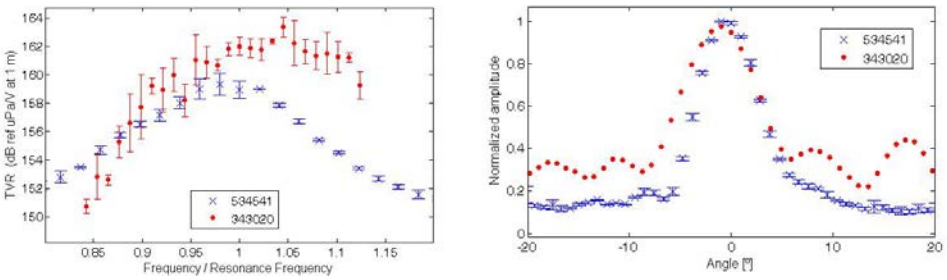

Figure 1. Left: TVR of UCE-534541 at F_R=490 kHz (blue x) and for UCE-343020 at F_R=890 kHz (red dot). Right: Directivity at 490 kHz for the UCE-534541 (blue x) and at 890 kHz for UCE-343020 (red dot).

2.6.5 Parametric Bipolar Pulse Emission.

The experiment of generating the bipolar pulse was carried out in the same water tank. The piezo-ceramic was connected to a linear 55 dB RF amplifier ENI 1040L to feed the emitter and generate a more powerful signal in order to achieve the non-linear parametric effect. The chosen receiver was the RESON-TC4034, this transducer is an omnidirectional, broad-band hydrophone with enough sensitivity to detect the primary beam (high frequency) and better sensitivity to lower frequencies for the bipolar pulse detection. Additionally it was connected to a charge amplifier CCA 1000 (Teledyne RESON©) which amplifies the received signal, especially the low frequency range. Here, we present the study performed with the UCE-343020 ceramic, hence, the signal for emission has been derived for parametric generation at 890 kHz as described in ref. [7]. The distance between the emitter and the receiver was 30 cm. The results with the UCE-534541 are reported in ref. [8], where the shapes of the primary beam and the secondary bipolar pulse can be observed in figure 3 of this reference.

Since the amplitude of the secondary bipolar signal is about 100 times smaller than the primary beam, it is necessary to use a band pass ([5 - 80] kHz) filter to be able to observe this signal. In order to check that the secondary beam has a non-linear behaviour, the amplitude of the parametric signal, as a function of the voltage applied to the transducer, was measured. Figure 2-Left shows the amplitude behaviour of the received signal, without filtering (original) and with the band pass filtering (the parametric bipolar signal, secondary beam). Linear behaviour can be observed for the amplitude of the primary beam, whereas, for the secondary received signal (parametric bipolar signal) the amplitude behaviour is proportional to the square of the amplitude of the input signal, showing the nonlinearity of the effect. On the other hand, in Figure 2-Right it can be observed that, despite the frequency content of both signals is so different, the directivity achieved is quite similar.

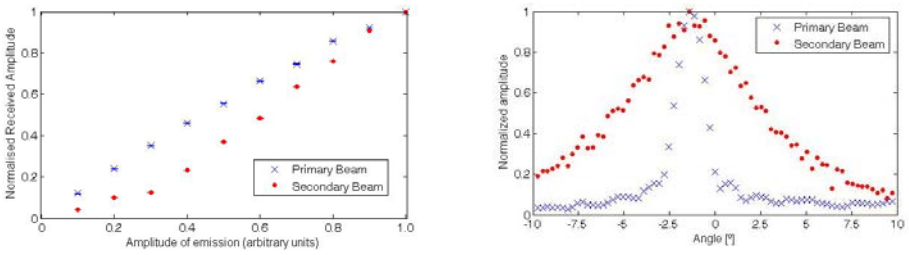

Figure 2. Left: Amplitude of the received primary beam and of the secondary bipolar pulse. Right: Directivity obtained for both signals.

2.6.6 Conclusions and Future steps.

The results obtained on the piezo-ceramics characterization show that both could be good candidates for being part of the future calibrator since they have an optimal sensitivity at both high and low frequency and narrow beam directivity at high frequencies which will lead, in turn, to a very directive low-frequency (parametric) pulse. Moreover, the first studies on the acoustic neutrino-like signals generation by using the parametric technique show that the signal reproduction is achieved.

The next steps will consist in completing the studies of the parametric emission for single and group of transducers, and moulding them. In addition, the electronics design will be finalized and tested. After this, the complete integration of the system and the tests at long distances will be performed before doing sea campaign tests.

2.6.7 Acknowledgements.

We acknowledge the financial support of the Spanish Ministerio de Economía y Competitividad, Grants FPA2012-37528-C02-02, and Consolider MultiDark CSD2009-00064, of the Generalitat Valenciana, Grants ACOMP/2015/175 PrometeoII/2014/079 and of the European FEDER funds.

2.6.8 References.

1. G.A. Askaryan, J. A. Energy **3**, 921 (1957).
2. J.A. Aguilar, et al., Nucl. Instrum. and Meth. A **626**, 128 (2009).
3. G. Riccobene, Nucl. Instrum. and Meth. A **604**, S149 (2009).
4. The KM3NeT Collaboration, KM3NeT Technical Design Report (2010) ISBN 978-90-6488-033-9, available on www.km3net.org.
5. M. Ardid, Nucl. Instrum. and Meth. A **604**, S203 (2009)
6. M. Ardid, Nucl. Instrum. and Meth. A **602**, 174 (2009).
7. M. Ardid et al., Sensors, **12**, 4113 (2012), pp. 4113-4132.

8. M. Saldaña et al., New design of an acoustic array calibrator for underwater neutrino telescopes. In Proceedings of the 2nd Int. Electron. Conf. Sens. Appl., 15–30 November 2015; Sciforum Electronic Conference Series,

2.7 Transducer development and characterization for underwater acoustic neutrino detection calibration.

M. Saldaña[1,*], C.D Llorens[1], I. Felis[1], J. A. Martínez-Mora[1] and M. Ardid[1]

[1]Institut d'Investigació per a la Gestió Integrada de les Zones Costaneres (IGIC), Universitat Politècnica de València (UPV), 46730 Gandia, València, España;

2.7.1 Abstract.

A short bipolar pressure pulse with 'pancake' directivity is produced and propagated when an Ultra-High Energy (UHE) neutrino interacts with a nucleus in water. Nowadays, acoustic sensor networks are being deployed in deep sea to detect the phenomenon, as a first step to build a neutrino telescope. In order to study the feasibility of the method, it is critical to have a calibrator able to mimic the neutrino signature. In previous works the possibility of using the acoustic parametric technique for this aim was proven. In this case, the array is operated at high-frequency and, by means of the parametric effect, the emission of the low-frequency acoustic bipolar pulse is generated mimicking the UHE neutrino acoustic pulse. In this paper, the development of the transducer to be used in the parametric array is described. The transducer design process, the characterization tests for the bare piezoelectric ceramic, and the addition of backing and matching layers are presented. The efficiencies and directivity patterns obtained for both primary and parametric beams confirm that the design fulfils all the requirements for the emitter.

Keywords: Acoustic calibrator; Piezo-ceramic tube transducers; Ultra High Energy neutrinos; Acoustic detection; Underwater neutrino telescopes; Parametric technique

2.7.2 Introduction.

Astrophysical neutrino detection is based on the measurement of the Cherenkov light induced by secondary leptons like muons produced by neutrino interactions with matter while passing across the Earth. Searches for cosmic ray neutrinos are ongoing detecting upward going muons from the Cherenkov light in either ice or water. The telescope IceCube, located at the South Pole, has recently discovered high-energy astrophysical neutrinos [1] boosting the neutrino astronomy field. Besides IceCube, the existing neutrino telescopes nowadays are NT200+ in lake Baikal [2], ANTARES [3] and a new optical-based deep-sea neutrino telescope under construction, the KM3NeT telescope [4], which will have a volume of several cubic kilometres.

Ultra High Energy (UHE) neutrinos (~10^{20} eV) became of high interest for the study of ultra-high-energy cosmic ray sources and to test fundamental physics due to the advantages of being high-energy, stable and weakly interacting elementary particles. Besides Cherenkov light, radio or acoustic wave techniques were proposed to detect the neutrino induced energy deposition in water, ice or salt. These techniques, with much

longer attenuation lengths, allow very large target volumes utilizing either large ice fields or dry salt domes for radio or ice fields and the oceans for the acoustic detection.

Acoustic detection of UHE neutrinos is based on the thermo-acoustic effect [5]. When an UHE neutrino interacts with a nucleus in water, its energy is released in a volume of about a centimetre in radius and several meters in length. This phenomenon induces a local heating in a very short period of time leading to a short pressure pulse signal with bipolar shape in time and a very directive pattern (pancake-like), being emitted mainly in the perpendicular plane of the shower axis [6].

Last decades, many experiments have been investigating on the acoustic neutrino detection in both water and ice mediums such as AMADEUS [7], SPATS [8], ACORNE [9] and SAUND [10]. The detection technique is still under study and could be implemented in a new optical neutrino telescope KM3NeT [11]. The acoustic detection would allow the combination of these two neutrino detection techniques for a hybrid underwater neutrino telescope, especially considering that the optical neutrino detection technique needs acoustic sensors as well for monitoring the position of the optical sensors [12].

Therefore, an emitter able to imitate the bipolar pulse signal generated by the neutrino in water will be extremely useful. For this purpose, an acoustic array calibrator is under design. The emissions from the emitter calibrator, which will be time controlled, will allow to train the sensors in the neutrino detection, as well as, to improve the classification and identification of the acoustic neutrino signals from noise or other transient signals background [13].

The acoustic calibrator will be deployed in the vicinity of the detector with a distance between the emitter calibrator and the detector that can vary from 0.5 km until 3.5 km. The furthest distances would occur when the calibrator is operated from the sea surface and the closest when operated from the seabed. Consequently, the acoustic calibrator requires to be considerably powerful in order to reach the detector with enough pressure level to be detected and recognized.

The objective of the acoustic array calibrator is the emission of bipolar pulse signals with similar characteristics of the signal produced by a 10^{20} eV neutrino interacting in water at a distance of 1 km, which would be detected with an amplitude of about 10 mPa in the low-ultrasonic frequency range (maximum amplitude between 5 kHz – 20 kHz) with an opening angle of about 1°. The proposed design for the acoustic calibrator is a compact array system composed of piezo-ceramic tube transducers emitting in the axial direction. The emission is amplified and controlled by specific electronics adapted to them. The emission of the low-frequency (tens of kHz) acoustic bipolar pulse is generated by using the parametric emission technique at high-frequency (hundreds of kHz).

2.7.3 Compact array calibrator based on the parametric acoustic source technique.

The use of the parametric acoustic source technique to generate neutrino-like signals allows to generate the low frequency signal with narrow directivity, which is essential in order to obtain bipolar signals with the 'pancake' directivity required. This technique was already validated in previous studies using cylindrical transducers [14]. The acoustic parametric effect occurs when two intense monochromatic beams with two close frequencies travel together through the medium. According to the linear theory, and as a consequence of the principle of superposition, the resulting sound field is composed only from the initial frequencies. However, due to the non-linearity of the medium the interaction of the two frequencies of the finite amplitude sound wave emerges a set of secondary frequencies, such as the sum and difference frequency components of the primary signals. This process of non-linear generation of new frequencies is limited to a certain distance from the transducer, called the array length, given by the distance of interaction or absorption length. This may be considered as a set of virtual acoustic sources (array) contained along the length of interaction; the source seems to be shaded exponentially as distance increases from the transmitter. The secondary beam is produced with a directivity pattern similar to the one of the primary beams, which offers the advantage of generating a low-frequency directive beam.

Applying the parametric technique for the emission of the low-frequency signal allows to design a compact array with fewer units with respect to classical solutions, and thus reducing costs and facilitating the deployment and operation issues of the calibrator. The proposed array calibrator under development will be constituted of three to five elements of the piezo tube ceramic structured in the same axis-line with a distance separation (d) between 10 cm to 20 cm, in order to obtain an opening angle of about 1º with phased emission of the array components. The transducer array will emit in axial direction and produce a bipolar pulse due to the interaction of parametric signals generated by each array element. Figure 1 shows a schematic diagram of the configuration and emission.

In order to increase the functionality of the calibrator and facilitate the calibration under different circumstances, it is designed to work in different operation modes. The three operation modes are: 1) at linear low frequency range by emitting long non-directive signals (easy to generate and easy to detect), 2) at high frequency range by emitting long parametric directive signals (signal processing techniques could be used to simplify detection of these signals), and 3) at high frequency range by emitting the transient and directive parametric bipolar signal (the most challenging case). Those operation modes will enable the array transmitter for different purposes, such as training and tuning of the acoustic detector, cross-checking of the detector hydrophones, and other marine applications. The proposed calibrator design and development was divided in three phases. In the first one, the study and selection of transducers was done. Once the transducers were selected, their characterization was performed and measures with the single bare transducer emitting parametric neutrino-like signals were realized. In a

second phase, the study and selection of backing and matching layer materials for optimizing the ceramic emission, as well as for holding and isolating the ceramics was made resulting in a final prototype transducer selected (backed and moulded) convenient for this application, Figure 2 shows a diagram of the transducer design with the backing and matching layer configuration. This paper is focused on those two phases. For future research a third phase is planned. It will be focused on the design of the complete array system composed of a few units of the transducer developed. In this future phase, electronics will be adapted to the array emitters in order to amplify the power of the signal emission, as well as including all the functionalities for the control and operation of the calibrator. Once completed the development, tests over long distances, and in situ tests in the detector vicinity will be performed.

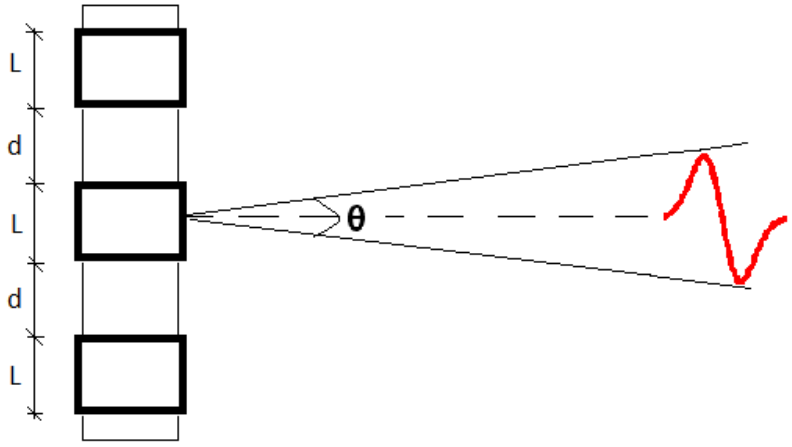

Figure 1. Schematic diagram of the transducer array configuration with 3 elements.

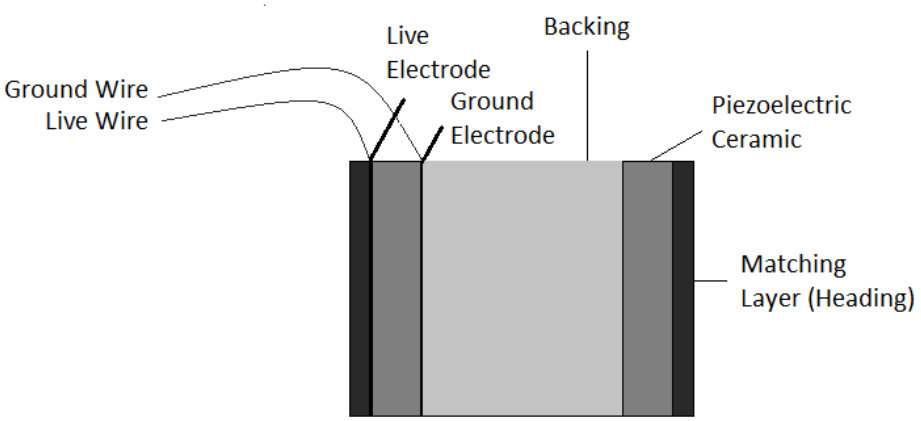

Figure 2. Drawing of the transducer design component; ceramic, backing and matching layer.

2.7.4 Transducer selection and characterization.

Two commercial piezo-ceramic tube transducers were selected as emitter candidates of the array calibrator. The selection was made in terms of resonance frequencies, power emission, dimensions, and costs. Both transducers permit high frequency signal emissions with high power exhibiting reasonable power levels at low frequency as well. The first candidate was the piezo-ceramic UCE-534541, hereinafter referred to as large tube, with dimensions: outer diameter of 5.3 cm, inner diameter of 4.5 cm and 4.1 cm of height. The large tube primary resonance frequency is around 490 kHz with a real impedance of 9 Ω, with a secondary resonance frequency at low frequency, around 35 kHz. The second candidate is the piezo-ceramic UCE-343020, hereinafter referred to as small tube, with dimensions: outer diameter of 3.4 cm, inner diameter of 3 cm and 2 cm of height. The small tube primary resonance frequency is located around 890 kHz with a real impedance of 6 Ω, with a secondary frequency resonance around 75 kHz. Figure 3 shows a picture of both ceramics and Figure 4 shows the admittance of the large tube, where the resonance frequencies are appreciated.

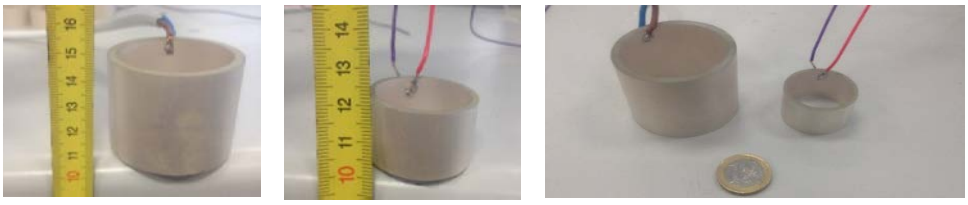

(a) (b) (c)

Figure 3. (a) Piezo-ceramic large tube (b) Piezo-ceramic small tube (c) Both piezo-ceramics.

.

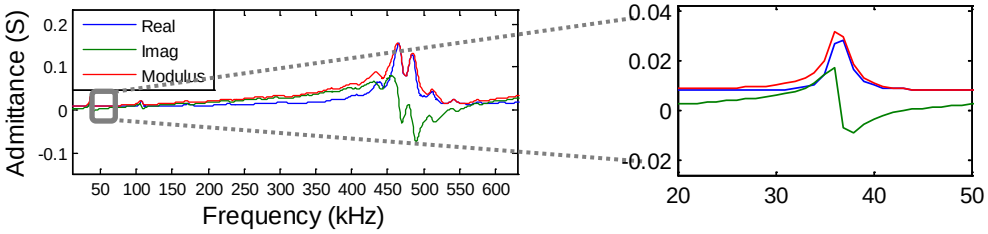

Figure 4. Admittance of the large tube.

2.7.4.1 Transmitting voltage response and directivity.

The piezo-ceramics were characterized both at high and low resonance frequencies in a water tank of 87.5 × 113 × 56.5 cm^3 with fresh-water at the laboratory. The calibration of the ceramics was performed in terms of the Transmitting Voltage Response (TVR), which is the ratio of the pressure signal emitted to the applied voltage, and the emission directivity along the axial direction of the cylinder using tone bursts at different frequencies. The hydrophones used for these measurements are omnidirectional, particularly, model RESON-TC4038 for the high frequency range and the model RESON-TC4034 for the low frequency range. Figure 5 shows the characterization of both ceramics. In Figure 5 (a) the sensitivity obtained at high frequency with resonance frequency (F_R) of 490 kHz for the large tube and 890 kHz for the small tube is depicted. The TVR of the large tube is 159 dB (re µPa/V at 1m) at F_R = 490 kHz with a directivity of Full Width Half Maximum (FWHM) of 10º (Figure 6). At low frequencies, the TVR varies between 132 – 140 dB (re µPa/V at 1m). On the other hand, the TVR of the small tube is 162 dB (re µPa/V at 1m) at F_R = 890 kHz with a FWHM directivity of 14º (Figure 6). The TVR at low frequencies varies between 132 – 143 dB (re µPa/V at 1m).

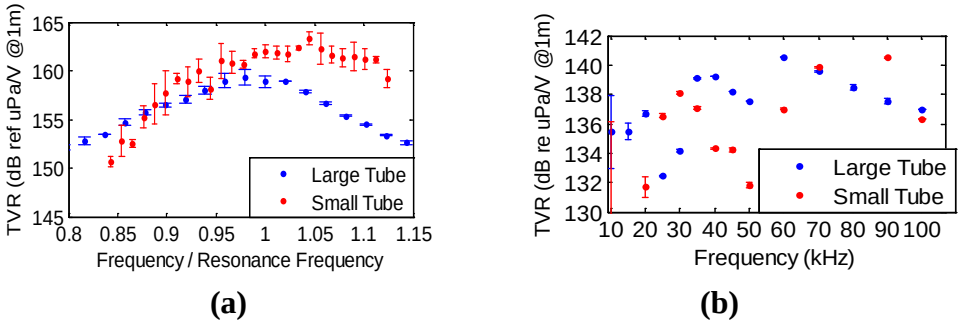

Figure 5. Characterization of the ceramics (a) TVR of large tube at F_R=490 kHz (blue dots) and for small tube at F_R=890 kHz (red dots) (b) TVR from 10 - 100 kHz.

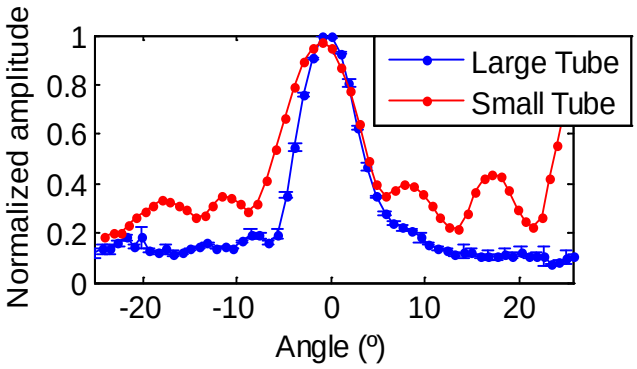

Figure 6. Directivity at 490 kHz for the large tube (blue) and at 890 kHz for small tube (red).

2.7.4.2 Backing.

Some backing materials are able to absorb the energy produced from the back of the active element (ceramic) and reflect part of it forward, providing more acoustic power in emission [15]. In addition, the backing element of the transducer will constitute the support of the complete future array calibrator, i.e., playing an important role in the mechanical design of the array (Figure 1). Different materials and thicknesses were studied in order to find the best option in terms of TVR and acoustic impedance. The materials studied as backings were epoxy and aluminium. Figure 7 shows the ceramics implemented with the backing elements studied.

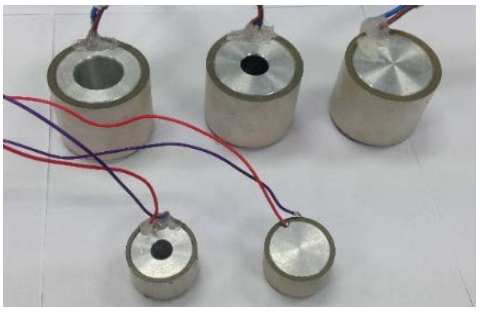

Figure 7. Piezo-ceramics with aluminium backings of different thicknesses.

According to the results obtained on the characterization of all backings for both ceramic types, the set of aluminium backing filling completely the tube ceramic gave the best results. For both ceramics the filled aluminium backing produced a flatter frequency response of the TVR. In the case of the backed large tube a 3 dB increment on the TVR , a resonance frequency shifting to 510 kHz, and an increment up to 30 Ω (real) in the

impedance was observed. About the small tube an increase of 5 dB on the TVR, a shift on the resonance frequency to 950 kHz, and an impedance increment to 50 Ω (real) was appreciated. Moreover, there was not any appreciable change on the directivity patterns of both tubes.

For the array, it is expect that the coupling effect of the backing will be minor since the elements are identical and they will be phased-emitted.

2.7.4.3 Matching layer.

Two interesting materials for moulding underwater transducers were acoustically studied in order to know the effect on the signal emitted. The reasons of moulding the bare ceramic are to ensure the protection, isolation and holding, and to match the impedance of the piezo-ceramic to the impedance media [16]. The matching materials under study were the resin RoyaPox 511 and the Polyurethane EL241F. Both materials exhibit interesting acoustic properties for matching the ceramic impedance to the media due to their specific acoustic impedance (Z), density (ρ) and sound speed (c_L). There is maximum transmission at the layer thickness of (2n-1) λ/4. Since for the first mode, λ/4, the obtained thickness values were too thin for an optimum covering, the matching layer thicknesses were set to accomplish the second mode with thickness 3λ/4 of the wavelength emitted at the ceramic resonance frequency, the advantage of this selection is that is thick enough to facilitate the covering and obtaining maximum length transmission. The matching layer mould used was a cylinder with the thickness space necessary to cover the ceramic, controlled by a precise metric rule with an estimated uncertainty of

± 0. 1mm.The acoustic properties of the materials and the thickness used are summarized in Table 1. In a first stage, in order to test both materials with the same ceramic, two large tubes with aluminium backing were moulded with each material. Figure 8 shows the ceramic covered with RoyaPox 511 (a) and with polyurethane EL241F (b). The best results in terms of TVR and directivity were obtained with the polyurethane. Afterwards, a small tube with aluminium backing was moulded with polyurethane, as shown in Figure 8 (c).

Table 1. Acoustic properties of the matching layer (ML) materials RoyaPox 511 and EL214F, and thickness (mm) obtained for accomplishing λ/4 or 3λ/4 of the emitted wavelength at the ceramic resonance frequency.

ACOUSTIC PROPERTIES	Large tube M.L RoyaPox 511	Large tube M.L EL214F	Small tube M.L EL214F
c_L (m/s)	2602	1600	1600
Z (MRayls)	2.82	1.857	1.857
ρ (kg/m^3)	1050	1160.7	1160.7
Frequency (kHz)	480	510	960
λ/4 Thickness (mm)	1.3	0.78	0.42
3λ/4 Thickness (mm)	4.0	2.4	1.3

(a) **(b)** **©**

Figure 8. (a) Piezo-ceramic large tube with aluminium backing and RoyaPox 511 moulding (b) Piezo-ceramic large tube with aluminium backing and and polyurethane EL241F moulding (c) Piezo-ceramic small tube with aluminium backing and polyurethane EL241F moulding.

The ceramic moulded with the RoyaPox 511 resin showed the same TVR level on the resonance frequency than before moulding. The resonance frequency shifted to 450 kHz, but the impedance and directivity were very similar to that obtained with the bare ceramic. For the case of the large tube moulded with the EL241F polyurethane, there was a TVR gain of 5 dB approximately in the resonance frequency compared within before moulding. The resonance frequency shifted to 495 kHz with a sensitivity of 169 dB (re µPa/V at 1m). The TVR curve for this case is shown in Figure 9 (a). The impedance at the resonance frequency was 12 Ω (real), that is, it was reduced as compared to itself only backed, but being still higher than bare. With respect to the directivity, the pattern did not show any significant variation. The TVR of the small tube moulded with the polyurethane is shown in Figure 9 (b). The graph is practically the same as before moulding for the 890 kHz – 1 MHz range. However, there was also a peak resonance at higher frequencies, for 1165 kHz with 169 dB (re µPa/V at 1m) with real impedance of 20 Ω. Directivity pattern did not vary with respect to the bare one.

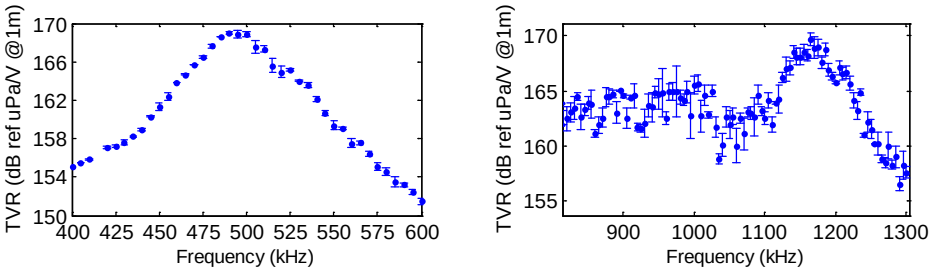

(a) **(b)**

Figure 9. (a) TVR of large tube with aluminium backing and moulded with polyurethane EL241F (b) TVR of small tube with aluminium backing and moulded with polyurethane EL241F.

To sum up, the design with the aluminium backing and the moulding with polyurethane EL241F produced an increase on the TVR at resonance of 9 dB for the large tube and of 7 dB for the small tube. For both ceramics, the design did not change the directivity pattern of the ceramics.

2.7.5 Studies on parametric emission.

The parametric acoustic source technique was evaluated by means of the low frequency-parametric generation of a sine sweep signal using the cross-correlation with the expected signal. Following this methodology, it is feasible to recognize the parametric signal, since the correlation produces a clear narrow peak on the signal arrival time, which allows distinguishing it from near echoes, as well as, an increase in the signal to noise ratio [17]. Then, the low frequency-parametric generation of a bipolar shape pulse signal in time was studied. The generation of the portable signal for the bipolar pulse generation is explained in Ref. [14]. These portable signals for the parametric generation were implemented with modulation at high frequency, e.g., at the frequency resonance of the ceramic, either 495 kHz or 1165 kHz.

In order to confirm the non-linear effect of the parametric signal received three studies in the different aforementioned stages were done. The first study was to compare the amplitude of primary and secondary beams by starting from low amplitude emission and increasing it to demonstrate the non-linear effect. The second measurement analysed the secondary non-linear beam generation in the medium by changing the distance between emitter and receiver. The last study compared the directivity patterns of both beams.

The experiment was done in the same water tank as described in Section 3.1. The piezo-ceramic was connected to a linear 55 dB (gain) RF amplifier ENI 1040L to feed the

emitter and generate a more powerful signal in order to achieve the non-linear parametric effect. The receiver was the RESON-TC4034. This transducer is an omnidirectional, broad-band hydrophone with enough sensitivity to detect the primary beam (high frequency) and being more sensitive to low frequency, i.e., for the bipolar pulse detection. Additionally, it was connected to a charge amplifier CCA 1000 (Teledyne RESON) which amplifies the received signal, especially for low frequency signals.

2.7.5.1 Parametric sine sweep signal.

The signal for the generation of the sine sweep signal was designed by modulating a sine sweep signal from 20 kHz to 50 kHz using a modulation frequency of 495 kHz; Figure 10 (a) shows the emission signal, where the modulation shape can be observed. The received signal was a mix of the primary beam at 495 kHz and the secondary beam at low frequency produced by parametric effect. In order to distinguish the secondary beam, a band pass ([5 - 80] kHz) filter was applied. Figure 10 (b) shows the received signal, primary (original) and secondary (filtered) beams. The analyses of the different parametric studies with this signal were obtained by taking the amplitude value of the correlation of the received signal with the primary beam signal (high frequency) and with the expected secondary beam signal (low frequency). Figure 10 (c) shows the correlation of the original received signal with the expected secondary beam signal. There is a clear correlation peak at the arrival time of the received signal.

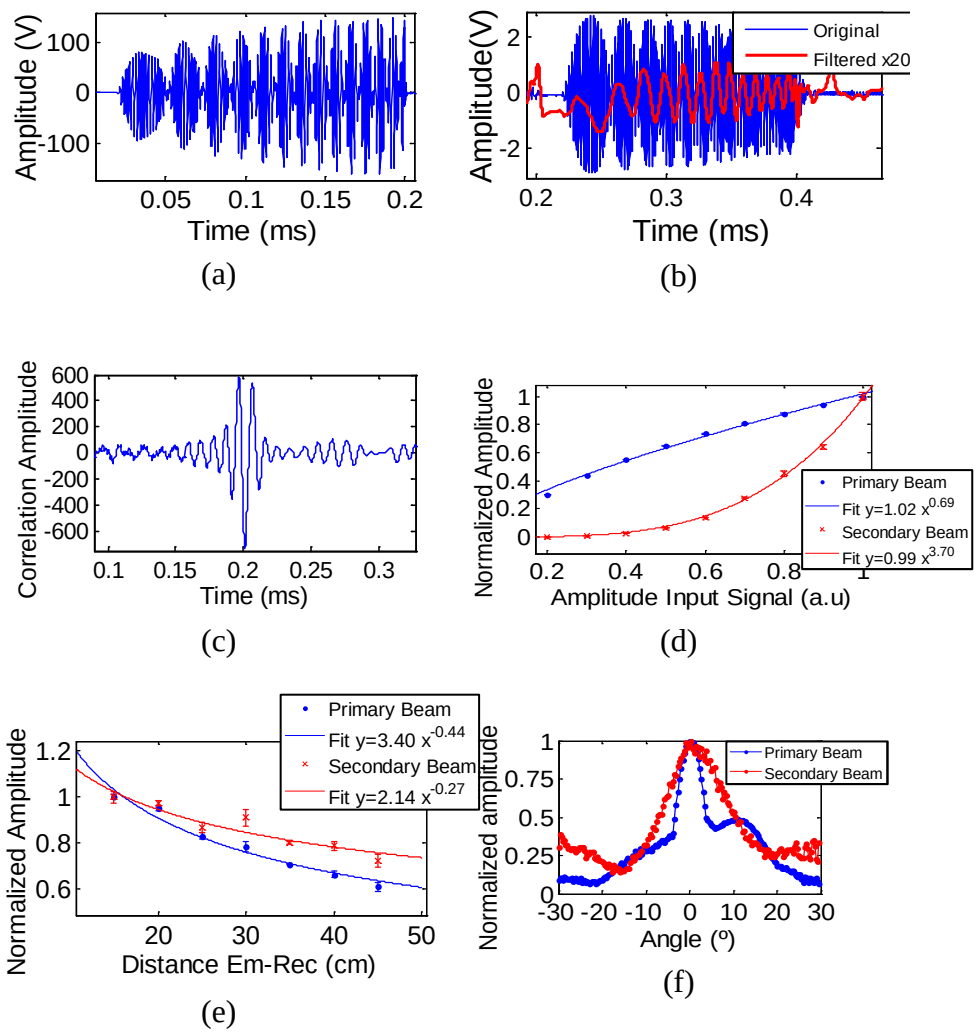

Figure 10. (a) Emitted signal for sine sweep (20 kHz – 50 kHz) generation, (b) received signal (blue line) and the band-pass filtered signal (red line), (c) correlation of the original received signal with the expected secondary beam, (d) correlation amplitude of the received signal with primary beam (blue points) and secondary beam (red points) as a function of the signal emitted amplitude, (e) correlation amplitude of the received signal with both beams as a function of the distance between emitter and receiver and (f) directivity pattern of both beams.

Figure 10 (d) shows the correlation amplitude behaviour of the received signal, without filtering (original) and with the band-pass filtering (secondary beam) as a function of the input signal amplitude. The data fitting to parameterizations shown that the exponent for the secondary beam is much larger than the one of the primary beam, being an evidence of the non-linear effect. The exponent value of the primary beam is 0.69±0.03 and for the secondary beam is 3.70±0.12. The exponent for the primary beam is slightly below one due to saturation effects of the amplifier. The evolution of both beams with the distance is shown in Figure 10 (e), clearly appreciating the different behaviour between them. The ratio of amplitudes between the primary and secondary beam increases as a function of the distance, which is an evidence of the secondary beam being generated in the medium. Parameterizations were fitted to the data obtaining a smaller exponent for the secondary beam, as expected. For the primary beam the value exponent is -0.44±0.04 while for the secondary beam is -0.27±0.06. The directivity patterns, shown in Figure 10 (f) is as well an evidence of the parametric effect for the secondary beam since the pattern for this beam is quite similar to the one of the primary beam, and more directive than the ceramic directly fed at low frequency. For instance, the open angle (FWHM) for direct feeding in the frequency range, 20 – 50 kHz, was 80º approximately.

2.7.5.2 Parametric bipolar pulse signal.

The emission signal for achieving the parametric generation of the bipolar-shape pulse signal was designed by using the portable signal at 495 kHz and implementing a different type of modulation. This signal is obtained thanks to the data from the shape of the secondary signal, which follows the second time derivative of the envelope of the primary signal in amplitude [18]. Figure 11 (a) shows the emitted signal-shape modulated. The received signal was a mix of the primary beam at 495 kHz and the secondary beam at low frequency produced by parametric effect. In order to distinguish the secondary beam, a band pass ([5 - 80] kHz) filter was applied. Figure 11 (b) shows the received signal, primary (original) and secondary (filtered) beams. The secondary beam (bipolar pulse) is multiplied by a factor of 30 in order to be visible together with the original received signal (non-filtered). As expected, the secondary beam has a bipolar pulse-shape. A peak after the bipolar pulse is appreciated, this is due to the signal response of the transducer, what can affect to the shape of the signal tail and generate an oscillation after the last signal pulse. The analysis of the different parametric studies with this signal were obtained by taking the amplitude value of the signal received at high frequency (primary beam) and of the bipolar pulse signal (secondary beam).

Figure 11 (c) shows the amplitude behaviour of the received signal, without filtering (original) and with the band-pass filtering (the parametric bipolar signal) as function of input signal amplitude. The fitting data to parameterizations shown that the exponent for the secondary beam is twice the exponent of the primary beam, representing the non-linear effect. The exponent value of the primary beam is 0.81±0.03 and for the secondary beam is 1.72±0.26. The exponent for the primary beam is slightly below one due to saturation effects of the amplifier. In Figure 11 (d) the evolution of both beams with the

distance can be observed. No conclusive results could be obtained from this due to the fluctuations observed in the measurements and on the detection of the bipolar secondary signal, since the exponent value for the primary beam is -0.53±0.01 and for the secondary beam is -0.51±0.05. The directivity pattern, shown in Figure 11 (e), is the best proof of the parametric effect for the secondary beam since both beams have similar directivities.

Considering all these results, the parametric generation was satisfactory validated. The large tube with aluminium backing and moulded with polyurethane EL241F, as matching layer, showed very good characteristics for being used as the transducer unit of the final array.

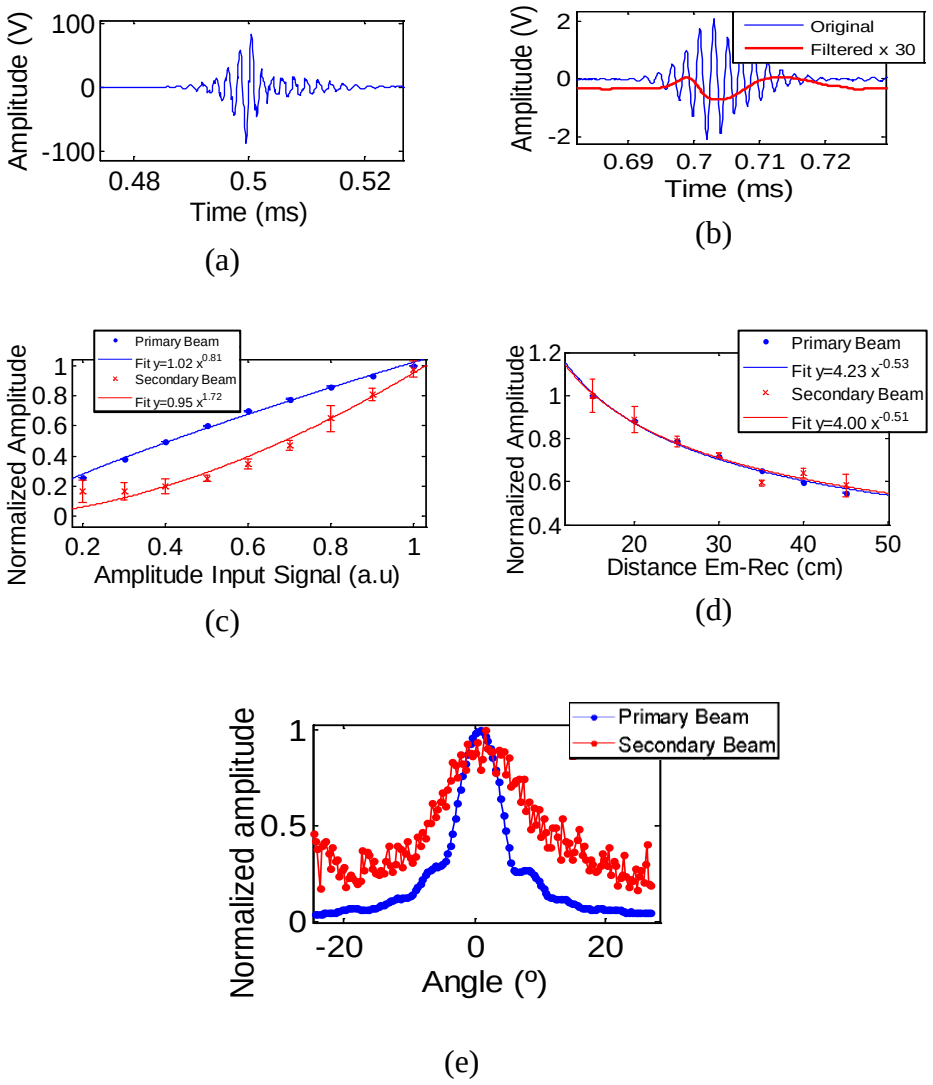

Figure 11 (a) Emitted signal for bipolar pulse generation, (b) received signal (blue line) and bipolar signal obtained after applying a band-pass filter (red line), (c) amplitude of the received (blue) and filtered signal (red) as function of input signal amplitude, (d) amplitude of the received signal for both beams as function of distance between emitter and receiver and (e) directivity pattern of both beams.

2.7.6 Future steps

The near future work will consist of adapting the electronics to the final transducer design to achieve the required power emission able to produce the parametric signals. The electronic board is based on the same philosophy as a previous electronic board designed [19], adapted to the particularities of the new transducer and application. The electronics will also incorporate the functionalities for communication, configuration, control and amplification of the signal, already developed in previous studies [20].

Then, the transducer array will be built, which will be composed of multi-emitters placed in the same line structure that will be a long tube of aluminium that will work as backing of the ceramics as well. Finally, after the characterization and final tests over longer distances, it will be either used in sea campaigns for emissions from a vessel, or incorporated in the KM3NeT deep-sea neutrino telescope infrastructure for performing the calibration tests of the acoustic systems of the telescope.

2.7.7 Conclusions.

The results obtained on the characterization of the transducers designed (piezo-ceramics with backing and matching layer) indicate that the best option as future element for the multi-element array calibrator is the large tube with aluminium backing and moulded with $3\lambda/4$ of polyurethane EL241F. An increment of 9 dB after backing and moulding was appreciated on the transducer compared to the bare ceramic, having a final sensitivity of 169 dB (re µPa/V at 1m) at 495 kHz. The parametric emission was validated for both parametric signals generated, the sine sweep and the bipolar pulse; the non-linearity effect of the parametric signal was seen in the studies performed, higher amplitude evolution and narrower directivity pattern. Moreover, the signal reproduction of the acoustic neutrino-like signals generation by using the parametric technique was achieved.

The future array of multi-elements emitting at linear or parametric modes with high-pressure sound level will become a very versatile and powerful system, which could be used in other kind of underwater acoustics applications, such as communication, localization, positioning and on-site sensor calibration.

2.7.8 Acknowledgments.

We acknowledge the financial support of Plan Estatal de Investigación, ref. FPA2015-65150-C3-2-P (MINECO/FEDER), and Consolider MultiDark CSD2009-00064 (MINECO) and of the Generalitat Valenciana, Grants ACOMP/2015/175 and PrometeoII/2014/079.

2.7.9 References and Notes.

1. IceCube Collaboration, Evidence for High-Energy Extraterrestrial Neutrinos at the IceCube Detector IceCube neutrino observatory. *Science* Vol.342, Issue 6161 (2013).

2. V. Aynutdinov et al., The Baikal neutrino experiment: Status, selected physics results, and perspectives, *Nucl. Instrum. and Meth. A* 588 (2008) 99-106.
3. ANTARES Collaboration. ANTARES: The first undersea neutrino telescope, *Nucl. Instrum. and Meth. A* 656 (2011) 11-38.
4. KM3NeT Collaboration. Letter of Intent for ARCA and ORCA. arXiv:1601.07459v1 (2016).
5. G.A. Askaryan. Hydrodynamical emission of tracks of ionising particles in stable liquids. J. A Energy 3 (1957) 921.
6. S.Bevan, Study of the acoustic signature of UHE neutrino interactions in water and ice. *Nucl.Instr. and Meth.A* 607 (2009) 398-411.
7. J.A. Aguilar, et al., AMADEUS, The acoustic neutrino detection test system of the ANTARES deep-sea neutrino telescope, *Nucl. Instr. and Meth. A* 2011, 626, 128-143.
8. IceCube Collaboration, Research and calibration of Acoustic Sensors in ice within the SPATS (South Pole Acoustic Test Setup) project. arXiv:10110.2313 (2010).
9. L.F.Thompson and J.D. Perkin, Acoustic Detection of UHE Neutrinos – the ACORNE project. *Journal of Physics: Conference Series 136 (2008) 042070*.
10. Vandenbroucke J, Gratta G and Lehtinen N, Experimental study of acoustic ultra-high-energy neutrino detection, *Astrophys. J.* 621(1) 301-12 (2005)
11. S. Viola et al., (KM3NeT Collaboration), Acoustic positioning system for *KM3NeT in proceedings of 34th ICRC*, PoS (ICRC2015)1169 (2015).
12. S. Viola et al., NEMO-SMO acoustic array: A deep-sea test of a novel acoustic positioning system for a km 3-scale underwater neutrino telescope, *Nucl. Instrum. Meth. A* 2013, 725, 207-210.
13. M. Ardid, Calibration in acoustic detection of neutrinos. *Nucl. Instr. and Meth. A* 2009, 604, S203.
14. M. Ardid, J.A. Martínez-Mora, M. Bou-Cabo, G. Larosa, S. Adrián-Martínez and C.D. Llorens ., Acoustic Transmitters for Underwater Neutrino Telescopes, *Sensors* 2012, 12, 4113-4132.
15. Kossof G., The effects of backing and matching on the performance of piezoelectric ceramic transducers, *IEEE Transactions on Sonics and Ultrasonics*, 1966, 13, 20-30.
16. Li, H.; Deng, Z.D.; Yuan, Y.; Carlson, T.J., Design Parameters of a Miniaturized Piezoelectric Underwater Acoustic Transmitter. *Sensors* 2012, 12, 9098-9109.
17. S. Adrián-Martínez, M. Ardid, M. Bou-Cabo, I.Felis, C. Llorens, J.A. Martínez-Mora, M. Saldaña, Acoustic signal detection through the cross-correlation method in experiments with different signal to noise ratio and reverberation conditions, *LNCS* 2015, 8629, 66-79.
18. Moffett, M.B.; Mello, P. Parametric acoustic sources of transient signals. *J. Acoust. Soc. Am*. 66 1979, 66, 1182-1187.

19. Llorens, C.D., M. Ardid, T. Sogorb, M. Bou-Cabo, J.A. Martínez-Mora, G. Larosa, S. Adrián-Martínez., The Sound Emission Board of the KM3NeT Acoustic Positioning System. *J. Instrum.* 2012, 7 (01), C01001.
20. S. Adrián-Martínez, M.Ardid, M. Bou-Cabo, G.Larosa, C.D. Llorens, J.A. Martínez-Mora, A compact acoustic calibrator for ultra-high energy neutrino detection, *Nucl. Instrum. Meth. A* 2013, 725, 219-222.

Capítulo 3
Discusión general de los resultados

En este capítulo se describen las aportaciones realizadas y se ponen en común todos los resultados presentados en el capítulo anterior. Cabe destacar que, si bien durante el desarrollo de la tesis se han publicado más artículos, finalmente se han seleccionado los siete expuestos ya que en ellos se puede ver de forma más clara la evolución de la investigación y los resultados principales.

Como se puede observar en el primer artículo la investigación partió de seleccionar unos transductores adecuados a las aplicaciones de posicionamiento, por un lado, y del array paramétrico, por otro. Una vez seleccionados dichos transductores, comenzó lo que sería mi tarea principal, el desarrollo de la electrónica que pudiese excitar dichos transductores con señales predefinidas en cuanto se recibiese una señal de disparo.

En un prototipo muy primitivo se trató de conseguir dicho objetivo mediante el uso de un DAC y sendos amplificadores integrados. Aunque este prototipo no aparece expuesto en los artículos presentados, sí que fue una primera prueba que nos permitió darnos cuenta de que dicha solución no era óptima para los requisitos altamente restrictivos que teníamos en los telescopios submarinos de neutrinos.

Es por ello que rápidamente nos decantamos por realizar una amplificación digital (clase D) ya que además de tener una alta eficiencia nos permitía almacenar la energía en los tiempos muertos entre emisiones para poder emplearla en las mismas, dado que este sistema de amplificación tiene muy poco consumo en reposo.

Para realizar la prueba de concepto del amplificador clase D se preparó una segunda placa de prototipo, que tampoco aparece reflejada en los artículos presentados, que mediante un microcontrolador y un transistor MOSFET, alimentaba el transductor a

través de un transformador bobinado a mano para la prueba. Una vez se validó la prueba de concepto se pasó a diseñar el prototipo que se describe en los artículos 1 y 2 presentados en el tema 2.

Para dicho prototipo se decidió montar un amplificador basado en un puente en H con unos transistores MOSFET suficientemente rápidos en su conmutación y con una muy baja resistencia, *Ron*. También se seleccionó un *driver* que fuese capaz de encenderlos y apagarlos lo bastante rápido (Anexo A.2). Por último, para generar las señales se seleccionó un microcontrolador DsPIC de la casa Microchip que mediante un dispositivo interno pensado para control de motores nos permitía generar las señales PWM necesarias para excitar el amplificador clase D (Anexo A.1).

Dicho prototipo fue ampliamente probado en laboratorio demostrando que se podían conseguir los requisitos propuestos para desarrollar el emisor acústico necesario para los sistemas de posicionamiento y calibración del telescopio de neutrinos.

Para poder realizar pruebas de campo más específicas se realizó una serie de prototipos que pudiesen ser integrados en los telescopios submarinos que estaban en activo en esas fechas (ANTARES y NEMO).

Como el grupo del Instituto de Física Corpuscular también estaba interesado en introducir en dichos telescopios su prototipo de calibrador laser y ya tenían diseñada una vasija para contenerlo. Decidimos poner nuestros esfuerzos en común e incluir en su vasija nuestro sistema emisor acústico y encargarnos nosotros de la parte de comunicación con el telescopio y del control de los modos de funcionamiento de su calibrador laser.

Para poder realizar la integración en ANTARES, que se puede ver en el primer artículo del tema 2, fue necesario adaptar las comunicaciones de la placa, que habían sido diseñadas para trabajar con RS232 y con protocolo propietario basado en comandos ASCII, a RS485 con protocolo MODBUS. Para poder realizar las pruebas pertinentes con dicho protocolo se desarrolló un software Windows que simulaba las comunicaciones con el protocolo.

Otras modificaciones realizadas en la placa fueron: la inclusión de un conector con entradas y salidas digitales y bus i2c que permitían controlar los diversos parámetros del calibrador laser y un relé que permitía conectar el transductor FFR-SX30 a una placa de adquisición externa.

Una vez realizadas las modificaciones se realizaron sendos viajes para poder probar la integración electrónica de nuestro prototipo y el calibrador laser con la electrónica de prueba *onshore* de cada telescopio. El resultado obtenido en ambos casos fue correcto y se pasó a la fase de integración en sendos telescopios.

Teniendo por fin situados nuestros dos prototipos en ambos telescopios pudimos pasar a analizar los datos obtenidos de nuestras emisiones junto con los datos realizados en el laboratorio y el puerto de Gandia. Uno de los objetivos que se pretendía demostrar con

el análisis de dicha información era que, además de tener un emisor funcional, podríamos mejorar las características del sistema de posicionamiento (precisión, alcance y relación señal ruido) mediante el uso de técnicas de procesado de señal.

El método que se suele usar en los sistemas posicionamiento acústico, se basa en la detección de la llegada de la señal por umbral. Pero dicho método tiene una serie de problemas inherentes, el primero sería la falta de precisión dado que se usan señales senoidales que se van atenuando con la distancia, el segundo problema sería debido a que los emisores acústicos suelen emitir los primeros ciclos más atenuados puesto que el transductor todavía no tiene inercia y esto podría hacer que el umbral se salte alguno de los primeros ciclos con lo que calcularía un tiempo de vuelo erróneo. También podría haber reflexiones en elementos del telescopio que se superpusieran coherentemente y por tanto su intensidad final depender del desfase entre la onda directa y la reflejada.

Es por esto que en las pruebas de laboratorio y de campo se ha optado por comparar el método tradicional con la correlación de señales de banda ancha (MLS y *frequency sweep*) demostrando con este segundo método que no solo se puede conseguir el tiempo de vuelo con mucha mayor precisión, dado que se tienen en cuenta todas las muestras de la señal, si no que se puede usar en entornos donde el fondo de ruido incluso enmascara completamente la señal recibida. Estos resultados son los que dieron lugar a los artículos tres y cuatro contenidos en el capítulo 2.

El siguiente paso fue adaptar el emisor acústico a los requisitos finales impuestos para el telescopio KM3NeT. Uno de los requerimientos era aumentar la presión acústica hasta los 180 dB re 1μPa a 1m. Para lo que se decidió aumentar directamente la tensión de alimentación del amplificador clase D desde los 12V previos hasta 60V (Anexo A.4.). Para mejorar las prestaciones del equipo se hizo que dicha tensión fuese configurable mediante comandos que modificaban el voltaje de carga del condensador de emisión. Es por esto que se modificó la parte de alimentación para incluir un *boost converter* y dos limitadores de corriente opto-acoplados que permitían cargar y descargar el condensador para llegar al valor deseado (Anexo A.6). Otro cambio importante fue la decisión de dividir la *sound emission board* en tres placas: control, alimentación y potencia, en vistas a reducir la posibilidad de que se produjesen interferencias electromagnéticas en el momento de la emisión. Y por último cabe destacar que se sustituyó tanto el interfaz uart/rs232 como el receptor de la señal de disparo por otros diseños que permitían aislar nuestro emisor acústico de la masa del telescopio evitando así interferencias electromagnéticas (Anexo A.5).

Otras mejoras que fueron introducidas en el sistema fueron introducir un sensor de temperatura y humedad en la placa de control, añadir un bus RS485 interno con el objetivo de realizar lecturas de la presión externa mediante un sensor de la marca KELLER, instalar un *bootloader* que permite la actualización remota del firmware de la placa, implementar un sistema que permite la ejecución de comandos de arranque y permitir la subida/descarga de señales acústicas mediante un protocolo simple así como

el guardado/recuperación/borrado de dichas señales en una memoria flash montada en la placa de control (Anexo A.5).

Una vez cumplidos estos requisitos se montaron 18 *acoustic beacons* en unas vasijas de aluminio anodizado diseñadas por la empresa Mediterráneo Señales Marítimas SLL que tras verificar su tolerancia a altas presiones en cámaras hiperbáricas y caracterizarlos acústicamente fueron entregados a KM3NeT para su integración en el telescopio. En el artículo número cinco del tema 2 se describe el desarrollo y producción del emisor acústico.

En cuanto al desarrollo del sistema de calibración acústica, cabe destacar que después de numerosos intentos de adaptar nuestro emisor acústico al array de transductores descritos en el primer artículo, pudimos ver que, aunque las pruebas de laboratorio habían dado resultados prometedores, el hecho de que tuviesen una impedancia tan baja hacia que los requisitos de potencia para el nivel de señal obtenida no fuese el óptimo, resultando necesario elevar la potencia muy por encima de las prestaciones del amplificador clase D diseñado. Debido a estos resultados se decidió continuar con la búsqueda de unos transductores que nos permitiesen reproducir los datos obtenidos con el anterior diseño, pero con una importante mejora en la sensibilidad. Esta búsqueda nos llevó hasta unos transductores piezo-ceramicos de la empresa UCE ultrasonic Co. LTD que tienen también una simetría similar a los FFR-SX83 puestos a prueba en el primer artículo.

En el sexto artículo presentado en el capítulo 2 se muestran la caracterización de dos de los nuevos transductores, para decidir cuál es el que mejor cumple con los requisitos a la hora de generar el pulso bipolar paramétricamente con el patrón de directividad *pancake*.

Por último, en el séptimo artículo se puede ver el proceso para obtener los mejores resultados posibles de los transductores piezo-ceramicos propuestos mediante el uso de un *backing* y un *matching layer* que han permitido mejorar la sensibilidad en 9 dB situándola cerca de los 170 dB re. 1μPa/V @ 1m, y por tanto adecuado como elemento básico para el array paramétrico.

Cabe mencionar también que diseñé un software para la localización y direccionamiento del calibrador acústico en las campañas marítimas (Anexo A.7).

En síntesis, los resultados obtenidos son:

- Se ha desarrollado un sistema emisor acústico con acabado comercial, que cumple perfectamente con los requisitos de KM3NeT para ser usados en su sistema de posicionamiento acústico.
- Se ha probado con éxito que usando procesado de señal (filtrado, interpolación, correlación) se puede mejorar enormemente la precisión, las prestaciones y el alcance del sistema de posicionamiento.
- Se han realizado grandes avances en el desarrollo de un calibrador acústico compacto para el telescopio de neutrinos.

Capítulo 4
Conclusiones

4.1 Cumplimiento de objetivos.

Conforme se puede ver el tema anterior, se ha desarrollado con éxito y con acabado comercial un sistema emisor acústico que cumple con todos los requisitos impuestos por el pliego de condiciones de KM3NeT.

También se ha diseñado y probado un nuevo sistema de procesado de señal que permite el cálculo del tiempo de la señal acústica con mucha mayor precisión y alcance que el sistema predecesor. Y se ha demostrado que además puede funcionar en entornos con peor relación señal ruido.

Se han desarrollado sendos prototipos de transductores acústicos que cumplen con los requisitos necesarios para formar parte de un calibrador acústico y compacto de neutrinos.

Se han desarrollado una serie de herramientas Software y Firmware que han aumentado la versatilidad de los emisores acústicos y que han facilitado el desarrollo de los diferentes test y pruebas a los que se han sometido los dispositivos diseñados.

4.2 Aportaciones realizadas.

Una de las principales aportaciones realizadas al proyecto ha sido, como no, la realización de un sistema emisor de ultrasonidos que tiene un alto nivel de confiabilidad, un muy buen rendimiento y unas prestaciones que nos han permitido formar parte del hardware fundamental del nuevo telescopio de neutrinos KM3NeT. Particularmente destacable ha sido el diseño y desarrollo de la *sound emission board*, que ha permitido, por un lado, explotar al máximo las características de los transductores elegidos y, por otro, una óptima integración en la infraestructura KM3NeT cumpliendo con los estándares y requisitos requeridos.

Paralelamente también he colaborado en la elección y diseño de los nuevos transductores propuestos para el calibrador acústico de neutrinos, así como en la elaboración de los *backing* y los moldes para la resina del *matching layer*.Así como he colaborado en el diseño de la estructura de soporte para el array del nuevo calibrador acústico. Además, desarrollé una aplicación para las campañas marítimas, que permitía posicionar el array emisor del calibrador mediante el uso de un Smartphone que enviaba su ubicación GPS y los datos del magnetómetro y los acelerómetros por UDP a un portátil que registraba los datos, indicaba hacia donde apuntar para que la señal llegase al telescopio desde el barco y por último enviaba los comandos necesarios mediante un script a la tarjeta electrónica emisora. De esta forma quedaba registrado tanto la posición y dirección de la emisión como el tipo de emisión realizada, y así poder cotejar los datos con las señales acústicas registradas por el telescopio.

En cuanto a la detección de la señal para el cálculo del tiempo de vuelo, promoví e hice los primeros cálculos para comprobar la viabilidad de usar señales de banda ancha y correlación en la recepción. También realicé pruebas para mejorar la precisión del sistema actual, que emplea conversores ADC de 200ksps por lo que tendría una precisión de unos 7,5mm (v=1500 m/s), aplicando una interpolación tanto en la señal recibida como la emitida para mejorar la precisión, entorno a un milímetro.

4.3 Líneas de investigación futuras.

Una vez vistos los resultados obtenidos queda plantear futuras líneas de trabajo para mejorar, aún más si cabe, el sistema emisor y así poder dar por finalizado el diseño del calibrador, así como una versión mejor del *acoustic beacon.*.

La primera modificación que sería interesante hacer con el *acoustic beacon* para lograr un sistema aún más potente y con mejor rendimiento sería mejorar la placa de potencia. Para ello se está barajando la idea de substituir los transistores MOSFET por IGBT que se pueden conseguir con una mayor capacidad de gestionar tensión y corriente.

Otro cambio interesante a realizar en la placa de potencia sería sustituir el driver por otro que permita proteger los transistores contra sobrecorrientes además de poder trabajar con un rango de tensiones mal alto que el actual.

Un cambio necesario en la placa de potencia es substituir el transformador bobinado por un transformador planar. Este cambio permitiría por un lado prescindir de depender de empresas externas para que nos los fabriquen, y por otro lado mejorar la homogeneidad del diseño.

Por último, también se está planteando la posibilidad de instalar un *TR switch* con asilamiento galvánico que permita aprovechar el transductor también para recepción sin emplear relés que tienen un ciclo de vida más limitado y un retardo de activación más alto.

En cuanto a la placa de alimentación se planteó la posibilidad de incluir un reloj de tiempo real (RTC) de alta precisión que permita encender la placa a intervalos pre-programados cuando está trabajando con un pack de baterías externo de forma autónoma.

Otra modificación interesante en dicha placa seria substituir el *boostconverter* por otro que permita ajustar la corriente y la tensión de salida de forma digital, lo que permitiría mejorar aún más el rendimiento del sistema.

Otra línea de actuación, sería aumentar la aplicabilidad del *acoustic beacon* desarrollado. Con unas modificaciones modestas, el emisor acústico se podría adaptar y utilizar como transceptor acústico para comunicación acústica, ecosonda, etc.

En cuanto al calibrador acústico de neutrinos para el diseño un array con los transductores propuestos en los artículos seis y siete se podría usar un amplificador independiente basado en un *pulser* de la casa Microchip que permite generar señales de unos 200Vpp y 2,5A que usando una red de adaptación debería proporcionar suficiente potencia. Con ello, se podría completar el calibrador compacto basado en generación paramétrica, que, tras la correspondiente caracterización y testeo, podría ser usado y/o incorporado en la infraestructura de los telescopios de neutrinos.

Bibliografia

[AAR13] M. G. Aartsen et al. (IceCube Collaboration), Evidence for High-Energy Extraterrestrial Neutrinos at the IceCube Detector, Science 342 (2013) 1242856.

[ADR12] S. Adrian-Martinez et al. (ANTARES Coll.), The Positioning System of the ANTARES Neutrino Telescope, J. Inst. 7 (2012) T08002.

[ADR16] S. Adrian-Martinez et al. (ANTARES Coll.), A search for Secluded Dark Matter in the Sun with the ANTARES neutrino telescope, JCAP 05 (2016) 016.

[ADR16b] S. Adrian-Martinez et al. (KM3NeT Coll.), Letter of intent for KM3NeT 2.0, J. Phys. G 43 (2016) no.8, 084001.

[AGE11] M. Ageron et al. (ANTARES Collaboration), ANTARES: the first undersea neutrino telescope, Nucl. Instrum. Meth. A 656 (2011) 11.

[AGU11] J.A. Aguilar, et al. (ANTARES Collaboration), AMADEUS, The acoustic neutrino detection test system of the ANTARES deep-sea neutrino telescope, Nucl. Instr. and Meth. A 626 (2011) 128.

[ARD09] M. Ardid for the ANTARES Collaboration, Positioning system of the ANTARES neutrino telescope, Nucl. Instrum. Meth. A 602 (2009) 174.

[ARD17] M. Ardid et al., Constraining Secluded Dark Matter models with the public data from the 79-string IceCube search for dark matter in the Sun, JCAP 04 (2017) 010.

[ASK57] G.A. Askaryan, Hydrodynamical emission of tracks of ionising particles in stable liquids. J. A Energy 3 (1957) 921.

[ASK79] G.A. Askarian et al, Acoustic Detection Of High-energy Particle Showers In Water, Nucl. Instrum. Meth. 164 (1979) 267.

[COY17] P. Coyle and C.W. James for the ANTARES Collaboration, Recent Results from the ANTARES Neutrino Telescope, 2017, arXiv:1701.02144.

[ENZ13] A. Enzenhöfer on behalf of the KM3NeT Consortium, Combined Opto-Acoustical Sensor Modules for KM3NeT, AIP Conf. Proc. 1535 (2013) 185.

[RIC09] G. Riccobene et al. (NEMO Collaboration), Long-term measurements of acoustic background noise in very deep sea, Nucl. Instrum. Meth. A 604 (2009) S149.

[RIC09b] C Richardt, et al., Reconstruction methods for acoustic particle detection in the deep sea using clusters of hydrophones, Astropart. Phys. 31 (2009) 19.

[THO08] L.F.Thompson and J.D. Perkin, Acoustic Detection of UHE Neutrinos – the ACORNE project. Journal of Physics: Conference Series 136 (2008) 042070.

[VAN05] J. Vandenbroucke, G. Gratta and N. Lehtinen, Experimental study of acoustic ultra-high-energy neutrino detection, Astrophys. J. 621 (2005) 301.

[VIO16] S. Viola et al., on behalf of the KM3NeT Collaboration, Acoustic positioning system for KM3NeT, PoS ICRC2015 (2016) 1169.

[WES63] P. J. Westervelt, Parametric Acoustic Array, J. Acoust. Soc. Am. 35 (1963) 535.

Co-autoría de artículos relacionados con la tesis

1) Adrián-Martínez, S., Ageron, M., Aiello, S., Albert, A., Ameli, F., Anassontzis, E.G., Andre, M., Androulakis, G., Anghinolfi, M., Anton, G., Ardid, M., Avgitas, T., Barbarino, G., Barbarito, E., Baret, B., Barrios-Mart, J., Belias, A., Berbee, E., van den Berg, A., Bertin, V., Beurthey, S., van Beveren, V., Beverini, N., Biagi, S., Biagioni, A., Billault, M., Bondì, M., Bormuth, R., Bouhadef, B., Bourlis, G., Bourret, S., Boutonnet, C., Bouwhuis, M., Bozza, C., Bruijn, R., Brunner, J., Buis, E., Buompane, R., Busto, J., Cacopardo, G., Caillat, L., Calamai, M., Calvo, D., Capone, A., Caramete, L., Cecchini, S., Celli, S., Champion, C., Cherubini, S., Chiarella, V., Chiarelli, L., Chiarusi, T., Circella, M., Classen, L., Cobas, D., Cocimano, R., Coelho, J.A.B., Coleiro, A., Colonges, S., Coniglione, R., Cordelli, M., Cosquer, A., Coyle, P., Creusot, A., Cuttone, G., D'Amato, C., D'Amico, A., D'Onofrio, A., De Bonis, G., De Sio, C., Di Palma, I., Díaz, A.F., Distefano, C., Donzaud, C., Dornic, D., Dorosti-Hasankiadeh, Q., Drakopoulou, E., Drouhin, D., Durocher, M., Eberl, T., Eichie, S., van Eijk, D., El Bojaddaini, I., Elsaesser, D., Enzenhöfer, A., Favaro, M., Fermani, P., Ferrara, G., Frascadore, G., Furini, M., Fusco, L.A., Gal, T., Galatà, S., Garufi, F., Gay, P., Gebyehu, M., Giacomini, F., Gialanella, L., Giordano, V., Gizani, N., Gracia, R., Graf, K., Grégoire, T., Grella, G., Grmek, A., Guerzoni, M., Habel, R., Hallmann, S., van Haren, H., Harissopulos, S., Heid, T., Heijboer, A., Heine, E., Henry, S., Hernández-Rey, J.J., Hevinga, M., Hofestädt, J., Hugon, C.M.F., Illuminati, G., James, C.W., Jansweijerf, P., Jongen, M., de Jong, M., Kadler, M., Kalekin, O., Kappes, A., Katz, U.F., Keller, P., Kieft, G., Kießling, D., Koffeman, E.N., Kooijman, P., Kouchner, A., Kreter, M., Kulikovskiy, V., Lahmann, R., Lamare, P., Larosa, G., Leisos, A., Leone, F., Leonora, E., Lindsey Clark, M., Liolios, A., Llorens Alvarez, C.D., Lo Presti, D., Löhner, H., Lonardo, A., Lotze, M., Loucatos, S., Maccioni, E., Mannheim, K., Manzali, M., Margiotta, A., Margotti, A., Marinelli, A., Maris, O., Markou, C., Martínez-Mora, J.A., Martini, A., Marzaioli, F., Mele, R., Melis, K.W., Michael, T., Migliozzi, P., Migneco, E., Mijakowski, P., Miraglia, A., Mollo, C.M., Mongelli, M., Morganti, M., Moussa, A., Musico, P., Musumeci, M., Navas, S., Nicolau, C.A., Olcina, I., Olivetto, C., Orlando,

A., Orzelli, A., Pancaldi, G., Papaikonomou, A., Papaleo, R., Păvălas, G.E., Peek, H., Pellegrini, G., Pellegrino, C., Perrina, C., Pfutzner, M., Piattelli, P., Pikounis, K., Pleinert, M.-O., Poma, G.E., Popa, V., Pradier, T., Pratolongo, F., Pühlhofer, G., Pulvirenti, S., Quinn, L., Racca, C., Raffaelli, F., Randazzo, N., Rauch, T., Real, D., Resvanis, L., Reubelt, J., Riccobene, G., Rossi, C., Rovelli, A., Saldaña, M., Salvadori, I., Samtleben, D.F.E., Sánchez García, A., Sánchez Losa, A., Sanguineti, M., Santangelo, A., Santonocito, D., Sapienza, P., Schimmel, F., Schmelling, J., Schnabel, J., Sciacca, V., Sedita, M., Seitz, T., Sgura, I., Simeone, F., Sipala, V., Spisso, B., Spurio, M., Stavropoulos, G., Steijger, J., Stellacci, S.M., Stransky, D., Taiuti, M., Tayalati, Y., Terrasi, F., Tézier, D., Theraube, S., Timmer, P., Tönnis, C., Trasatti, L., Travaglini, R., Trovato, A., Tsirigotis, A., Tzamarias, S., Tzamariudaki, E., Vallage, B., Van Elewyck, V., Vermeulen, J., Versari, F., Vicini, P., Viola, S., Vivolo, D., Volkert, M., Wiggers, L., Wilms, J., de Wolf, E., Zachariadou, K., Zani, S., Zornoza, J.D., Zúñiga, J.

Intrinsic limits on resolutions in muon- and electron-neutrino charged-current events in the KM3NeT/ORCA detector

(2017) Journal of High Energy Physics, 2017 (5), art. no. 8.

2) Saldaña, M., Llorens, C.D., Felis, I., Martínez-Mora, J.A., Ardid, M.

Transducer development and characterization for underwater acoustic neutrino detection calibration

(2016) Sensors (Switzerland), 16 (8), art. no. 1210.

3) Ardid, M., Camarena, F., Felis, I., Herrero, A., Llorens, C.D., Martínez-Mora, J., Saldaña, M.

A compact array calibrator to study the feasibility of acoustic neutrino detection

(2016) EPJ Web of Conferences, 116, art. no. 03001.

4) Adrián-Martínez, S., Aiello, S., Ameli, F., Anghinolfi, M., Ardid, M., Barbarino, G., Barbarito, E., Barbato, F.C.T., Beverini, N., Biagi, S., Biagioni, A., Bouhadef, B., Bozza, C., Cacopardo, G., Calamai, M., Calì, C., Calvo, D., Capone, A., Caruso, F., Ceres, A., Chiarusi, T., Circella, M., Cocimano, R., Coniglione, R., Costa, M., Cuttone, G., D'Amato, C., D'Amico, A., De Bonis, G., De Luca, V., Deniskina, N., De Rosa, G., di Capua, F., Distefano, C., Enzenhöfer, A., Fermani, P., Ferrara, G., Flaminio, V., Fusco, L.A., Garufi, F., Giordano, V., Gmerk, A., Grasso, R., Grella, G., Hugon, C., Imbesi, M., Kulikovskiy, V., Lahmann, R., Larosa, G., Lattuada, D., Leismüller, K.P., Leonora, E., Litrico, P., Llorens Alvarez, C.D., Lonardo, A., Longhitano, F., Lo Presti, D., Maccioni, E., Margiotta, A., Marinelli, A., Martini, A., Masullo, R., Migliozzi, P., Migneco, E.,

Miraglia, A., Mollo, C.M., Mongelli, M., Morganti, M., Musico, P., Musumeci, M., Nicolau, C.A., Orlando, A., Orzelli, A., Papaleo, R., Pellegrino, C., Pellegriti, M.G., Perrina, C., Piattelli, P., Pugliatti, C., Pulvirenti, S., Raffaelli, F., Randazzo, N., Real, D., Riccobene, G., Rovelli, A., Saldaña, M., Sanguineti, M., Sapienza, P., Sciacca, V., Sgura, I., Simeone, F., Sipala, V., Speziale, F., Spitaleri, A., Spurio, M., Stellacci, S.M., Taiuti, M., Terreni, G., Trasatti, L., Trovato, A., Ventura, C., Vicini, P., Viola, S., Vivolo, D.

Long term monitoring of the optical background in the Capo Passero deep-sea site with the NEMO tower prototype

(2016) European Physical Journal C, 76 (2), art. no. 68, pp. 1-11. Cited 2 times.

5) Adrián-Martínez, S., Ageron, M., Aharonian, F., Aiello, S., Albert, A., Ameli, F., Anassontzis, E.G., Androulakis, G.C., Anghinolfi, M., Anton, G., Anvar, S., Ardid, M., Avgitas, T., Balasi, K., Band, H., Barbarino, G., Barbarito, E., Barbato, F., Baret, B., Baron, S., Barrios, J., Belias, A., Berbee, E., van den Berg, A.M., Berkien, A., Bertin, V., Beurthey, S., van Beveren, V., Beverini, N., Biagi, S., Biagioni, A., Bianucci, S., Billault, M., Birbas, A., Boer Rookhuizen, H., Bormuth, R., Bouché, V., Bouhadef, B., ourlis, G., Boutonnet, C., Bouwhuis, M., Bozza, C., Bruijn, R., Brunner, J., Cacopardo, G., Caillat, L., Calamai, M., Calvo, D., Capone, A., Caramete, L., Caruso, F., Cecchini, S., Ceres, A., Cereseto, R., Champion, C., Château, F., Chiarusi, T., Christopoulou, B., Circella, M., Classen, L., Cocimano, R., Coleiro, A., Colonges, S., Coniglione, R., Cosquer, A., Costa, M., Coyle, P., Creusot, A., Cuttone, G., D'Amato, C., D'Amico, A., De Bonis, G., De Rosa, G., Deniskina, N., Destelle, J.-J., Distefano, C., Di Capua, F., Donzaud, C., Dornic, D., Dorosti-Hasankiadeh, Q., Drakopoulou, E., Drouhin, D., Drury, L., Durand, D., Eberl, T., Elsaesser, D., Enzenhöfer, A., Fermani, P., Fusco, L.A., Gajanana, D., Gal, T., Galatà, S., Garufi, F., Gebyehu, M., Giordano, V., Gizani, N., Gracia Ruiz, R., Graf, K., Grasso, R., Grella, G., Grmek, A., Habel, R., van Haren, H., Heid, T., Heijboer, A., Heine, E., Henry, S., Hernández-Rey, J.J., Herold, B., Hevinga, M.A., van der Hoek, M., Hofestädt, J., Hogenbirk, J., Hugon, C., Hößl, J., Imbesi, M., James, C.W., Jansweijer, P., Jochum, J., de Jong, M., Jongen, M., Kadler, M., Kalekin, O., Kappes, A., Kappos, E., Katz, U., Kavatsyuk, O., Keller, P., Kieft, G., Koffeman, E., Kok, H., Kooijman, P., Koopstra, J., Korporaal, A., Kouchner, A., Kreykenbohm, I., Kulikovskiy, V., Lahmann, R., Lamare, P., Larosa, G., Lattuada, D., Le Provost, H., Leismüller, K.P., Leisos, A., Lenis, D., Leonora, E., Lindsey Clark, M., Llorens Alvarez, C.D., Löhner, H., Lonardo, A., Loucatos, S., Louis, F., Maccioni, E., Mannheim, K., Manolopoulos, K., Margiotta, A., Mariş, O., Markou, C., Martínez-Mora, J.A., Martini, A., Masullo, R., Melis, K.W., Michael, T., Migliozzi, P., Migneco, E., Miraglia, A., Mollo, C.M., Mongelli, M., Morganti, M., Mos, S., Moudden, Y., Musico, P., Musumeci, M., Nicolaou, C., Nicolau, C.A., Orlando, A., Orzelli, A., Papaikonomou, A., Papaleo, R., Păvălaş, G.E., Peek, H., Pellegrino, C., Pellegriti, M.G., Perrina, C., Piattelli, P., Pikounis, K., Popa, V., Pradier, T., Priede, M., Pühlhofer, G., Pulvirenti, S., Racca, C.,

Raffaelli, F., Randazzo, N.,Rapidis, P.A., Razis, P., Real, D., Resvanis, L., Reubelt, J., Riccobene, G., Rovelli, A., Saldaña, M., Samtleben, D.F.E., Sanguineti, M., Santangelo, A., Sapienza, P., Schmelling, J., Schnabel, J., Sciacca, V., Sedita, M., Seitz, T., Sgura, I., Simeone, F., Sipala, V., Spitaleri, A., Spurio, M., Stavropoulos, G., Steijger, J., Stolarczyk, T., Stransky, D., Taiuti, M., Terreni, G., Tézier, D., Théraube, S., Thompson, L.F., Timmer, P., Trasatti, L., Trovato, A., Tselengidou, M., Tsirigotis, A., Tzamarias, S., Tzamariudaki, E., Vallage, B., Van Elewyck, V., Vermeulen, J., Vernin, P., Vicini, P., Viola, S., Vivolo, D., Werneke, P., Wiggers, L., Wilms, J., de Wolf, E., van Wooning, R.H.L., Zonca, E., Zornoza, J.D., Zúñiga, J., Zwart, A.

The prototype detection unit of the KM3NeT detector: KM3NeT Collaboration

(2016) European Physical Journal C, 76 (2), art. no. 54, pp. 1-12. Cited 7 times.

6) Saldaña, M., Adrián-Martínez, S., Bou-Cabo, M., Felis, I., Larosa, G., Llorens, C.D., Martínez-Mora, J.A., Ardid, M.

Ultrasonic Transmitter for Positioning of the Large Underwater Neutrino Telescope KM3NeT

(2015) Physics Procedia, 63, pp. 195-200.

7) Adrián-Martínez, S., Bou-Cabo, M., Felis, I., Llorens, C.D., Martínez-Mora, J.A., Saldaña, M., Ardid,M.

Acoustic signal detection through the cross-correlation method in experiments with different signal to noise ratio and reverberation conditions

(2015) Lecture Notes in Computer Science (including subseries Lecture Notes in Artificial Intelligence and Lecture Notes in Bioinformatics), 8629, pp. 66-79. Cited 3 times.

8) Adrián-Martínez, S., Ageron, M., Aharonian, F., Aiello, S., Albert, A., Ameli, F., Anassontzis, E.G., Anghinolfi, M., Anton, G., Anvar, S., Ardid, M., de Asmundis, R., Balasi, K., Band, H., Barbarino, G., Barbarito, E., Barbato, F., Baret, B., Baron, S., Belias, A., Berbee, E., van den Berg, A.M., Berkien, A., Bertin, V., Beurthey, S., van Beveren, V., Beverini, N., Biagi, S., Bianucci, S., Billault, M., Birbas, A., Boer Rookhuizen, H., Bormuth, R., Bouché, V., Bouhadef, B., Bourlis, G., Bouwhuis, M., Bozza, C., Bruijn, R., Brunner, J., Cacopardo, G., Caillat, L., Calamai, M., Calvo, D., Capone, A., Caramete, L., Caruso, F., Cecchini, S., Ceres, A., Cereseto, R., Champion, C., Château, F., Chiarusi, T., Christopoulou, B., Circella, M., Classen, L., Cocimano, R., Colonges, S., Coniglione, R., Cosquer, A., Costa, M., Coyle, P., Creusot, A., Curtil, C., Cuttone, G., D'Amato, C., D'Amico, A., De Bonis, G., De Rosa, G., Deniskina, N.,

Destelle, J.-J., Distefano, C., Donzaud, C., Dornic, D., Dorosti-Hasankiadeh, Q., Drakopoulou, E., Drouhin, D., Drury, L., Durand, D., Eberl, T., Eleftheriadis, C., Elsaesser, D., Enzenhöfer, A., Fermani, P., Fusco, L.A., Gajana, D., Gal, T., Galatà, S., Gallo, F., Garufi, F., Gebyehu, M., Giordano, V., Gizani, N., Gracia Ruiz, R., Graf, K., Grasso, R., Grella, G., Grmek, A., Habel, R., van Haren, H., Heid, T., Heijboer, A., Heine, E., Henry, S., Hernández-Rey, J.J., Herold, B., Hevinga, M.A., van der Hoek, M., Hofestädt, J., Hogenbirk, J., Hugon, C., Hößl, J., Imbesi, M., James, C., Jansweijer, P., Jochum, J., de Jong, M., Kadler, M., Kalekin, O., Kappes, A., Kappos, E., Katz, U., Kavatsyuk, O., Keller, P., Kieft, G., Koffeman, E., Kok, H., Kooijman, P., Koopstra, J., Korporaal, A., Kouchner, A., Koutsoukos, S., Kreykenbohm, I., Kulikovskiy, V., Lahmann, R., Lamare, P., Larosa, G., Lattuada, D., Le Provost, H., Leisos, A., Lenis, D., Leonora, E., Lindsey Clark, M., Liolios, A., Llorens Alvarez, C.D., Löhner, H., Lo Presti, D., Louis, F., Maccioni, E., Mannheim, K., Manolopoulos, K., Margiotta, A., Mariş, O., Markou, C., Martínez-Mora, J.A., Martini, A., Masullo, R., Michael, T., Migliozzi, P., Migneco, E., Miraglia, A., Mollo, C., Mongelli, M., Morganti, M., Mos, S., Moudden, Y., Musico, P., Musumeci, M., Nicolaou, C., Nicolau, C.A., Orlando, A., Orzelli, A., Papageorgiou, K., Papaikonomou, A., Papaleo, R., Păvălaş, G.E., Peek, H., Pellegrino, C., Pellegriti, Terms and conditions Privacy policy Copyright © 2017 Elsevier B.V. All rights reserved. Scopus® is a registered trademark of Elsevier B.V. M.G., Perrina, C., Petridou, C., Piattelli, P., Pikounis, K., Popa, V., Pradier, T., Priede, M., Pühlhofer, G., Pulvirenti, S., Racca, C., Raffaelli, F., Randazzo, N., Rapidis, P.A., Razis, P., Real, D., Resvanis, L., Reubelt, J., Riccobene, G., Rovelli, A., Royon, J., Saldaña, M., Samtleben, D.F.E., Sanguineti, M., Santangelo, A., Sapienza, P., Savvidis, I., Schmelling, J., Schnabel, J., Sedita, M., Seitz, T., Sgura, I., Simeone, F., Siotis, I., Sipala, V., Solazzo, M., Spitaleri, A., Spurio, M., Stavropoulos, G., Steijger, J., Stolarczyk, T., Stransky, D., Taiuti, M., Terreni, G., Tézier, D., Théraube, S., Thompson, L.F., Timmer, P., Trapierakis, H.I., Trasatti, L., Trovato, A., Tselengidou, M., Tsirigotis, A., Tzamarias, S., Tzamariudaki, E., Vallage, B., Van Elewyck, V., Vermeulen, J., Vernin, P., Viola, S., Vivolo, D., Werneke, P., Wiggers, L., Wilms, J., de Wolf, E., van Wooning, R.H.L., Yatkin, K., Zachariadou, K., Zonca, E., Zornoza, J.D., Zúñiga, J., Zwart, A.

Deep sea tests of a prototype of the KM3NeT digital optical module: KM3NeT Collaboration

(2014) European Physical Journal C, 74 (9), art. no. 3056, 8 p. Cited 10 times.

9) Adrián-Martínez, S., Ardid, M., Bou-Cabo, M., Felis, I., Larosa, G., Llorens, C., Martínez-Mora, J.A., Saldaña, M.

A versatile compact array calibrator for UHE neutrino acoustic detection

(2013) AIP Conference Proceedings, 1535, pp. 190-194.

10) Adrian-Martinez, S., Ageron, M., Aguilar, J.A., Aharonian, F., Aiello, S., Albert, A., Alexandri, M., Ameli, M., Anassontzis, E.G., Anghinolfi, M., Anton, G., Anvar, S., Ardid, M., Assis Jesus, A., Aubert, J.-J., Bakker, R., Ball, A.E., Barbarino, G., Barbarito, E., Barbato, F., Baret, B., De Bel, M., Belias, A., Bellou, N., Berbee, E., Berkien, A., Bersani, A., Bertin, V., Beurthey, S., Biagi, S., Bigongiari, C., Bigourdan, B., Billault, M., De Boer, R., Boer Rookhuizen, H., Bonori, M., Borghini, M., Bou-Cabo, M., Bouhadef, B., Bourlis, G., Bouwhuis, M., Bradbury, S., Brown, A., Bruni, F., Brunner, J., Brunoldi, M., Busto, J., Cacopardo, G., Caillat, L., Calvo Díaz-Aldagalán, D., Calzas, A., Canals, M., Capone, A., Carr, J., Castorina, E., Cecchini, S., Ceres, A., Cereseto, R., Chaleil, Th., Chateau, F., Chiarusi, T., Choqueuse, D., Christopoulou, P.E., Chronis, G., Ciaffoni, O., Circella, M., Cocimano, R., Cohen, F., Colijn, F., Coniglione, R., Cordelli, M., Cosquer, A., Costa, M., Coyle, P., Craig, J., Creusot, A., Curtil, C., D'Amico, A., Damy, G., De Asmundis, R., De Bonis, G., Decock, G., Decowski, P., Delagnes, E., De Rosa, G., Distefano, C., Donzaud, C., Dornic, D., Dorosti-Hasankiadeh, Q., Drogou, J., Drouhin, D., Druillole, F., Drury, L., Durand, D., Durand, G.A., Eberl, T., Emanuele, U., Enzenhöfer, A., Ernenwein, J.-P., Escoffier, S., Espinosa, V., Etiope, G., Favali, P., Felea, D., Ferri, M., Ferry, S., Flaminio, V., Folger, F., Fotiou, A., Fritsch, U., Gajanana, D., Garaguso, R., Gasparini, G.P., Gasparoni, F., Gautard, V., Gensolen, F., Geyer, K., Giacomelli, G., Gialas, I., Giordano, V., Giraud, Terms and conditions Privacy policy Copyright © 2017 Elsevier B.V. All rights reserved. Scopus® is a registered trademark of Elsevier B.V. J., Gizani, N., Gleixner, A., Gojak, C., Gómez-González, J.P., Graf, K., Grasso, D., Grimaldi, A., Groenewegen, R., Guédé, Z., Guillard, G., Guilloux, F., Habel, R., Hallewell, G., Van Haren, H., Van Heerwaarden, J., Heijboer, A., Heine, E., Hernández-Rey, J.J., Herold, B., Van De Hoek, M., Hogenbirk, J., Hößl, J., Hsu, C.C., Imbesi, M., Jamieson, A., Jansweijer, P., De Jong, M., Jouvenot, F., Kadler, M., Kalantar-Nayestanaki, N., Kalekin, O., Kappes, A., Karolak, M., Katz, U.F., Kavatsyuk, O., Keller, P., Kiskiras, Y., Klein, R., Kok, H., Kontoyiannis, H., Kooijman, P., Koopstra, J., Kopper, C., Korporaal, A., Koske, P., Kouchner, A., Koutsoukos, S., Kreykenbohm, I., Kulikovskiy, V., Laan, M., La Fratta, C., Lagier, P., Lahmann, R., Lamare, P., Larosa, G., Lattuada, D., Leisos, A., Lenis, D., Leonora, E., Le Provost, H., Lim, G., Llorens, C.D., Lloret, J., Löhner, H., Lo Presti, D., Lotrus, P., Louis, F., Lucarelli, F., Lykousis, V., Malyshev, D., Mangano, S., Marcoulaki, E.C., Margiotta, A., Marinaro, G., Marinelli, A., Maris, O., Markopoulos, E., Markou, C., Martínez-Mora, J.A., Martini, A., Marvaldi, J., Masullo, R., Maurin, G., Migliozzi, P., Migneco, E., Minutoli, S., Miraglia, A., Mollo, C.M., Mongelli, M., Monmarthe, E., Morganti, M., Mos, S., Motz, H., Moudden, Y., Mul, G., Musico, P., Musumeci, M., Naumann, Ch., Neff, M., Nicolaou, C., Orlando, A., Palioselitis, D., Papageorgiou, K., Papaikonomou, A., Papaleo, R., Papazoglou, I.A., Păvălas, G.E., Peek, H.Z., Perkin, J., Piattelli, P., Popa, V., Pradier, T., Presani, E., Priede, I.G., Psallidas, A., Rabouille, C., Racca, C., Radu, A., Randazzo, N., Rapidis P.a., Razis, P., Real, D., Reed, C., Reito, S., Resvanis, L.K., Riccobene, G., Richter, R., Roensch, K., Rolin, J., Rose, J., Roux, J., Rovelli, A., Russo,

A., Russo, G.V., Salesa, F., Samtleben, D., Sapienza, P., Schmelling, J.-W., Schmid, J., Schnabel, J., Schroeder, K., Schuller, J.-P., Schussler, F., Sciliberto, D., Sedita, M., Seitz, T., Shanidze, R., Simeone, F., Siotis, I., Sipala, V., Sollima, C., Sparnocchia, S., Spies, A., Spurio, M., Staller, T., Stavrakakis, S., Stavropoulos, G., Steijger, J., Stolarczyk, Th., Stransky, D., Taiuti, M., Taylor, A., Thompson, L., Timmer, P., Tonoiu, D., Toscano, S., Touramanis, C., Trasatti, L., Traverso, P., Trovato, A., Tsirigotis, A., Tzamarias, S., Tzamariudaki, E., Urbano, F., Vallage, B., Van Elewyck, V., Vannoni, G., Vecchi, M., Vernin, P., Viola, S., Vivolo, D., Wagner, S., Werneke, P., White, R.J., Wijnker, G., Wilms, J., De Wolf, E., Yepes, H., Zhukov, V., Zonca, E., Zornoza, J.D., Zúñiga, J.

Expansion cone for the 3-inch PMTs of the KM3NeT optical modules

(2013) Journal of Instrumentation, 8 (3), art. no. T03006, . Cited 7 times.

11) Adrián-Martínez, S., Ageron, M., Aguilar, J.A., Aharonian, F., Aiello, S., Albert, A., Alexandri, M., Ameli, F., Anassontzis, E.G., Anghinolfi, M., Anton, G., Anvar, S., Ardid, M., Assis Jesus, A., Aubert, J.-J., Bakker, R., Ball, A.E., Barbarino, G., Barbarito, E., Barbato, F., Baret, B., De Bel, M., Belias, A., Bellou, N., Berbee, E., Berkien, A., Bersani, A., Bertin, V., Beurthey, S., Biagi, S., Bigongiari, C., Bigourdan, B., Billault, M., De Boer, R., Boer Rookhuizen, H., Bonori, M., Borghini, M., Bou-Cabo, M., Bouhadef, B., Bourlis, G., Bouwhuis, M., Bradbury, S., Brown, A., Bruni, F., Brunner, J., Brunoldi, M., Busto, J., Cacopardo, G., Caillat, L., Calvo Díaz-Aldagalán, D., Calzas, A., Canals, M., Capone, A., Carr, J., Castorina, E., Cecchini, S., Ceres, A., Cereseto, R., Chaleil, T., Chateau, F., Chiarusi, T., Choqueuse, D., Christopoulou, P.E., Chronis, G., Ciaffoni, O., Circella, M., Cocimano, R., Cohen, F., Colijn, F., Coniglione, R., Cordelli, M., Cosquer, A., Costa, M., Coyle, P., Craig, J., Creusot, A., Curtil, Terms and conditions Privacy policy Copyright © 2017 Elsevier B.V. All rights reserved. Scopus® is a registered trademark of Elsevier B.V. C., D'Amico, A., Damy, G., De Asmundis, R., De Bonis, G., Decock, G., Decowski, P., Delagnes, E., De Rosa, G., Distefano, C., Donzaud, C., Dornic, D., Dorosti-Hasankiadeh, Q., Drogou, J., Drouhin, D., Druillole, F., Drury, L., Durand, D., Durand, G.A., Eberl, T., Emanuele, U., Enzenhöfer, A., Ernenwein, J.-P., Escoffier, S., Espinosa, V., Etiope, G., Favali, P., Felea, D., Ferri, M., Ferry, S., Flaminio, V., Folger, F., Fotiou, A., Fritsch, U., Gajanana, D., Garaguso, R., Gasparini, G.P., Gasparoni, F., Gautard, V., Gensolen, F., Geyer, K., Giacomelli, G., Gialas, I., Giordano, V., Giraud, J., Gizani, N., Gleixner, A., Gojak, C., Gómez-González, J.P., Graf, K., Grasso, D., Grimaldi, A., Groenewegen, R., Guédé, Z., Guillard, G., Guilloux, F., Habel, R., Hallewell, G., Van Haren, H., Van Heerwaarden, J., Heijboer, A., Heine, E., Hernández-Rey, J.J., Herold, B., Hillebrand, T., Van De Hoek, M., Hogenbirk, J., Hößl, J., Hsu, C.C., Imbesi, M., Jamieson, A., Jansweijer, P., De Jong, M., Jouvenot, F., Kadler, M., Kalantar-Nayestanaki, N., Kalekin, O., Kappes, A., Karolak, M., Katz, U.F., Kavatsyuk, O., Keller, P., Kiskiras, Y., Klein, R., Kok, H., Kontoyiannis, H., Kooijman, P., Koopstra, J., Kopper, C., Korporaal, A., Koske, P., Kouchner, A., Koutsoukos, S., Kreykenbohm, I., Kulikovskiy, V., Laan, M., La Fratta,

C., Lagier, P., Lahmann, R., Lamare, P., Larosa, G., Lattuada, D., Leisos, A., Lenis, D., Leonora, E., Le Provost, H., Lim, G., Llorens, C.D., Lloret, J., Löhner, H., Lo Presti, D., Lotrus, P., Louis, F., Lucarelli, F., Lykousis, V., Malyshev, D., Mangano, S., Marcoulaki, E.C., Margiotta, A., Marinaro, G., Marinelli, A., Mariş, O., Markopoulos, E., Markou, C., Martínez-Mora, J.A., Martini, A., Marvaldi, J., Masullo, R., Maurin, G., Migliozzi, P., Migneco, E., Minutoli, S., Miraglia, A., Mollo, C.M., Mongelli, M., Monmarthe, E., Morganti, M., Mos, S., Motz, H., Moudden, Y., Mul, G., Musico, P., Musumeci, M., Naumann, C., Neff, M., Nicolaou, C., Orlando, A., Palioselitis, D., Papageorgiou, K., Papaikonomou, A., Papaleo, R., Papazoglou, I.A., Păvălaş, G.E., Peek, H.Z., Perkin, J., Piattelli, P., Popa, V., Pradier, T., Presani, E., Priede, I.G., Psallidas, A., Rabouille, C., Racca, C., Radu, A., Randazzo, N., Rapidis, P.A., Razis, P., Real, D., Reed, C., Reito, S., Resvanis, L.K., Riccobene, G., Richter, R., Roensch, K., Rolin, J., Rose, J., Roux, J., Rovelli, A., Russo, A., Russo, G.V., Salesa, F., Samtleben, D., Sapienza, P., Schmelling, J.-W., Schmid, J., Schnabel, J., Schroeder, K., Schuller, J.-P., Schussler, F., Sciliberto, D., Sedita, M., Seitz, T., Shanidze, R., Simeone, F., Siotis, I., Sipala, V., Sollima, C., Sparnocchia, S., Spies, A., Spurio, M., Staller, T., Stavrakakis, S., Stavropoulos, G., Steijger, J., Stolarczyk, T., Stransky, D., Taiuti, M., Taylor, A., Thompson, L., Timmer, P., Tonoiu, D., Toscano, S., Touramanis, C., Trasatti, L., Traverso, P., Trovato, A., Tsirigotis, A., Tzamarias, S., Tzamariudaki, E., Urbano, F., Vallage, B., Van Elewyck, V., Vannoni, G., Vecchi, M., Vernin, P., Viola, S., Vivolo, D., Wagner, S., Werneke, P., White, R.J., Wijnker, G., Wilms, J., De Wolf, E., Yepes, H., Zhukov, V., Zonca, E., Zornoza, J.D., Zúñiga, J.

Detection potential of the KM3NeT detector for high-energy neutrinos from the Fermi bubbles

(2013) Astroparticle Physics, 42, pp. 7-14. Cited 21 times.

12) Larosa, G., Ardid, M., Llorens, C.D., Bou-Cabo, M., Martínez-Mora, J.A., Adrian-Martínez, S.

Development of an acoustic transceiver for the KM3NeT positioning system

(2013) Nuclear Instruments and Methods in Physics Research, Section A: Accelerators, Spectrometers, Detectors and Associated Equipment, 725, pp. 215-218. Cited 1 time.

13) Viola, S., Ardid, M., Bertin, V., Enzenhofer, A., Keller, P., Lahmann, R., Larosa, G., Llorens, C.D.

NEMO-SMO acoustic array: A deep-sea test of a novel acoustic positioning system for a km3-scale underwater neutrino telescope

(2013) Nuclear Instruments and Methods in Physics Research, Section A: Accelerators, Spectrometers, Detectors and Associated Equipment, 725, pp. 207-210. Cited 11 times.

14) Adrian-Martínezn, S., Ardid, M., Bou-Cabo, M., Larosa, G., Llorens, C.D., Martínez-Mora, J.A.

A compact acoustic calibrator for ultra-high energy neutrino detection

(2013) Nuclear Instruments and Methods in Physics Research, Section A: Accelerators, Spectrometers, Detectors and Associated Equipment, 725, pp. 219-222. Cited 1 time.

15) Ardid, M., Martínez-Mora, J.A., Bou-Cabo, M., Larosa, G., Adrián-Martínez, S., Llorens, C.D.

Acoustic transmitters for underwater neutrino telescopes

(2012) Sensors, 12 (4), pp. 4113-4132. Cited 10 times.

16) Simeone, F., Ameli, F., Ardid, M., Bertin, V., Bonori, M., Bou-Cabo, M., Calì, C., D'Amico, A., Giovanetti, G., Imbesi, M., Keller, P., Larosa, G., Llorens, C.D., Masullo, R., Randazzo, N., Riccobene, G., Speziale, F., Viola, S.

Design and first tests of an acoustic positioning and detection system for KM3NeT

(2012) Nuclear Instruments and Methods in Physics Research, Section A: Accelerators, Spectrometers, Detectors and Associated Equipment, 662 (SUPPL. 1), . Cited 3 times.

17) Llorens, C.D., Ardid, M., Sogorb, T., Bou-Cabo, M., Martínez-Mora, J.A., Larosa, G., Adrin-Martínez, S.

The sound emission board of the KM3NeT acoustic positioning system

(2012) Journal of Instrumentation, 7 (1), art. no. C01001, . Cited 10 times.

18) Adrián, S., Ardid, M., Bou-Cabo, M., Larosa, G., Llorens, C.D., Martínez-Mora, J.A.

Development of a compact transmitter array for the acoustic neutrino detection calibration

(2011) Proceedings - 8th IEEE International Conference on Mobile Ad-hoc and Sensor Systems, MASS 2011, art. no. 6076708, pp. 916-921.

19) Ardid, M., Bou-Cabo, M., Camarena, F., Espinosa, V., Larosa, G., Llorens, C.D., Martnez-Mora, J.A.

R&D towards the acoustic positioning system of KM3NeT

(2011) Nuclear Instruments and Methods in Physics Research, Section A: Accelerators, Spectrometers, Detectors and Associated Equipment, 626-627 (SUPPL.), . Cited 10 times.

20) Ameli, F., Ardid, M., Bertin, V., Bonori, M., Bou-Cabo, M., Cal, C., D'Amico, A., Giovanetti, G., Imbesi, M., Keller, P., Larosa, G., Llorens, C.D., Masullo, R., Randazzo, N., Riccobene, G., Speziale, F., Viola, S.

R&D for an innovative acoustic positioning system for the KM3NeT neutrino telescope

(2011) Nuclear Instruments and Methods in Physics Research, Section A: Accelerators, Spectrometers, Detectors and Associated Equipment, 626-627 (SUPPL.), . Cited 11 times.

21) Ardid, M., Bou-Cabo, M., Camarena, F., Espinosa, V., Larosa, G., Llorens, C.D., Martínez-Mora, J.A.

A prototype for the acoustic triangulation system of the KM3NeT deep sea neutrino telescope

(2010) Nuclear Instruments and Methods in Physics Research, Section A: Accelerators, Spectrometers, Detectors and Associated Equipment, 617 (1-3), pp. 459-461. Cited 10 times.

Glosario

PMTs	Foto Multiplicadores.
ORCA	KM3NeT, Determinación de la masa Jerarquía de neutrinos.
ARCA	KM3Net, detección de neutrinos de alta energía de origen cósmico.
GZK	Límite Greisen-Zatsepin-Kuzmin.
MLS	Maximum length sequence.
FFR	Free Flooded Ring.
GeV	Giga electron voltio.
UPV	Universidad Politécnica de Valencia.
IFIC	Instituto de Física Corpuscular.
MODBUS	Protocolo de comunicaciones de nivel 7 de OSI.
OSI	Modelo de interconexión de sistemas abiertos.
RS232	Interfaz de comunicación serie.
RS485	Interfaz de comunicación serie sobre bus diferencial
MOSFET	Metal Oxide Semiconductor Field Effect Transistor.
IGBT	Insulated Gate Bipolar Transistor.
RTC	Reloj de Tiempo Real.
UDP	User Datagram Protocol.
ADC	Analog To Digital Converter.
TR switch	Conmutador entre Transmisión y Recepción.

Anexos

A.1 Esquemático de la parte de control del prototipo instalado en Antares y Nemo.

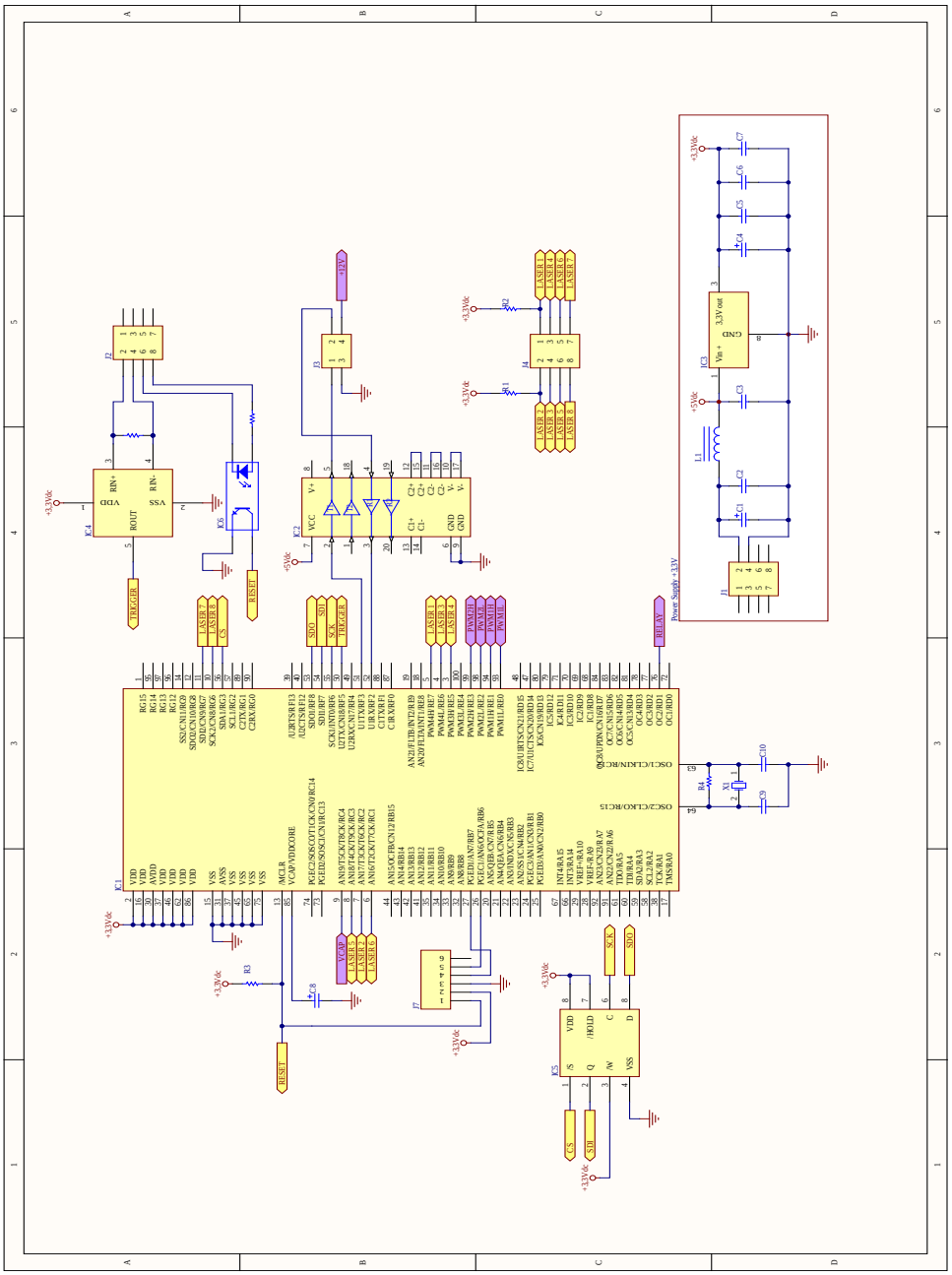

A.2 Esquemático de la parte de potencia del prototipo instalado en Antares y Nemo.

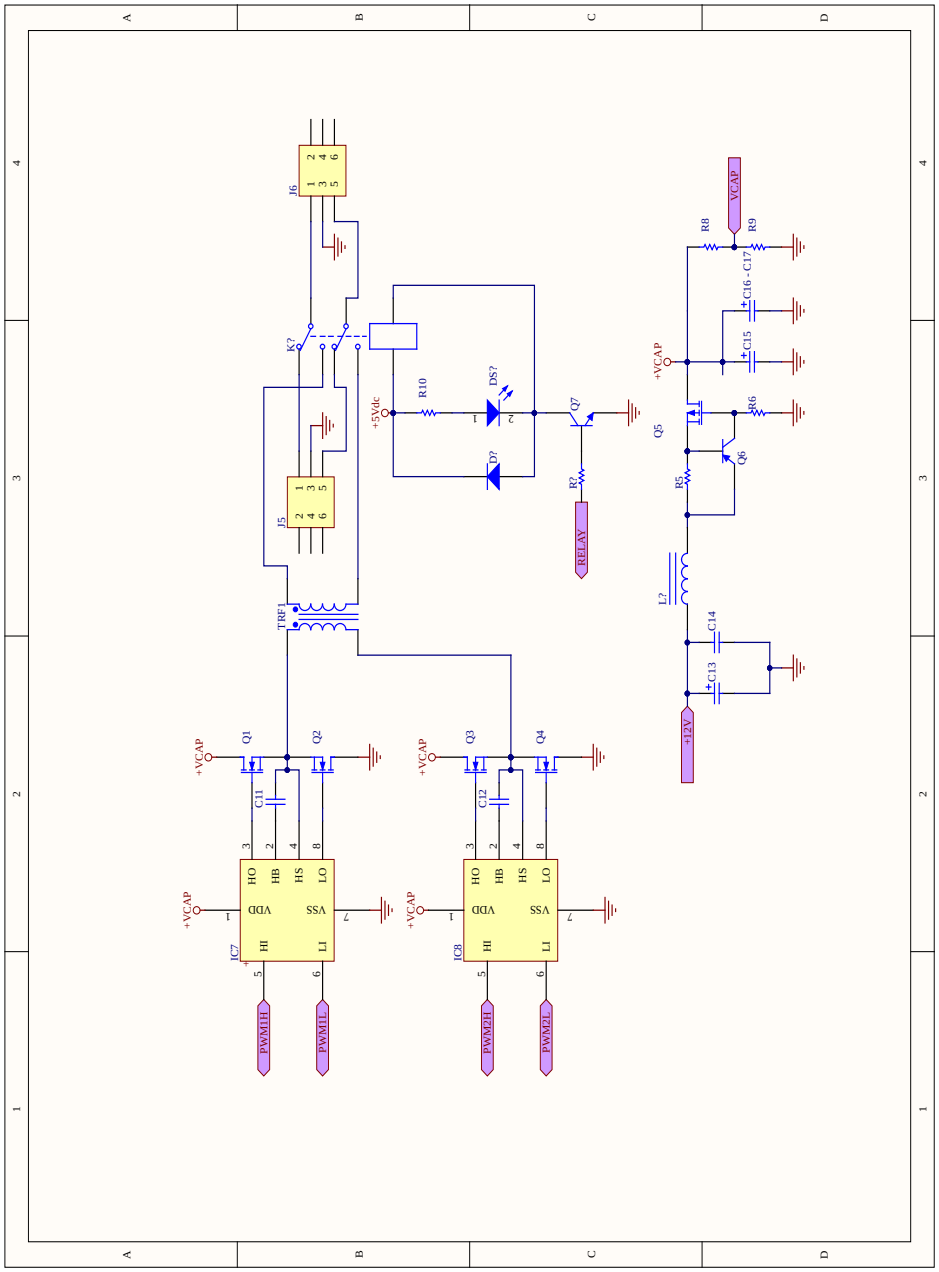

A.3 Esquematico módulo de control potencia del acoustic beacon de KM3NeT.

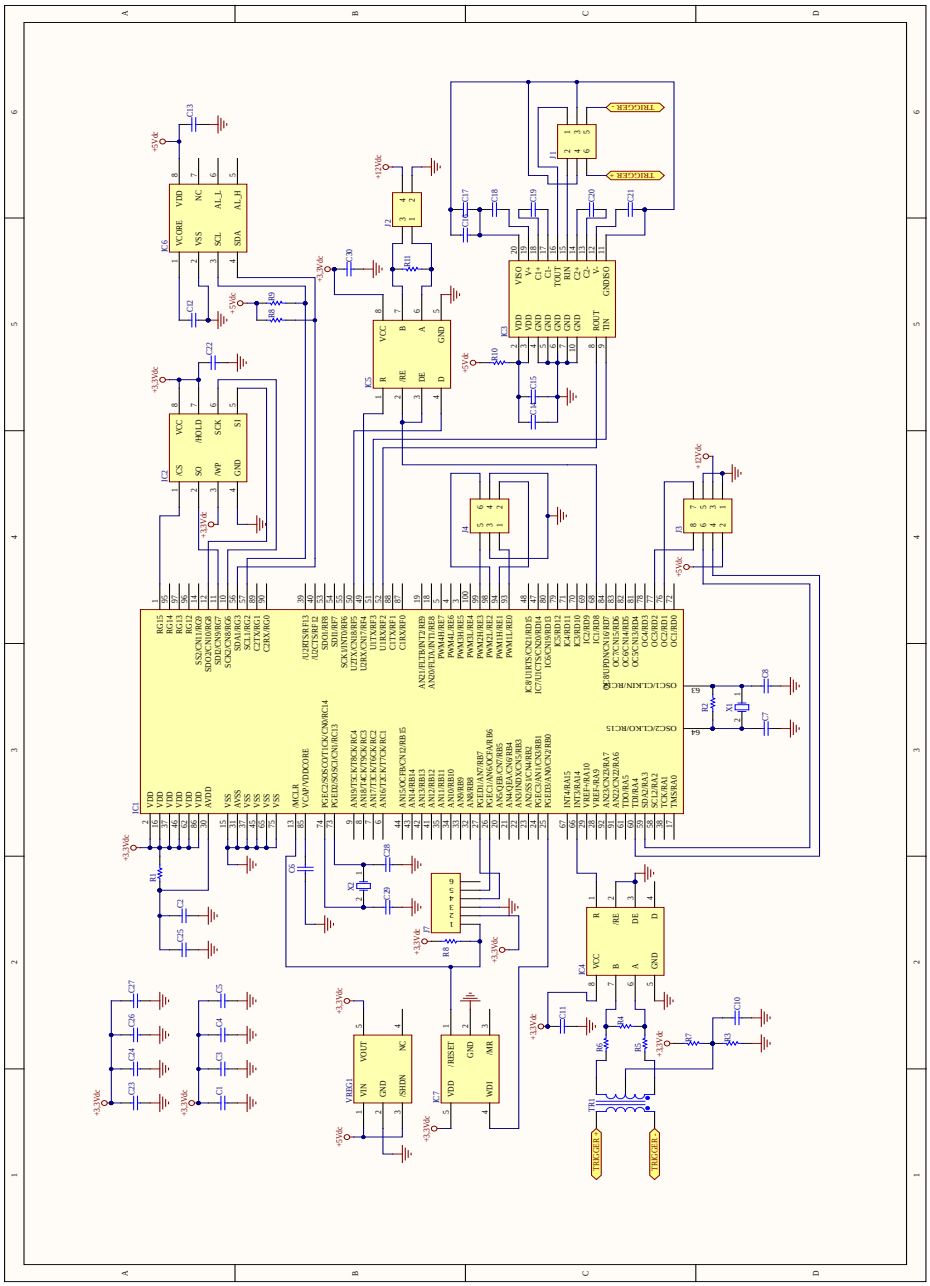

A.4 Esquemático del módulo de potencia del *acoustic beacon* de KM3NeT.

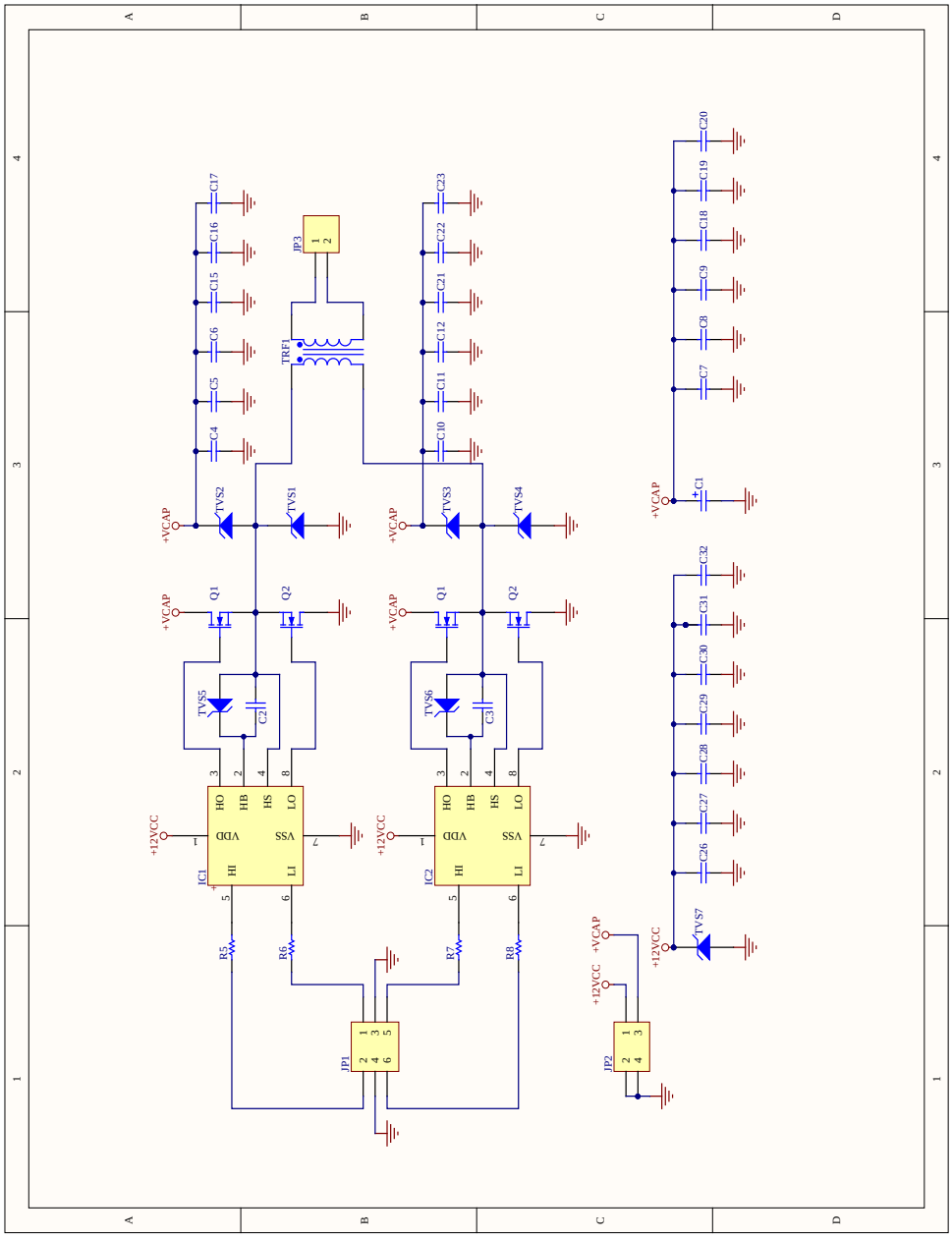

A.5 Esquemático del módulo de alimentación del *acoustic beacon* de KM3NeT.

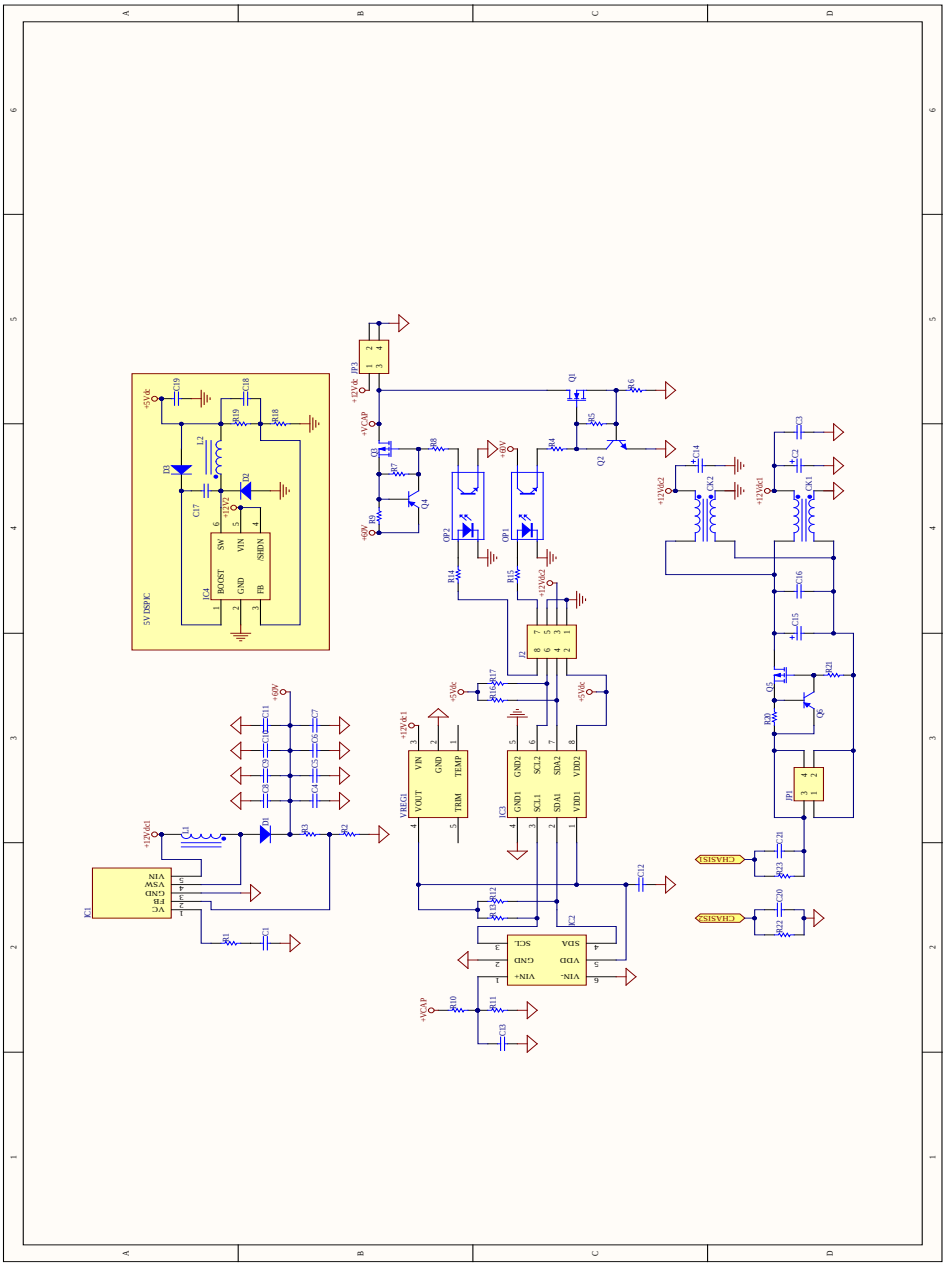

A.6 Diagrama de cableado del del *acoustic beacon* de KM3NeT.

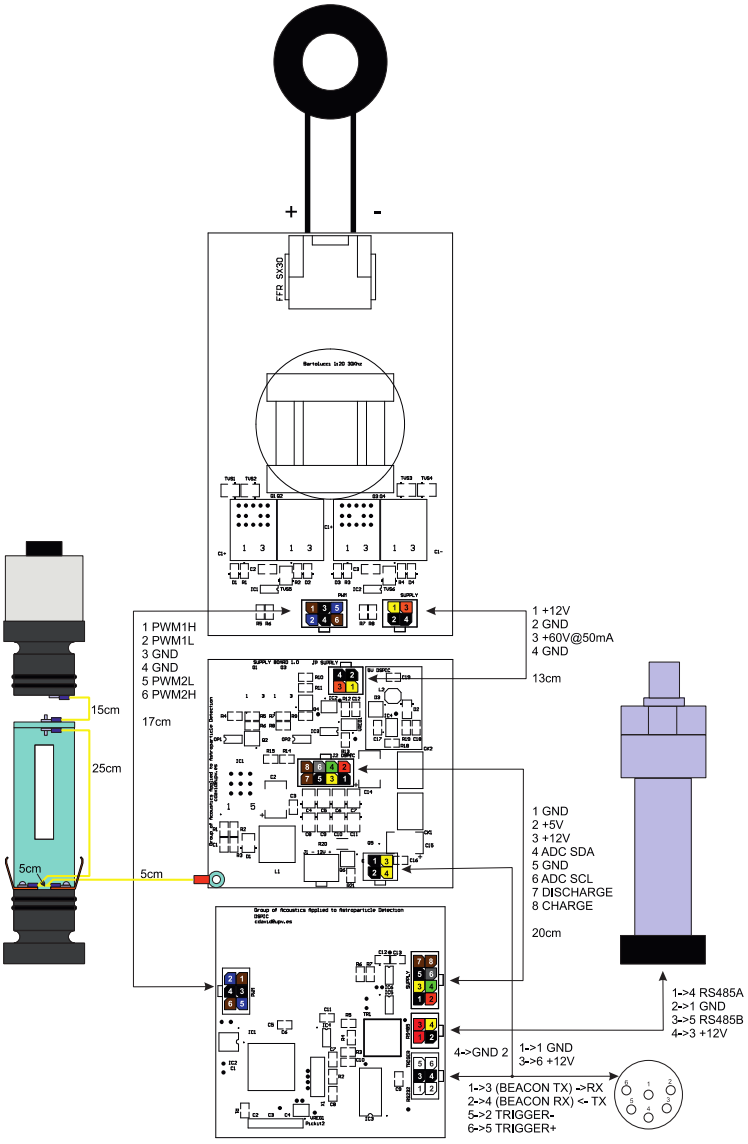

A.7 Pantalla principal del Software desarrollado para las campañas marítimas.